5-1-2014

# Improved Wind Turbine Control Strategies for Maximizing Power Output and Minimizing Power Flicker

Quan Chen
*University of Wisconsin-Milwaukee*

# IMPROVED WIND TURBINE CONTROL STRATEGIES FOR MAXIMIZING POWER OUTPUT AND MINIMIZING POWER FLICKER

**by**

**Quan Chen**

**A Thesis Submitted in**

**Partial Fulfillment of the**

**Requirements for the Degree of**

**Master of Science**

**in Engineering**

**at**

**The University of Wisconsin-Milwaukee**

**May 2014**

# ABSTRACT

# IMPROVED WIND TURBINE CONTROL STRATEGIES FOR MAXIMIZING POWER OUTPUT AND MINIMIZING POWER FLICKER

**by**

**Quan Chen**

**The University of Wisconsin-Milwaukee, 2014**
**Under the Supervision of Professor Ronald Perez**

For reducing the cost of energy (COE) for wind power, controls techniques are important for enhancing energy yield, reducing structural load and improving power quality. This thesis presents a study on innovative control strategies for wind turbine operation, from the perspectives of both maximizing power output and reducing power flicker and structural load.

First, a self-optimizing robust control scheme is developed with the objective of maximizing the power output of a variable-speed wind turbine with doubly-fed induction generator (DFIG) operated in Region 2. The process of wind power generation can be divided into two stages: conversion from aerodynamic power to rotor (mechanical) power and conversion from rotor power to the electrical (grid) power. In this work, the maximization of power generation is achieved by a two-loop control structure in which the power control for each stage has intrinsic synergy. The outer loop is an Extremum Seeking Control (ESC) based generator torque regulation via the rotor power feedback. The ESC can search for the optimal torque constant to maximize the rotor power without

wind measurement or accurate knowledge of power map. The inner loop is a vector-control based scheme that can both regulate the generator torque requested by the ESC and also maximize the conversion from the rotor power to grid power. In particular, an$\mathcal{H}_\infty$ controller is synthesized for maximizing, with performance specifications defined based upon the spectrum of the rotor power obtained by the ESC. Also, the controller is designed to be robust against the variations of some generator parameters. The proposed control strategy is validated via simulation study based on the synergy of several software packages including the TurbSim and FAST developed by NREL, Simulink and SimPowerSystems.

Then, a bumpless transfer scheme is proposed for inter-region controller switching scheme in order to reduce the power fluctuation and structural load under fluctuating wind conditions. This study considers the division of Region 2, Region 2.5 and Region 3 in the neighborhood of the rated wind speed. When wind varies around the rated wind speed, the switching of control can lead to significant fluctuation in power and voltage supply, as well as structural loading. To smooth the switch and improve the tracking, two different bumpless transfer methods, Conditioning and Linear Quadratic techniques, are employed for different inter-region switching situations. The conditioning bumpless transfer approach adopted for switching between Region 2 maximum power capture controls to Region 2.5 rotor speed regulation via generator torque. For the switch between Region 2.5 and Region 3, the generator torque windup at rated value and pitch controller become online to limit the load of wind turbine. LQ technique is posed to reduce the discontinuity at the switch between torque controller and pitch controller by using an extra compensator. The flicker emission of the turbine during the switching is

calculated to evaluate power fluctuation. The simulation results demonstrated the effectiveness of the proposed scheme of inter-region switching, with significant reduction of power flicker as well as the damage equivalent load.

# TABLE OF CONTENTS

# LIST OF FIGURES

# LIST OF TABLES

# ACKNOWLEDGEMENTS

I would like to acknowledge my advisors, Dr. Ronald Perez and Dr. Yaoyu Li at University of Wisconsin-Milwaukee, and co-advisor Dr. John Seem, from Johnson Controls, Inc, for all of their guidance and support that helped me through the past years. Their invaluable encouragement and support make me to perform the work described in this thesis.

I am grateful to the Wind Energy Group at the College of Engineering & Applied Sciences of UW-Milwaukee, for sharing their broad knowledge and excellent research in wind energy. I also want to thank my colleagues from the Mechatronics lab of UW-Milwaukee. They gave me great help when various problems were encountered during my research. In particular, I would like to thank Justin Creaby and Zhongzhou Yang. Justin has made a great contribution about using Extremum Seeking method in wind turbine control, and the simulation study of FAST as well as CART models and data. Zhongzhou Yang gave me great help on the fatigue load analysis of the wind turbine.

Finally, I would like to acknowledge the financial support from We Energies 2008 Renewable Energy Research Grant Program.

# 1. Introduction

This chapter introduces the background and the problems of interest for this thesis research. In the first section, the basic information of the wind energy will be introduced. Then, Section 1.2 provides a brief overview of the state-of-the-art advancement in wind turbine controls, which leads to the two main problems of interest for this study, i.e. maximizing the power output and reducing power fluctuation.

## 1.1. Wind Energy

Wind energy is free, clean, and endless. The use of wind power has a history of thousands of years before modern plants were developed[1]. Since ancient times wind power has been recognized as a valuable resource for different purposes, e.g. building windmills for milling grain and pumping water. Wind power technology has experienced an important development in the past two decades, originated from the oil crisis in early 1970s, and spurred by more recent pressure in energy and environmental sustainability. According to a 2012 report by a clean energy consulting group, the cost of the electricity produced by new wind farms is at 5-8 cents per kWh which is comparable with the conventional energy source electricity price, for instance, fossil based power plants[2]. Wind power has transitioned from research prototyping to a mainstream renewable power technology with bring perspective for utility generation.

With over 280 GW[3] capacity installed by the end of 2012, wind power has now become the most important renewable energy source worldwide. The U.S has so far the second largest installed capacity of wind power in the world, surpassed 60GW by the end of 2012[3]. The global wind power capacity has increased by 22.5% during the year of

2010. It is expected that wind energy accounts for just over 1.5% of the electricity produced in the U.S in 2009, the Department of Energy aims a 20% wind power generation by 2030, approximately 300GW[4]. Figure 1.1 shows an example of a modern wind farm[5].

Figure 1.1 Big Horn Wind Farm at Bickelton, Washington

Wind energy technology is advanced by decreasing the cost of energy (COE) and improving the power quality of the wind power. The first goal leads to various technical innovations in enhancing energy capture and reducing the cost of installation and maintenance, and development of advanced control strategies is a critical aspect. Controls for maximizing power capture and reducing fatigue loads both serve for such purpose. To improve power quality, electrical controls, as well as mechanical controls, have been widely developed.

## 1.2.Wind Turbine Control Systems

From the power flow perspective, control of wind turbine can be divided into two stages. The first stage is to control the turbine to convert aerodynamic power into the mechanical (rotor) power (i.e. the product of rotor torque and rotor speed), while the second stage is to control the generator to convert the mechanical power into the electrical power (i.e. grid power for most occasions).Figure 1.2 shows the power vs. wind speed curve for variable speed pitch regulated turbine[1].

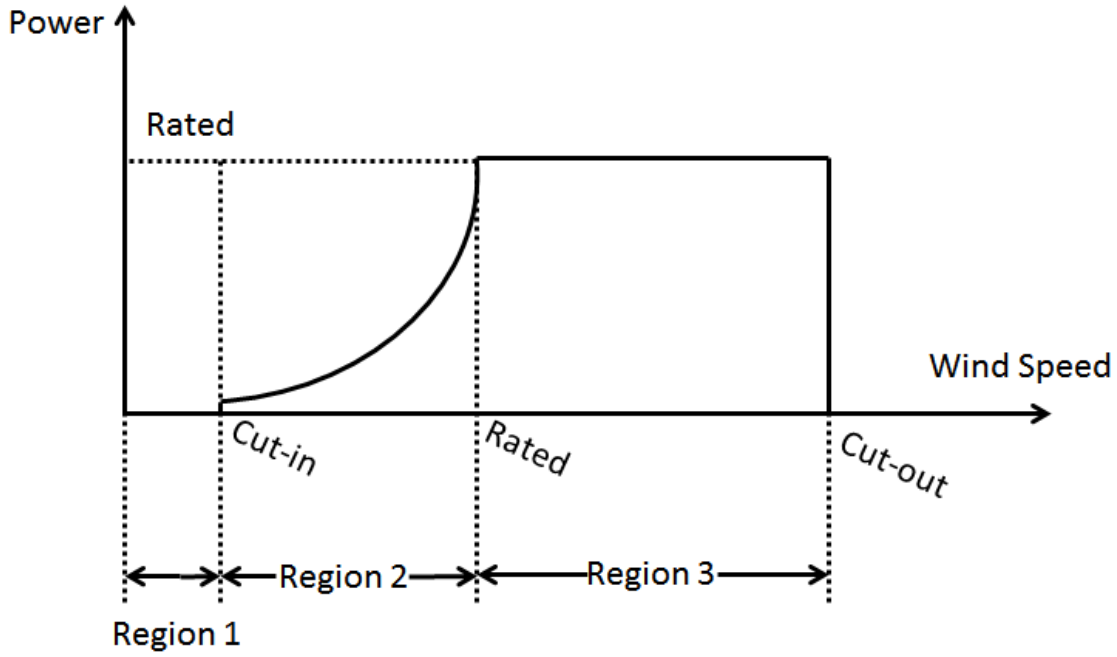


Figure 1.2 Power-Wind Speed Curve for Variable-speed Pitch-regulated Turbine

There are different configurations for wind turbines. For utility wind turbines, the most popular and efficient is the variable-speed and variable-pitch turbine. With different wind speed and control objectives, the control of variable-speed variable-pitch wind turbine can be categorized into three control regions [1, 6, 7]. The wind speed below the cut-in speed (usually 3-5m/s) is classified as Region 1. Turbine operation is not started

yet in this region. The wind speed between the cut-in speed and rated wind speed is classified as Region 2. The objective for Region 2 control is maximizing the capture of mechanical rotor power. Above rated wind speed is Region 3, the turbine operates at the rated power of the generator, and pitch is used to reduce the mechanical load. When the wind is above the cut-out speed, the turbine will shut down to protect turbine.

The control development for wind power generation always focuses on Region 2 and Region 3 operations. For Region 2, the challenge is in order to achieve maximize power operation, controller needs to find out the optimal rotor speed and blade pitch under variable wind. For Region 3, the control objective is to regulate the power output at the rated level and minimizing the turbine load at the same time to ensure the reliability.

As more and more wind turbines have been and will be installed in medium to low wind areas, i.e. more frequently operated in Region 2,enhancing power capture in this region is an critical issue for wind power development. Wind power capture can be enhanced with better turbine design and/or advanced control strategy. Developing advanced control strategies is often a more cost-effective way for energy capture enhancement and also can be applied easily to those turbines already installed.

Improving power quality of grid connected wind turbine is as same important as increasing power capture. Especially for weak grid situations, such as islanding and microgrid, the power quality is strongly affected by the fluctuating nature of wind source, and thus receives remarkable concern. The power fluctuation due to grid connected wind turbines can be affected by numerous factors, such as wind variations, grid conditions, type of turbine, the control algorithm, and the tower shadow effect. One cause of power fluctuation is the transient of controller switching when turbine operation experiences

transition between two neighbored regions (typically between Region 2 and Region 3). In Section 1.2.2, more details on improving power quality via reducing power fluctuation during inter-region operation of wind turbine will be described.

Variable-speed variable-pitch (VSVP) wind turbine is chosen for this study for the reason that it has better performances in energy capture and power quality compared with the conventional fixed speed fixed pitch wind turbines [8, 9, 10].Among different options of generators available for VSVP wind turbine, the doubly fed induction generator (DFIG) drew attention in industry and became the mainstream choice for utility wind power, with intensive research has been done in its dynamic modeling, stability analysis and control [11, 12, 13, 14, 15]. The DFIG is an attractive choice for variable-speed wind turbine systems with moderate variable speed range, i.e. ±30% of synchronous speed of the generator [16, 17]. For DFIG based VSVP turbine, due to the lower power rating required, the converter losses will be reduced as compared to those systems with the full power scale converter (e.g. permanent magnet synchronous generators), and in consequence, the cost of the power electronics is reduced. Therefore, in this thesis study, the DFIG is selected as the generator for the simulated system.

As summary of the foregoing considerations, this thesis study has two aims: Region 2 operation and the inter-region transition between the Region 2 to Region 3, i.e. how to maximize the wind power generation in Region 2 and minimize the power fluctuation in inter-region transition on DFIG base VSVP wind turbine.

### 1.2.1 Maximum Power Capture for Region 2 Control

To achieve maximum power capture in Region 2, it is important to maximize the conversion for both rotor power and electrical power. For rotor power maximization,

typical control actions adjust blade pitch and rotor speed (or tip speed ratio). For variable speed turbines in Region 2 operation, it is typical to control the generate torque to adjust the rotor speed as the optimal pitch angle does not vary as much. Most existing rotor control strategies are based on a statistic wind power map, which in consequence needs wind measurement as well. Considering the significant variation in wind, low fidelity in wind power models, variation of turbine characteristics, and uncertainties in wind measurement, it is desirable to develop control strategies that can maximize power capture while not relying on either high-fidelity power maps or accurate wind measurements. Therefore, adaptive control, which is much less dependent on the accuracy of the reference model, has received quite some attention for energy capture control.

Johnson *et al*. [6] used a method to measure the average power coefficient during every adaptation period and then adjust the torque control gain based on the result. The main limitation of this method is the need for wind measurement for the feedback signal in adaptation, which has difficulty in decoupling the power variation due to the wind variation from the adjustment of torque control gain. The 3-hour adaptation period appeared too long for practical operation. Such performance is not ideal for field operation. Bianchi *et al*. [7] used a model based approach to select the appropriate torque control value based on the wind speed. Again accurate wind speed measurements are required, and this method relies on precise modeling, which can be inaccurate [18].

Extremum Seeking Control (ESC) is a nearly model-free self-optimizing control strategy that can dynamically optimize an unknown and slowly time-varying performance index. The only measurement needed is the performance index output. ESC based wind

turbine control was studied in [19] to search for the optimum pitch angle based on captured power for a simple quadratic model of a fixed speed wind turbine. Recently, a multi-variable ESC controller was developed by Creaby *et al*. [20]via tuning pitch angle and generator torque. Simulation results demonstrated encouraging performance in improving energy capture under fluctuating turbulent winds. However, this work was limited in several aspects. The ESC scheme in [20] was designed with the nominal Hessian (or the $2^{nd}$-order derivative) of the power map, without considering the robustness of the ESC scheme. More importantly, [20] was limited to maximization of rotor power, without addressing the maximization of electrical power conversion.

In order to achieve the maximization of ultimate power generation, the work in [20] should be extended to incorporate the conversion from rotor power to the electrical power. Design of generator controllers for converting rotor power to electrical power is not independent from the rotor power control. With the broad-spectrum nature of the turbulent wind input, the rotor power obtained from the rotor control is determined by both the wind characteristics and the rotor controllers. Therefore, for the generator controller to be designed, the performance specifications for power conversion need to cover appropriate bandwidth so as to capture the dominant frequency components of the rotor power. Meanwhile, the designed controller needs to be robust against the variations in system parameters such as winding resistance/inductance and frequency.

### 1.2.2 Power Fluctuation Issue for Interregional Control

The power fluctuation due to grid connected wind turbines is affected by numerous factors, such as wind variation, grid condition, turbine type, control algorithm, and tower shadow effect. As more mid-size turbines will be installed in severe turbulent wind area

and weak grid condition, it is important to develop a smooth inter-region switch control scheme to improve wind power quality [21].

The controller switching during inter-region operation of wind turbine can induce significant fluctuation of the grid-side power output. The switching transient is due to the different control strategies between Region 2 and Region 3.When the turbine operates in wind fluctuating around the rated wind speed, the rotor speed will vary around the reference/rated speed, which may result in frequent switch between the Region-2 controller and the Region-3 controller. After the Region-3 controller is activated, the pitch control is used to limit the load, this will result in a short transient, which possibly reduce the rotor speed to the rated value and the turbine controller will switch back to the Region-2 operation. Such frequent switching, as shown in Fig. 1.3, canlead to significant flicker emission when the turbine is connected to grid.

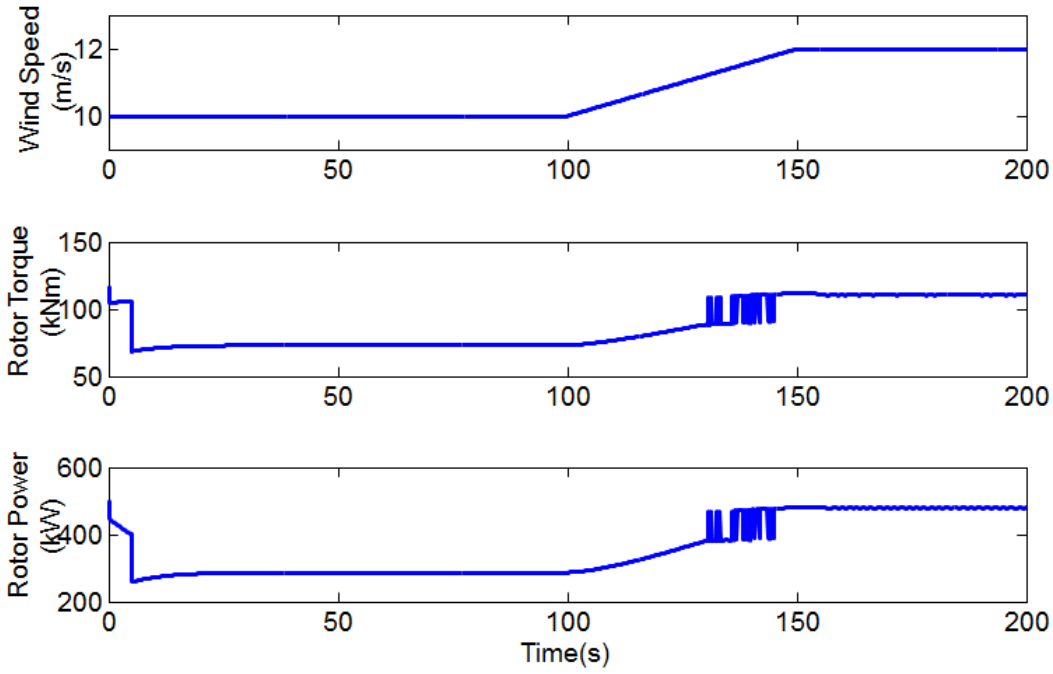


Figure 1.3 Controller Switching transient of a Variable-speed Pitch-regulated Turbine

There have been some studies related to inter-region switching control for wind turbine [22, 23]. When the turbine operates in turbulence wind above the rated wind speed, the rotor speed will vary around the reference rotor speed and this will result in a switch between the Region 2 controller and Region 3 controller. After the Region 3 controller is activated, the pitch control is triggered to limit the rotor load, this will result in rotor speed decreasing and less than rated value and the turbine controller will switch back to Region 2 operation. This fluctuation can produce power flicker at the grid side, which deteriorates the power quality. Electrical flicker is a measure of the voltage variation, which may cause disturbance for the consumer. The International Electrotechnical Commission (IEC) has designed IEC 61400-21 to procedures standard test for wind turbines for grid connection with respect to the impact on the power quality y[24]. This testing includes assessment of power flicker and harmonics levels. In this study, an inter-region switching control strategy based on bumpless transfer methods is presented to reduce the flicker and improve the transient during the controller switching of wind turbine during Region 2 and 3 operations.

## 1.3.Problem Statements

Based on the consideration described in the previous section, the research problems addressed by this thesis can be stated as follows.

Problem Statement #1

*Develop a self-optimizing control strategy for Region 2 operation, which can maximize both energy capture in turbine rotor and the power conversion to the grid for a DFIG based variable-speed wind turbine without dependency on wind speed measurement.*

Problem Statement #2

*Develop a bumpless transfer based inter-region controller switching scheme, which can reduce the power fluctuation due to the switching between Region 2 and Region 3 operations.*

## 1.4.Research Approach

The self-optimizing robust control strategy for maximizing power output includes two control loops: the outer loop is the self-optimizing search for the maximum rotor power based on Extremum Seeking Control (ESC), while the inner loop is an $\mathcal{H}_\infty$ robust controller that can maximize the conversion from rotor power to grid power against generator parameter variations.

The advantage of using ESC is its model-free and can dynamically optimize an unknown cost function. This can enable us maximizing the power capture independent on an accurate wind turbine model and wind measurement. The $\mathcal{H}_\infty$ control method is selected to convert the rotor power to the electrical power with performance specification of covering the appropriate bandwidth in order to capture the dominant frequency components of the rotor power. Meanwhile the controller is synthesized to be robust against the variation in the system parameters.

Bumpless transfer method is introduced to deal with the transient during the controller switching. The switching can be divided into two steps, i.e. Region 2 to Region 2.5 and Region 2.5 to Region 3. Bumpless transfer method can improve in each step of switching. The LQ bumpless transfer method and conditioned bumpless transfer method are studied and compared under different wind profile.

The problem statement in the previous section leads to the five aspects of control design as to be addressed in the later chapters:

1) ESC based maximizing wind energy capture
2) Modeling of DFIG based wind power conversion system
3) $\mathscr{H}_\infty$ controller for maximizing DFIG wind power conversion
4) Inter-region controller switching for variable-speed variable-pitch wind turbine
5) Bumpless transfer methods for minimizing power fluctuation

This research is focused on the simulation study. The turbine model of this study is the CART (controls Advanced Research Turbine) facility located at the National Renewable Energy Laboratory (NREL) at Golden, Colorado. This turbine model has been used in previous wind turbine control research [6, 25] and is a well-known test model in the wind power community. Simulation packages used in this research includes Matlab and Simulink/SimPower Systems, and wind turbine simulation software developed by NREL, i.e. FAST, AeroDyn, and TurbSim. The FAST (Fatigure, Aerodynamics, Structures and Turbulence) software is widely recognized as quality aeroelastic software for wind turbine control simulation. AeroDyn is used for the aerodynamic calculations for obtaining load profiles and will input to FAST. TurbSim is a stochastic, turbulent wind simulator.

The DFIG model and grid simulation is developed in Simulink/SimPowerSystems. The $\mathscr{H}_\infty$ controller is synthesized by Matlab robust control toolbox. After the turbine and generator model is developed, the controller is designed and tested with the different wind profiles. Simulation from smooth wind to turbulent wind allows for analysis of data and testing of the designed controllers. Finally, the controller is simulated under realistic operating conditions. In this research, we use the actual wind file recorded from the wind field.

As the reliability and operating life is critical for wind turbine control. It is also important to evaluate the stability of the control method introduced and test the damage equivalent load induced by proposed controllers. Flicker emission is needed to evaluate to analysis the improvement of the power quality from the bumpless transfer methods.

## 1.5. Organization of the Thesis

There are seven chapters in this thesis. The second chapter reviews the literatures in the modern wind turbine control methods and DFIG modeling and control methods previous developed for wind turbine with DFIG. The three control region of wind turbine will be introduced and inter-region controller switching of wind turbine will be reviewed. The bumpless transfer control method will be introduced for minimal the transient during the inter-region controllers switching.

Chapter 3 presents the simulation tools for this study. The software packages used in this study are described. FAST, AeroDyn, TurbSim are developed by National Renewable Energy Laboratory (NREL) for wind turbine simulation. The controllers are developed in Matlab, with DFIG model is developed using SimPowerSystems Toolbox. Robust Control Toolbox is used to synthesize $\mathscr{H}_\infty$ controller to achieving robust performance and stabilization.

Chapter 4 presents the model of DFIG based wind power system. The mathematical model will be analyzed and state-space representation of DFIG is developed. The grid side converter and rotor side converter is introduced and the controller strategies is analyzed respectively

Chapter 5 presents the comprehensive study of self-optimizing scheme that can maximize the power generation for a variable speed wind turbine with DFIG operated in

Region 2. Power generation optimized through two stages: conversion from aerodynamic power to rotor power and conversion from rotor power to the electrical power. In this chapter, the maximization of power generation is achieved by a two-loop control structure in which the power control of each stage has intrinsic synergy. The outer loop is an Extremum ESC based generator torque regulation via the rotor power feedback. The ESC can search for the optimal generator torque constant to maximize the rotor power without wind measurement or accurate knowledge of power map. The inner loop is a vector-control based scheme that can both regulate the generator torque requested by the ESC and also maximize the conversion from the rotor power to grid power. In particular, an $\mathscr{H}_\infty$ controller is synthesized for maximizing, with performance specifications defined based upon the spectrum of the rotor power obtained by the ESC. Moreover, the controller is designed to be robust against the variations of some generator parameters. The proposed control strategy is validated via simulation study based on the synergy of simulation packages described in Chapter 4.

Chapter 6 presents a bumpless transfer based control switch scheme for the inter-region operation of variable-speed variable-pitch wind turbines, with the objective of reducing the associated power fluctuation. This study considers the division of Region 2, Region 2.5 and Region 3 in the neighborhood of the rated wind speed. It has been known that wind variations around the rate wind speed can lead to significant fluctuation in power and voltage supply. To smooth the switch and improve the tracking, two different bumpless transfer methods, Conditioning and Linear Quadratic techniques, are employed for different inter-region switching situations. The conditioning bumpless transfer approach adopted for switching between Region 2 maximum power capture control to

Region 2.5 rotor speed regulation via generator torque. During the switch between Region 2.5 and Region 3, the generator torque windup at rated value and pitch controller become online to limit the load of wind turbine. LQ technique is posed to reduce the discontinuity at the switch between torque controller and pitch controller by using an extra compensator. The simulation results demonstrated the effectiveness of the proposed scheme of inter-region switching, with significant reduction of power fluctuation. Therefore, the power quality can thus be improved.

Chapter 7 concludes this research. The contribution of this thesis work is concluded and the future work of this research is also summarized.

## 1.6. Summary

In summary, more wind turbines have been and will be built in the U.S and the worldwide in the future decades. A large number of wind turbines will be installed in areas with lower wind speeds which are closer to larger populations for more economical distribution and maintenance. The turbines will be operating mostly in Region 2 where the control goal is to maximize the power capture. And it is important to convert as much rotor power to the grid as possible for Region 2 operation. The two step optimizing control will help to reduce the COE of the wind energy.

As more midsize and small wind turbines will be installed in the micro-grid and isolated locations, there is demand of power quality improvement research for wind turbine control. The power fluctuation will occur during the inter-region controller switching of wind turbine. The bumpless transfer method is needed to reduce and minimize the power fluctuation when the turbine is operated with the neighborhood of

the region 2 and region 3 transitions. The power flicker emission needs to be reduced with the inter-region operation of wind turbine for grid integration.

# 2. Literature Review

In this chapter, we review the relative previous work about wind turbine research and control of Doubly-Fed Induction Generation (DFIG) based wind turbine. It is important to understand the current wind turbine control strategies and what research has been done especially for the DFIG based variable speed turbine control. This chapter starts from the review of general wind turbine control, followed by the studies of DFIG modeling and control of DFIG based wind turbine. Then Section 2.4 focuses on the discussion of the control of wind turbine through inter-region operating, and how the bumpless transfer control method will improve the transient of controller switching.

## 2.1 Wind Turbine Control

### 2.1.1 Historical Background of Wind Power

Wind power was used to provide mechanical power for milling grain and pumping water before the development of modern plants. It has about three thousands of year's history, and is gaining increasing importance throughout the world especially due to the energy crisis. As modern wind power plants can provide a more consistent power source and their cheap fossil fuels, the use of the fluctuating wind power is demised until the early $20^{th}$ century. In the early 1970s, with the oil shortage, the wind power technology re-emerged the public interest. Instead of providing mechanical energy, the modern wind power technology focus on using wind to producing electrical power. In the early $20^{th}$ century, the first wind turbine for electricity generation had been developed. The energy crisis encouraged the development of wind turbine technology. The reliability of the turbine is greatly improved and the cost of the energy (COE) is reduced at the same time

due to new turbine designs and new materials were developed. The cost of the wind power has fallen to about one sixth of the cost in the early 1980s, dropped to less than 5 cents per kWh today[4]. Wind turbine technology moved very fast in increasing dimensions. In late 1980s, a 300kW wind turbine with a 30 meter rotor diameter was state of the art. in 1990s, 2MW turbines with a rotor diameter of around 80 meters were available. In the 21$^{st}$ century, 3 to 3.6MW turbines are commercially available with a rotor diameter of around 90 meter.

### 2.1.2 Wind Energy Conversion System

A wind energy conversion system (WECS) is used for extracting kinetic energy from the wind and transforming into the electrical energy[1]. WECS can be divided into two types, depending on propelled by aerodynamic lift or drag force. Early WECS utilized the drag principle with vertical axis wind wheels which have a very low power coefficient at a maximum of round 0.16 [26]. Modern wind turbines technology is mostly based on aerodynamic lift. The lift devices use blades to interact with the incoming wind. Wind turbines using aerodynamic lift can be further cataloged into the orientation of the spin axis into horizontal axis and vertical axis turbines. Vertical axis turbines were developed and commercially produced in the 1970s until the end of the 1980s. The horizontal axis approach is currently dominates the wind turbine development and applications. A horizontal axis wind turbine (Figure 2.1 [1]) is typically consists of a tower and a nacelle which contains the generator, gearbox and the rotor. Different number of blades can be used on horizontal axis wind turbines depending on the sizes and technology of the wind turbine, usually are two-bladed or three bladed.

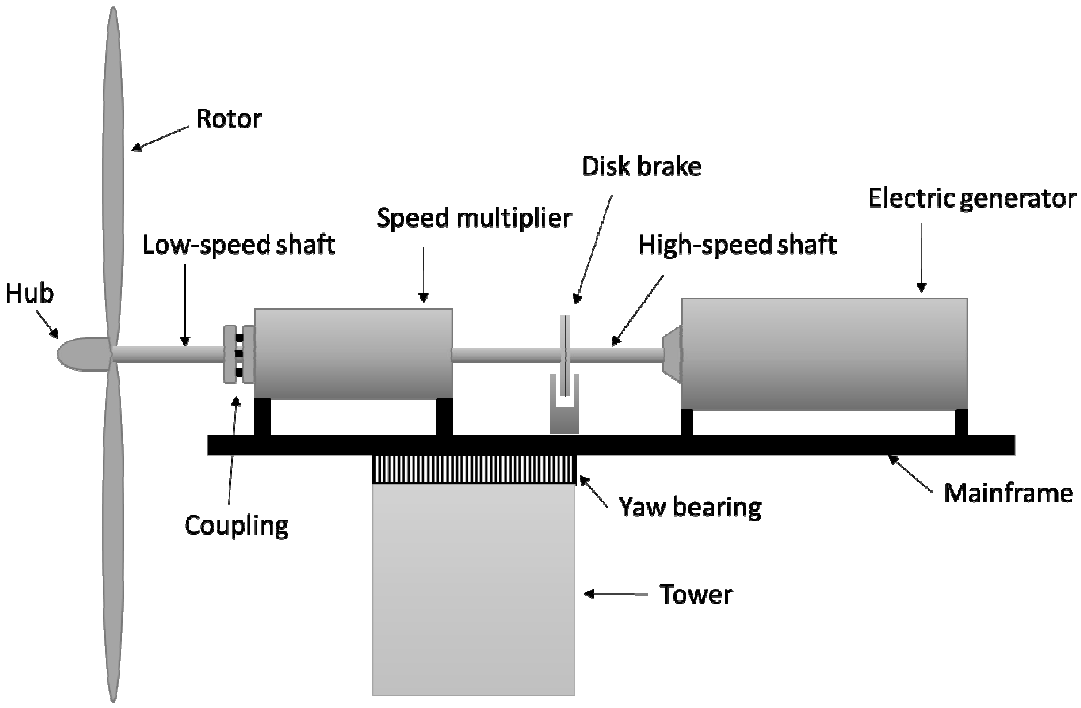


Figure 2.1 Main Elements of a Two-bladed Horizontal Axis Wind Turbine

The energy conversion of wind turbine chain can be organized into two steps:

- The aerodynamic torque results in the production of mechanical power
- The turbine rotor then drives a rotating generator which transform the kinetic energy into electrical power

The actual energy conversion process of wind turbine uses the basic aerodynamic lift force to produce a net positive torque on a rotating shaft. To achieve this, the wind turbine is basically consisted of four subsystems:

1) Aerodynamic subsystem, including the turbine rotor, which is composed of blades, and turbine hub to support the blades
2) Drive train, consisting low-speed shaft (coupled with the turbine hub), speed multiplier and high-speed shaft (drive the generator)
3) Electromagnetic subsystem, consisting of the electric generator for electrical power conversion

4) Electric subsystem, composed of the grid connection and local grid

### 2.1.4 Wind Turbine Control Objectives

Power generation capability of wind turbine respect to the wind speed is shown in Figure 2.2 [1, 6]. Follows the available wind power under different wind speed, the control of wind turbine can be classified into 3 control regions. The wind speed below 5m/s is classified as Region 1, representing the wind speed is too slow, the turbine is not stated in this region. The wind speed between 5m/s to 14 m/s is classified as Region 2[6]. Above the 14m/s wind, is in Region 3, which the turbine operates at the rated power of the generator. This can be done by limiting the mechanical load of the turbine via pitch control. When the wind speed is above 22m/s, the turbines need to be shut down for protection the equipment [6, 27].

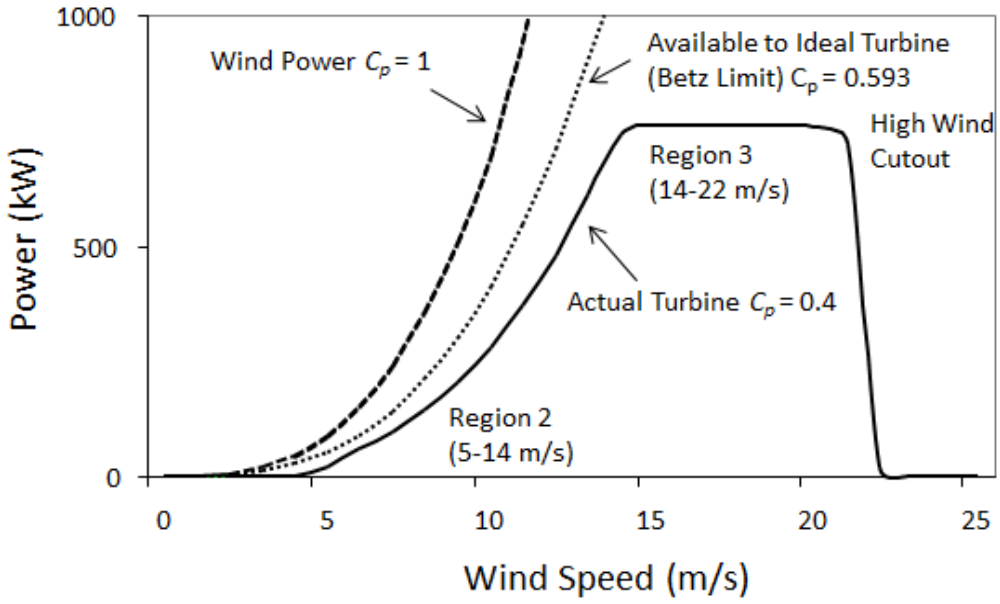


Figure 2.2 Wind Power Generation under Different Wind Speeds

Based on the above analysis, the objectives of wind turbine control can be summarized as

1) Controlling the wind turbine to capture as more power as possible when the rated wind speed is not reached
2) Controlling the wind turbine to maintain rated power capture for speed larger than the rated
3) Alleviating the mechanical load and guarantee the reliability of the mechanical parts
4) Transferring the mechanical power captured by the rotor to the grid and meeting the power quality standards.

The wind turbine control system usually takes use of a number of sensors, actuators on the wind turbine and a computer to processes the control signals. The three main areas of mechanical control consist of torque, pitch, and yaw control. Torque control is focus on the regulation of the rotational speed of the turbine which is generally used in the Region 2 control. Pitch control is typically used to regulate the rated power output in above rated winds, and yaw control is used to turn the turbine to face the wind. This research is focused on the Region 2 and Region 3 control design of wind turbine. The startup, shut shown or the grid fault are not taken into consideration in this research.

### 2.1.5 Electrical Power Generation Systems

The electrical power generation system of wind turbine consists of electrical generator and power electronics converter and electrical transformer which used to ensure the grid voltage compatibility [1]. The configurations of the power generation systems can be generally divided into two types: fixed speed and Variable speed, depends on the electric machine types and its grid interface [1, 28].

a) Fixed Speed Wind Turbine

For the fixed speed wind turbine, the rotor speed is fixed and determined by the grid frequency regardless of the wind speed. A fixed speed wind turbine (Figure 2.3) is typically equipped with a squirrel-cage induction generators (SCIG), soft starter and capacitor bank and directly connects to the grid.

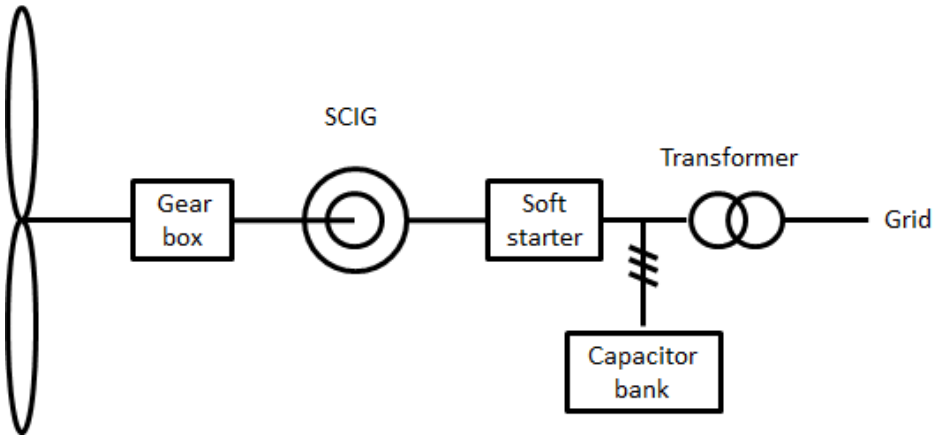


Figure 2.3 Scheme of a Fixed Speed Wind Turbine

To start, the induction machine is connected in motoring regime such that in steady-state, the rotational speed exceeds the synchronous speed and the electromagnetic torque is negative, which will generate electrical power. As the SCIG is directly connected to the grid, the generator works on its natural mechanical characteristic given by the rotor resistance. The rotational speed of the generator is close to the synchronous speed imposed by the grid frequency, and the turbulence in wind speed will induce only small variations in generator speed. SCIG are preferred in fixed speed wind turbine system for their mechanical simplicity and high efficiency with low maintenance cost. However, with the unique relation between the active power, reactive power, terminal voltage and rotor speed, SCIG based wind turbine need capacitor banks to limit the reactive power absorption from the grid in order to increase the power factor.

As SCIG based wind turbine are designed to achieve maximum power efficiency at a

unique wind speed. The generator of some fixed speed turbine has equipped two winding set in order to increase the power efficiency thus the turbine can operation at two speeds. The advantage of the fixed speed wind turbine system is its simple, robust and also reliable due to the simple and inexpensive electric systems. At the same time, the fixed-speed operation will induce significant mechanical stress to the drive train components. Furthermore, from the rotor speed point of view, fixed speed operation has very limited controllability. The fluctuation in wind speed is transmitted into the mechanical torque and later into the electrical power fluctuation into grid.

b) DFIG based Variable Speed Wind Turbine

Variable speed wind turbine is currently the most commonly used in wind energy due to its power variable speed operation can capture more power compare to the fixed speed operation.

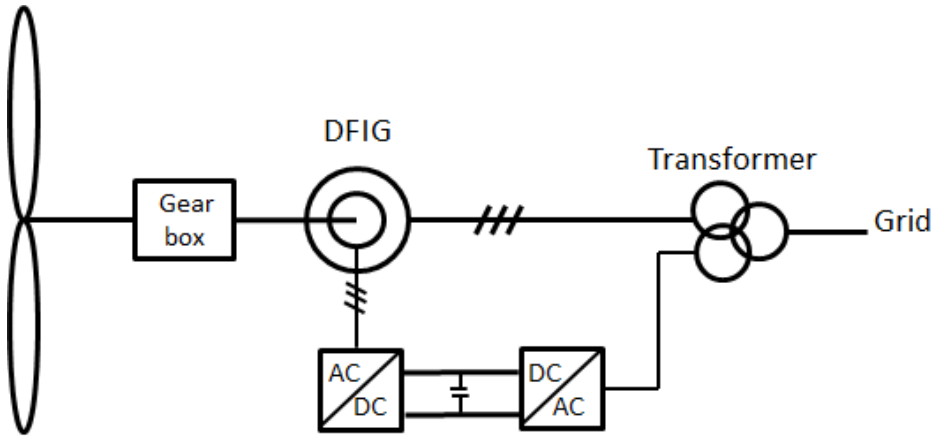


Figure 2.4 Scheme of a DFIG based Variable Speed Wind Turbine

The doubly-fed induction generator (DFIG) is most used by the wind turbine industry. As shown in Figure 2.4, the DFIG is consist of wound rotor induction generator with the stator windings connected directly to the grid and the rotor windings connected to a back-to-back AC-DC-AC voltage source converter [29]. The stator voltage is applied from the

grid and the rotor voltage is applied from the power converter. The stator output power into the grid all the time, while the rotor is feeding power into the grid when in over-synchronous operation and absorbs power from the grid when in the sub-synchronous operation[30]. The DFIG based wind turbine allows variable speed operation over a large but still restricted range limited by the scale of the power electronics converter and its controllers.

The power electronics converter used for DFIG based wind turbine is comprises of two IGBT converters: rotor side converter and grid side converter with a DC-link connection. The rotor side converter controls the generator in terms of active and reactive power, while the grid side converter controls the DC-link voltage and ensures operation at a large power factor.

DFIG based variable speed wind turbines are highly controllable, allowing maximum power capture over a large range of wind speeds, typically of ±40% around the synchronous speed. Furthermore, the active and reactive power control is decoupled by in dependently controlling the rotor currents via the power electronics converters. This study focuses on the modeling and control for DFIG based variable-speed wind turbine.

c) Full Variable Speed Wind turbine

DFIG based variable speed wind turbine is partially variable speed operation wind turbine depends on the size of the converter. Full variable speed wind turbine can be very flexible with both induction generator (SCIG) and synchronous generator i.e. wound-rotor synchronous generator (WRSG) or permanent-magnet synchronous generator (PMSG). PMSG is mostly used by the wind turbine industry with the back-to-back power converter has the similar size to the generator power. The PMSG has the advantage of

operation at high power factor and efficiency due to its self-excitation[28]. However, cooling system is critical to PMSG based wind turbines due to the magnetic materials in PMSG are sensitive to temperature and can lose their magnetic properties under high temperatures condition.

## 2.2 Modeling of DFIG

DFIG is the most attractive choice for variable speed wind turbine systems from the latest state-of-art in wind power industry. With limited variable speed range, i.e. ±30% of synchronous speed of the generator [16, 17], DFIG based variable speed wind turbine systems has better energy capture performance and flexible power control ability. In DFIG scheme, the power electronic converter only has to take care of partial of the total power, normally 20%~30%. The advantage of this is that the power electronic converter's losses will be reduced compared to a system with the total power scale converter. In addition, the cost of the power converter system is reduced. The DFIG system with a back-to-back converter is shown in Fig. 2.5[1].

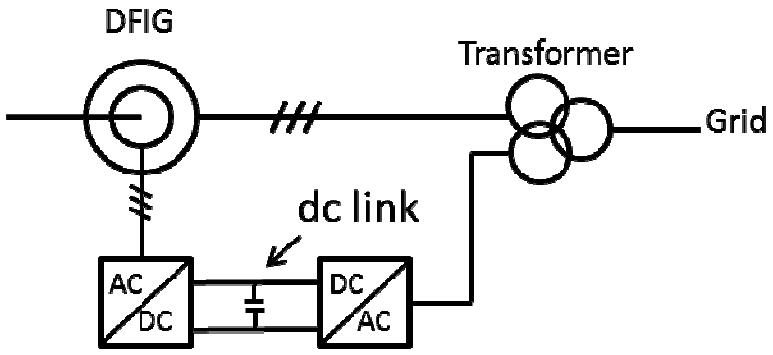


Figure 2.5 Schematic of a DFIG Wind Energy System with a Back-to-back Converter

The DFIG configuration allows a relatively wide range of rotor speed variations via the super-synchronous to sub-synchronous operation modes. In the super-synchronous mode,

the rotor speed is greater than the synchronous speed, and the generator provides the required energy from the mechanical energy for the rotor and the stator. While in the sub-synchronous mode, the rotor speed is less than the synchronous speed, the generator provides the energy to the stator from the rotor and the mechanical energy.

The back-to-back converter consists of two converters, i.e. rotor-side converter and grid-side converter, which are connected as “back-to-back”. Between the two converters, a dc link capacitor is connected to both side converters, in order to keep the voltage variations in the dc-link voltage small. The rotor-side converter makes it possible to control the torque or the speed of the generator and also the power factor at the stator terminals. The control objective for the grid-side converter is to keep the voltage of dc link constant. The DFIG can operate both in the motor mode and the generator mode, with a rotor-speed range of $\pm\Delta\omega_r^{max}$ around the synchronous speed. A typical speed-torque characteristics plot of the DFIG can be given as Fig. 2.6, where the $\omega_s$ is the synchronous speed of DFIG.

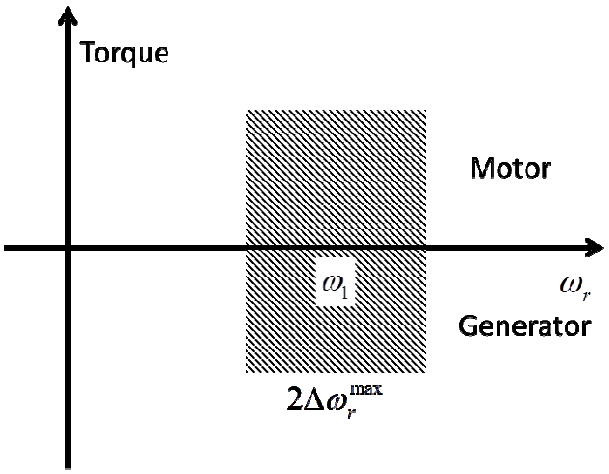


Figure 2.6 Speed-torque Characteristics of DFIG

DFIG is most commercial used for wind turbine industry, as mentioned earlier, for their limited speed range operation. Besides wind turbines application, the DFIG systems are also used in pumped storage power plants [31], stand-alone diesel systems [32], flywheel energy storage system [33], etc.

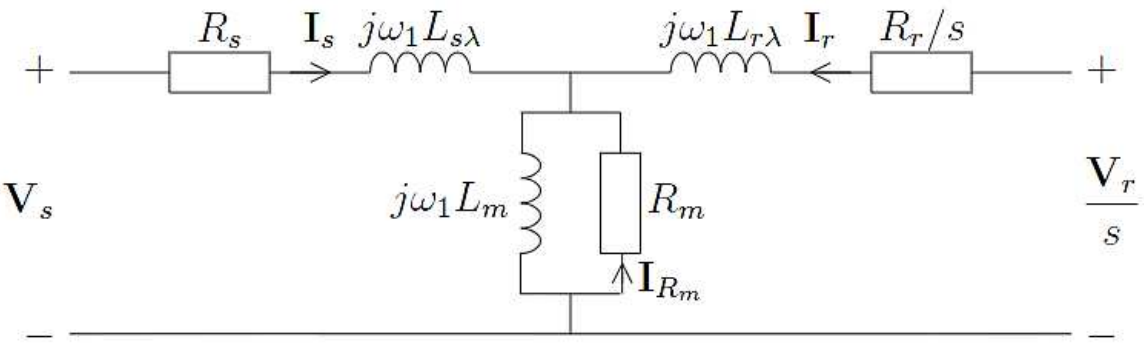


Figure 2.7 Equivalent Circuit of DFIG

As shown in Fig. 2.7,this equivalent circuit of DFIG is valid for one equivalent Y phase and for steady state calculations[1]. For Δ-connection, the equivalent Y representation of the generator can still be obtained via the Δ-Y transformation. Applying Kirchhoff voltage law to the circuit in Fig. 2.7, we can get,

$$V_s = R_s I_s + j\omega_1 L_{s\lambda} I_s + j\omega_1 L_m (I_s + I_r + I_{R_m}) \tag{2.6}$$

$$\frac{V_r}{s} = \frac{R_r}{s} I_r + j\omega_1 L_{r\lambda} I_r + j\omega_1 L_m (I_s + I_r + I_{R_m}) \tag{2.7}$$

$$0 = R_m I_{R_m} + j\omega_1 L_m (I_s + I_r + I_{R_m}) \tag{2.8}$$

where, $V_s$ and $V_r$ are the stator voltage and rotor voltage respectively; $R_s$, $R_r$ are the stator/rotor resistance; $R_m$ is magnetizing resistance, $L_{s\lambda}$, $L_{r\lambda}$ is stator/rotor leakage inductance; $L_m$ is magnetizing inductance; $I_s$, $I_r$ are the stator/rotor current; $I_{Rm}$ is magnetizing resistance current; $\omega_1$ is stator frequency and $s$ is slip. The slip s can be calculated by

$$s = \frac{\omega_1 - \omega_r}{\omega_1} = \frac{\omega_2}{\omega_1} \tag{2.9}$$

where the $\omega_r$ is rotor speed, $\omega_2$is the slip frequency. Equations (2.6) through (2.8) can be rewritten with the air-gap flux, stator flux and rotor flux, i.e.

$$V_s = R_s I_s + j\omega_1 \Psi_s \tag{2.10}$$

$$\frac{V_r}{s} = \frac{R_r}{s} I_r + j\omega_1 \Psi_r \tag{2.11}$$

$$0 = R_m I_{R_m} + j\omega_1 \Psi_m \tag{2.12}$$

where,

$$\Psi_m = L_m (I_s + I_r + I_{R_m}) \tag{2.13a}$$

$$\Psi_s = L_{s\lambda} I_s + L_m (I_s + I_r + I_{R_m}) = L_{s\lambda} I_s + \Psi_m \tag{2.13b}$$

$$\Psi_r = L_{r\lambda} I_r + L_m (I_s + I_r + I_{R_m}) = L_{r\lambda} I_r + \Psi_m \tag{2.13c}$$

The resistive losses of the induction generator are

$$P_{loss} = 3\left( R_s \left| I_s \right|^2 + R_r \left| I_r \right|^2 + R_m \left| I_{R_m} \right|^2 \right) \tag{2.14}$$

The electro-mechanical torque of the generator, $T_e$, can be calculated as

$$T_e = 3n \,\mathrm{Im}\left[ \Psi_s I_r^* \right] = 3n \,\mathrm{Im}\left[ \Psi_r I_s^* \right] \tag{2.15}$$

Where $n$ is the number of pole pairs.

## 2.3 Control of DFIG based Wind Turbine

In this section, different control method of DFIG based wind turbine system will be described. The DFIG based wind turbine has recently become the dominant choice for wind power industry [1, 22].A great advantage of DFIG based variable speed wind turbine is its voltage control capacity. The partial scale frequency converters in DFIG

enable the turbine to generate reactive power via delivering to the stator by the grid-side converter. However, the grid-side converter normally operates at unity power factor and does not exchange reactive power between the turbine and grid, with the only exception for the case of weak grid. As this study is focused on the power conversion in the region-2 operation, maximum active power conversion is assumed. As a simple treatment, the reactive load is not considered in the current stage of work. Therefore, the DFIG is controlled at the unity power factor and reactive power control is not considered.

Control of DFIG is more complicated when compared to a standard induction generator. The rotor current of the DFIG is controlled by an AC/DC/AC power electronic converter in the rotor circuit. The performance of a DFIG depends on the vector control applied to the generator and also which the orientation frame is chosen[34]. In[16][35], Leonhard introduces a vector control method which can be used to control the torque and excitation current independently. In [36], Pena *et al*. presents a detailed design of a grid connected DFIG with two back-to-back PWM converters. Their experimental validation shows that the vector control of the rotor-side converter provides wide speed-range operation as well as good speed tracking performance. The most common way of vector control for DFIG is based on PI control designed in a synchronous reference frame with the stator-flux [16, 36, 37, 38, 39, 40, 41] or stator-voltage orientation[42, 43]. In [39], the stator flux-oriented approach is presented for the control of both the active and the reactive power of the DFIG within variable speed range. In [41], a stator-flux orientation strategy is presented with the stator-flux vector is estimated based on the measurement of stator voltage and rotor current. Whereas in [40], the stator–flux vector position is estimated by adding a 90° delay to the stator voltage vector. In [44, 45], a direct power control

strategy using the stator flux-oriented approach is developed for a DFIG based wind power conversion system. The stator-voltage orientation is not the general choice for real and reactive power control for DFIG [34]. In [46, 47], the stator-voltage orientation approach is proposed to deal with unbalanced grid voltage condition. A comparison of real and reactive power control for DFIG based on stator-voltage orientation and stator-flux orientation for wind power system is presented in [34]. The simulation results conclude that both control methods have comparable performance.

In this research, the control strategy of the DFIG uses a vector control scheme based on the *d-q* synchronous reference frame. The stator flux vector is forced to control with *d*-axis of the synchronous frame in order to achieve decoupled control of the active and reactive powers.

In the *d-q* frame, the DFIG's electromagnetic torque $T_{em}$ can be expressed as

$$T_{em} = \frac{M}{L_s} p(\Phi_{ds} I_{qr} + \Phi_{qs} I_{dr}) \tag{2.25}$$

Where $p$ is the number of pole pairs. The mechanical power $P_m$ and the stator electric power output $P_S$ are

$$P_m = T_m \omega \tag{2.26}$$

$$P_s = T_{em} \omega_s \tag{2.27}$$

respectively, where $T_m$ is the mechanical torque applied to rotor. In this study, the field oriented control strategy adopted follows the scheme presented in [48, 49]. The control of DFIG in this research is consisting of two control loops. The inner loop is the rotor-flux control and the outer loop is the regulation of the stator-voltage magnitude. For the outer loop, the controlled outputs are stator voltages $V_{ds}$ and $V_{qs}$; while for the inner loop, the

controlled outputs are the rotor fluxes $\Phi_{dr}$ and $\Phi_{qr}$. The rotor and stator voltages can be expressed as function of rotor fluxes, and therefore the controls of the stator-voltage magnitude and the frequency are decoupled from $V_{ds}$'s dependence on $\Phi_{dr}$, and $V_{qs}$'s dependence on $\Phi_{qr}$.

In Region 2 of wind turbine system, the generator control deals mainly with the power conversion efficiency optimization. This is achieved by adjusting the rotor speed so that the optimum tip speed ratio is maintained. At this tip speed ratio, the power coefficient, $C_p$, is maximized. Thus the aerodynamic power captured by the rotor is maximized. The aerodynamic torque $T_{aero}$ is known to be

$$T_{aero} = \left( \frac{1}{2} \rho \pi R^5 \frac{C_{p\max}}{\lambda^2} \right) \omega^2 \tag{2.28}$$

where$\rho$ is the air density, $R$ is blade length, $C_{pmax}$ is maximum power coefficient, and $\lambda$ is the tip speed ratio. Based on this physical relationship, the demand of the generator torque $T_g$ is set to be proportional the square of rotor speed $\omega$, i.e.

$$T_g = k\omega^2 \tag{2.29}$$

where $k$ is the torque gain. The actual electrical power output, measured at the grid terminal, is compared with the reference power obtained from the product of the torque command and the rotor speed, and used to regulate the reference of the stator current $I_{ds}$ and $I_{qs}$. Following the DFIG control scheme described above, the rotor voltage is regulated and used to control the rotor side converters. Thus DFIG is controlled to follow the desired torque command of the wind turbine via the regulation of the $q$-axis current of the rotor.

The difficulty of the DFIG operation in a generating mode is from the disturbance derivative terms which are difficult to implement with the simulation [48]. In [48], the control variables are chosen as the rotor flux components of the machine in order to allow direct control over the rotor voltage. Compared to the rotor current inner loop method, this method allows minimum harmonics introduced by a nonlinear load, in our case, the turbulent wind speed.

## 2.4 Extremum Seeking Control

Extremum seeking control was first proposed by Leblanc's paper [50] in 1922, where ESC was applied to control of electric railways and became the original method of adaptive control. In 1951, Draper and Li provides details of extremum seeking control algorithm and its performance in English literature pape r[51] for the first time. This work gives solution to choose ignition timing to maximize power output of an internal combustion engine. Since this publication, internal combustion engine becomes a popular application for extremum seeking for a long time.

Adaptive control draws a significant interest in the mid 1950 with the strong driving force of flight control. Like all other forms of adaptive control, extremum seeking became very popular in 1950s and 1960s [52, 53]. Most work in the 1950s and 1960s focused on exploring extremum seeking performance for particular application and problems[54]. There's a lacking of clear definitions, a systematic analysis and design framework of extremum seeking algorithm. In 1980, Stern by [55] provides a useful survey paper of extremum seeking control. Astrom and Wittenmark [56] describe the extremum control as the most promising areas for adaptive control, consider it far from mature.

Wang and Krstić's [57] provide the first rigorous proof of the stability of an extremum seeking feedback scheme was provided by employing the tools of averaging and singular perturbation analysis. This proof allows the plant to be a general nonlinear dynamic system is more general scheme in which the plant is considered as a static nonlinear map in previous extremum seeking result. Krstić adds a dynamic compensator to the integrator in the Extremum seeking algorithm in [58]. This compensator is more effective in accounting for the plant dynamics than previously more often used phase shifting of the demodulation signal, and provides stability guarantees and fast tracking of plant operating condition variations for single parameter extremum seeking. After the publication of [57][58], extremum seeking witnessed a resurgence of interest.

Rotea [59] and Walsh [60] appeared to be the first to study multivariable extremum seeking algorithm. Rotea proposes a simple model for stability and performance calculation of multi-parameter extremum seeking algorithms in [59]. This model guarantees stability and performance even when measurement of the system is corrupted by noise or additional process dynamics. A systematic approach for the analysis of extremum seeking algorithms is also been provided in this work. Walsh provides a new control law for multi-parameter set-points and a proof of exponential stability for the averages system[60]. However, their results are limited for plants with constant parameters and the stability criteria requires use of slow forcing and consequent slow convergence for strictly proper output dynamics. In [61, 62], multivariable extremum seeking scheme is first applied to systems with general time-varying parameters by Ariyur and Krstic. A SISO format is used to derive a stability test and a systematic design algorithm is provided to satisfy the stability test based on standard LTI control

techniques. This work supplies an analytical quantification of the level of design difficulties and removes the adaptation speed limitation for plants with strictly proper output dynamics in earlier works.

The applications of extremum seeking for maximum wind power capture is investigated by Creaby and Li in [20]. A multivariable extremum seeking control is used to control torque and pitch angle based on only measurement of the rotor power. The simulation is tested under field recorded wind speed conditions and the results demonstrated significant improvement in energy capture compared to the standard control methods.

## 2.5 Review of Robust Control of Wind Turbine

Although the classical control methods are traditionally applied for wind turbine controls, they cannot assure the robustness and the performance of the system at the same time, especially with associated uncertainties in the model. During latest two decades, $\mathcal{H}_\infty$ control is introduced to control of wind energy conversion system and been proven successful for guaranteeing closed loop performance and robustness against plant uncertainties. Connor first applied $\mathcal{H}_\infty$ control method in wind turbine control in 1992 [63]. In his work, a $\mathcal{H}\infty$ controller is applied to reduces fatigue damage of a wind turbine and maintain the system to be robust. In [38], Bongers proposes the synthesis of low order $\mathcal{H}_\infty$ controllers in control design of a flexible wind turbine. In this work, a set of linear models of nominal model is discussed. The developed controller is tested to be stable with a set of linear models which represent the wind turbine under various operating condition. He continued this work on designing a $\mathcal{H}_\infty$ controller for variable-speed wind turbine system for load reduction in [37]. The $\mathcal{H}_\infty$ controller is applied for

reduction rotor shaft torque variations under model uncertainties without excessive variations in DC-current, generator speed or delay angle. In 2003, Rocha presents a multivariable controller for wind energy conversion system [62]. Pitch angle and generator torque are adjusted aiming to maximum energy conversion and the reduction of detrimental loads. A multivariable $\mathcal{H}_\infty$ controller is applied with weighting compensators are specified with considering rotor speed regulation, load reduction of mechanical stress and system stability. In [61], Rocha compares performance between multivariable controllers for wind energy conversion system designed using $\mathcal{H}_2$and $\mathcal{H}_\infty$ methodologies.

In the simulation, the $\mathcal{H}_\infty$ controller performs more conservative and more robust compared to $\mathcal{H}_2$ controller. However, $\mathcal{H}_2$ controller has a faster dynamic response than $\mathcal{H}_\infty$ methodology.

In this work, we consider the control for converting rotor power to electrical power is not independent from the rotor power control. With the broad-spectrum nature of the turbulent wind, the rotor power is determined by both the wind characteristics and the rotor controllers. Therefore, for the DFIG controller to be designed, the performance specifications for power conversion need to cover appropriate and width so as to capture the dominant frequency components of the rotor power. Meanwhile, the designed controller needs to be robust against the variations in system parameters such as winding resistance/inductance and frequency. Such control can be well dealt with by the $\mathcal{H}_\infty$ control method.

## 2.6 Wind Turbine Inter-region Controls

Generally, the control of variable-speed variable-pitch turbine consists of two controllers: a generator controller with a power versus rotor speed reference in Region 2 and a blade pitch controller with a PI controller to regulate the rotor speed during Region 3 operation [22, 23]. The two controllers are designed to operate independently and the transition between regions can cause problems such as power flickers and fatigue loads etc. [9, 64].

The generator controller can be designed with the power set-point for the generator as a tabulated function of the generator speed [23]. The speed signal input is the low-pass filtered RPM signal of the generator. The blade pitch controller is a PI controller with the input of the generator speed and the output is the pitch servo set-point. As in the Region 2 operation, the generator may not operate at its maximum power point. When the turbine is accelerated to above the rated speed for higher wind, the generator power is kept at a constant rated value. Then the generator torque can no longer regulate the rotor speed, and the pitch controller will start to reduce the mechanical load of the turbine and maintain the rotor speed.

A more advanced control of variable speed turbine is that in Region 2 operation, the rotor speed can be adjusted in proportion to the wind speed so that the optimum TSR is maintained [22]. At this TSR, the power coefficient $C_p$ is maximized. Once the rated torque is reached, the turbine will start to speed up as the load torque no further increase. Pitch control is then used to regulate the rotor speed, with the load torque held constant. Thus the control switches from Region 2 generator control to Region 3 pitch control.

To improve the transition during the switch between Region 2 to Region 3, it is worthwhile to introduce Region 2.5 [65]. In Region 2, the controller provides rotor torque

less than the rated, when turbine reaches the rated speed. Because Region 3 requires turbine operates at the rated power, the torque reference is set to be at the rated torque. Therefore, a bump occurs at the generator toque reference when switching between Regions 2 and 3. The Region 2.5 control is thus introduced to increase the generator torque to regulate the rotor speed instead of maintaining the torque at the optimal power point operation. The switching point between the Region 2 to Region 2.5 can be determined by the rotor speed. The controllers provide optimal TSR control under the rated rotor speed and regulate the rotor speed with generator torque to maintain the rated rotor speed. The switching point between the Region 2.5 to Region 3 is set as the generator torque reaching the rated value, thus the controller will switch from torque control to pitch control. In[65], the Region 2.5 is defined as a straight line in the torque-rotor-speed plot with a 5%slip. The high slip is chosen to prevent excessive torque oscillations during switching. Although the above approach provides a solution to reducing the bump during switching, there is no design guideline for the torque slip and no guarantee the bump is minimized. In [66], a trajectory tracking Region 2.5 control approach is presented based on the utilization of LiDAR wind preview measurements to smooth transitions. The main drawback of this method includes elaborate optimization effort to generate the reference trajectory and the extra cost of adding LiDAR wind speed measurement.

## 2.7 Bumpless Transfer Control

It is well known that transients will occur when switching between different controllers happens. These transients can lead to unacceptable system behavior, and arise out of discontinuity both in system states and controllers output. In most malicious situations,

the bump produced by controller switching can lead to instability when switch occurs. As can be seen from the previous sections, the wind turbine has three control regions, and the controller need to switching between region 2 and 3 during operation. Bumpless transfer technique [67, 68, 69] can be introduced to smooth the transition during wind turbine inter-region operation.

It is often happened in industry when the input of a controlled system is temporarily different from the output. The two main reasons to cause this discrepancy are limitations and substitutions. Limitations are generally caused by saturation on the system applied, for instance the physical limits of the actuator[70], and this phenomena is also called windup. A common approach to reducing this adverse impact is adding an extra compensator. This method is also referred as anti-windup [50, 59, 60, 71]. Substitutions occur when switching between two controllers for example, switching from manual to automatic control. In the case of substitution, the mismatch of the inputs can significantly deteriorate the expected system response, which is called bump transfer[70, 72]. A bumpless transfer can be achieved by modifying the controller states so as to minimize the switching induced bump. Since both substitutions and limitations cause control performance to deteriorate by involving the inadequacy of the controller state, these two phenomena can be treated in a similar manner[70, 73].

In[55], Hanus gives a solution of bumpless transfer to prevent nonlinearities by restore the consistency of the controller states. In [73], an generalized anti-windup observer is introduced into controller structure to deal with windup phenomena by Astrom and Wittenmark. The Conditioning Technique, proposed by Hanus in [55, 70, 72], corrects the off-line controller states to those of the online controller via synthesizing a ‘realisable

reference’ signal. The Conditioning Technique is considered as a special case of the generalized anti-windup compensator approach when the controller is linear and it can be applied to wider applications including nonlinear controllers and cascaded controllers[74].

The linear quadratic bumpless transfer was first introduced in [75]. The main idea of this approach is the introduction of a static feedback matrix, F, as referred as ‘bumpless transfer compensator’. This matrix F drives the offline controller so that its output match the online controller output. Then in [76], Turner adds a low-pass filter in the output vector of matrix F to ensure a smooth transition during the controller switching. This method makes can be applied to a great deal of applications with the use of two constant weighting matrices to adjust for different control objectives.

In this research, a switching scheme is proposed for wind turbine power fluctuation reduction with two different approaches. The first is to adopt the conditioned transfer method [77], which is introduced to improve the tracking performance of bumpless transfer based on conditioning technique. The second approach is applied LQ theory to the Bumpless transfer problem[69, 75]. The LQ bumpless transfer has the advantage of its static matrix which enables little extra on-line computation.

# 3. Wind Turbine System Control Simulation

Simulation model are important for component study and control development. Without appropriate modeling and simulation study, the developed controller could lead to an unsatisfactory control performance with low power capture or even failure in power conversion on the turbine. Therefore dynamic modeling and simulation study is essential for control design of wind turbine systems.

In this chapter, we will describe the software packages used in this research for wind turbine control simulation. The main wind turbine simulation codes in this study is FAST[78], AeroDyn [79] and TurbSim [80], developed by National Renewable Energy Laboratory (NREL). NREL is the leader in developing codes in the U.S. and offers the public a variety of wind turbine modeling tools. The DFIG model is simulated by SimPowerSystems™ 5.2.1 developed by Mathworks. This study presents highly multi-physical domains of simulation, ranging from aerodynamics to power electronics. The interaction among the three simulation codes is describing in Figure 3.1.

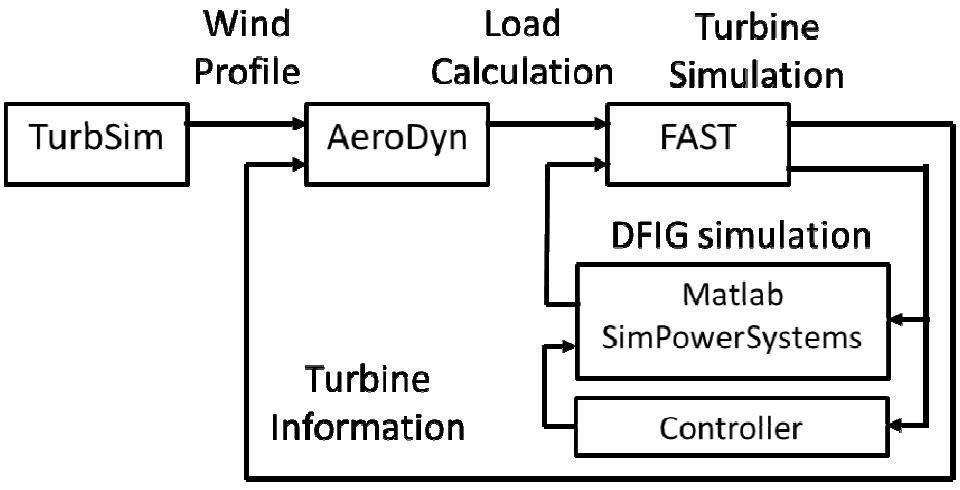


Figure 3.1 Block Diagram of Simulation Code Interaction

## 3.1 FAST Simulation Platform for Wind Turbine Simulation

In this thesis study, the dynamic modeling and simulation of the wind turbine is performed using NREL's FAST software [78]. Developed by the National Wind Technology Center (NWTC), FAST is an aeroelastic design code for two- or three-bladed HAWT design. FAST set up the equations of motion (EOM) using the Kane's method [81, 82, 83]and solvevia numerical integration scheme. Based on the definition of partial velocities, the Kane's method can be considered as an automated process for setting up the EOM's. A minimal set of dynamics equations will be obtained, in which dispensable reaction forces and torques are not included. The implemented method eliminates the need for separate constraint equations by using the generalized coordinates.

In FAST, the wind turbine is modeled as a combination of rigid and flexible bodies. For example, the model of a two-bladed, teetering-hub turbine, as shown in Figure 3.2,isconsist of four flexible bodies and four rigid ones. The rigid bodies include the earth (or foundation), nacelle, hub, and optional tip brakes (point masses), while the flexible bodies contain blades, tower, and drive shaft. The connections of these bodies have multiple degrees of freedom (DOF), such as tower bending, blade bending, nacelle yaw, rotor teeter, rotor speed, and torsional flexibility of the drive shaft. The flexible blades include two flapwise modes and one edgewise mode per blade. The flexible tower allows two modes each in the fore-aft and side-to-side directions. These DOF can be turn on or off individually in the analysis by adding a switch in the input file.

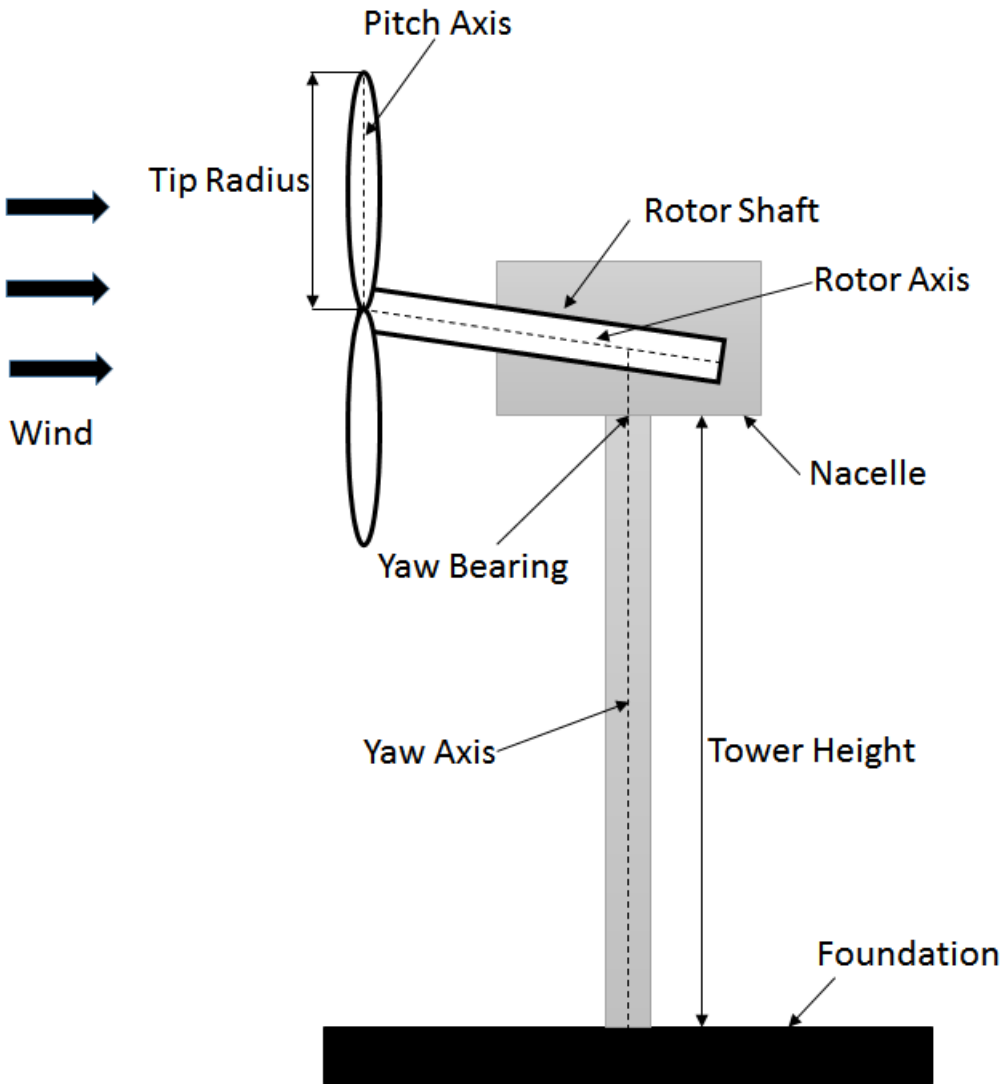


Figure 3.2 Layout of Conventional, Upwind, Three Blade Turbines

AeroDyn is used along-side FAST to simulate aerodynamic forces on the turbine blades. Simulink®[84] is a dynamics and controls simulation tool incorporated with Matlab®[85] that allows the use of S-function with custom Fortran routines. The FAST subroutines have been connected with a Matlab standard gateway subroutine in order to call the FAST EOM's in an S-Function that can be used in a Matlab Simulink model. The advantage is that the simulation of wind turbine allows great flexibility in controls implementation. For example, generator torque control, nacelle yaw control as well as

pitch control can be designed in the Simulink environment while the simulation still take the advantage of FAST with the entire nonlinear aeroelastic wind turbine EOM. Figure 3.3 shows an example of Simulink block for FAST based wind turbine model that takes yaw, pitch and generator torque as inputs. There are hundreds of output measurements available in FAST. The variables of interest in this study include pitch angle, generator torque, yaw angle, rotor speed, rotor power, wind speed, and wind direction.

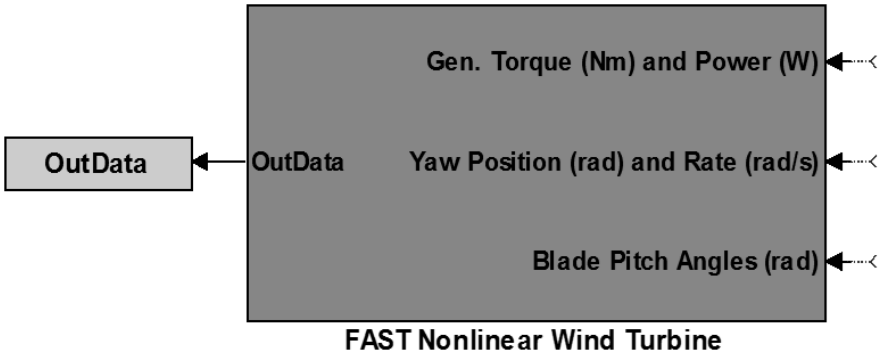


Figure 3.3 Example of Wind Turbine Block for Use with Simulink

In 2005, NREL announced that FAST can be used for worldwide turbine certification[86]. Another code which is used for turbine certification is ADAMS (Automatic Dynamic Analysis of Mechanical Systems) [87]. ADAMS has the ability to model unlimited degrees of freedom and is considered very accurate. One disadvantage is the large effort and extended computing time needed to model a wind turbine. Results from FAST models have been shown to correlate well with those from more complex ADAMS models [88]. The version of FAST used in this thesis work is v6.01.

## 3.2 AeroDyn

AeroDyn[79], developed by Windward Engineering, is an element level simulation code for aerodynamics analysis of HAWT. It takes wind speed trajectories and calculates the

aerodynamic loads on wind turbine blade elements. AeroDyn presents two models for computing the effect of wind turbine wakes: the blade element momentum(BEM) theory and the generalized dynamic-wake (GDW) theory [89].

The BEM theory is the widely adopted by most wind turbine designers, while the GDW theory is a more recent modeling technique for modeling skewed and unsteady wake dynamics [90]. The BEM theory is composed of the blade element theory and the momentum theory[89]. In the blade element theory, blades are assumed to be divided into infinite small pieces that act independently of the surroundings and operate aerodynamically as two-dimensional airfoils of which the computation of aerodynamic forces can be analyzed with local flow conditions. These elemental forces are summed across the blade to compute the total forces and moments of the turbine. The momentum theory points out that the loss of pressure or momentum in the rotor plane is induced by the airflow passing through the rotor plane on the blade elements. According to the momentum theory, the induced velocities can be calculated from the momentum lost in the flow in the axial and tangential directions. These induced velocities influence the inflow in the rotor plane and consequently also make impacts on the forces calculated by blade element theory. These two theories constitute the BEM theory and proposes an iterative process to compute the aerodynamic forces and also the induced velocities near the rotor [79, 89].

In practice, the BEM theory is implemented by breaking the wind turbine blades into infinite small elements along the span. Rotation of these elements in the rotor plane forms annular regions, as demonstrated in Figure 3.4 [91], across which the momentum balance holds. These annular regions are also used to analysis the change of the local flow

velocity at the rotor plane caused by induced velocities from the wake. BEM allows analyzing stream tubes across the rotor disk, which is smaller than the annular regions and with more computational fidelity. However, AeroDyn only computes annular regions. When using the BEM theory, various corrections can be chosen by the user, including incorporating the aerodynamic effects of tip losses, hub losses, and skewed wakes.

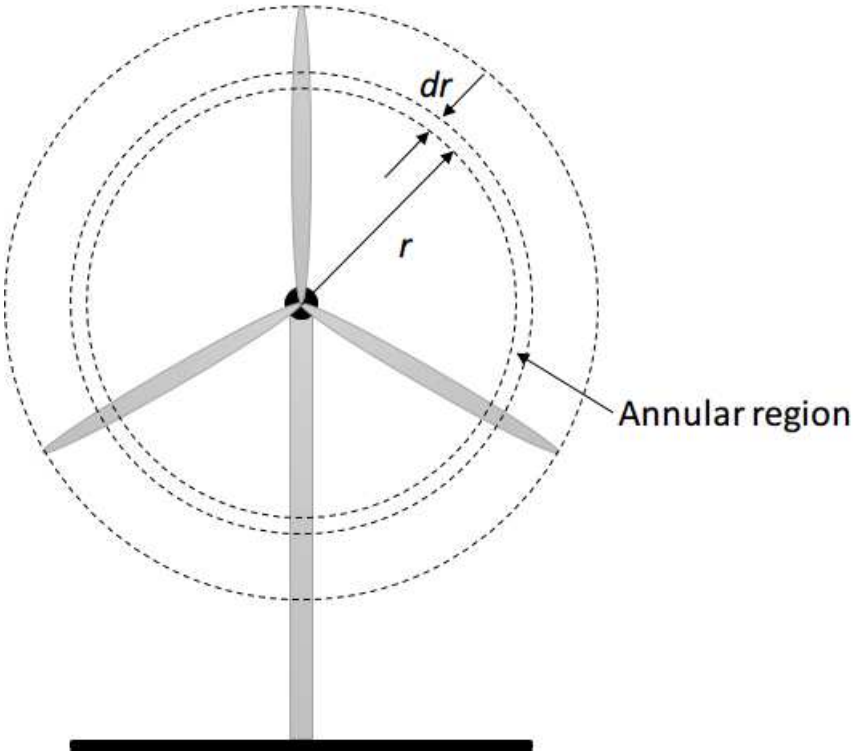


Figure 3.4 Incremental Annulus in Rotor Plane for the BEM Analysis

The GDW model of AeroDyn is developed on the base of Peters and He's work [92, 93] and the implementation is using Suzuki' code[94]in his Ph.D. dissertation at the University of Utah. The GDW theory was developed as an intermediate level unsteady induced-flow theory suitable for rotorcraft aeroelastic stability, vibration, control, and aeroelastic tailoring studies. It was developed because previous rotorcraft aeroelasticity and aeromechanics analysis models were either too simple to capture necessary physical

reality or too involved to carry out any system eigenvalue analysis or system design. This model, also called as *acceleration potential method*, was originally introduced for the helicopter design. Suzuki[95] modified the GDW theory for use with wind turbine rotor applications and implemented it in the YawDyn/AeroDyn codes for wind turbine dynamics simulations. Compared with the BEM theory, a benefit of this method is that it enables a more general distribution of pressure across a rotor plane. The GDW model, developed based on *Pitt and Peters's Model*[96], allows more flow states and a fully nonlinear implementation to calculate turbulence and spatial variation of the inflow. Pitt and Peters[96]developed the dynamic inflow theory which is used for the majority of flight dynamics models of single rotor helicopters.

AeroDyn can be interfaced with dynamics analysis software packages such as YawDyn, FAST and ADAMS. The AeroDyn code takes information about the wind turbine from the dynamics analysis routine (in this case, FAST) and returns the aerodynamic loads for each blade element to the dynamics routine. AeroDyn allows variable formats of wind input, including single-point hub-height wind files and multiple-point turbulent wind.

AeroDyn provides FAST with data such as tower shadow, the hub height, air density and detailed information about the blade elements. During simulation, AeroDyn takes wind data from TurbSim and turbine information, such as rotor speed, tower bending and blade bending, from FAST to calculate the aerodynamic loading. Detailed wind input files with full field turbulence can be created with codes like TurbSim or simple uniform wind files, or manually using a standard text editor. In this study, the simple steady wind profiles were created manually using a text editor, while TurbSim was used to generate turbulent wind profiles. The version of AeroDyn used in this thesis work is v12.58.

## 3.3 TurbSim for Wind Simulation

TurbSim [80] is a simulation code that creates a three dimensional rectangular grid of stochastic, full field turbulent wind. This wind file can then be used as input to AeroDyn and FAST. The TurbSim input file allows the user to specify options from a number of different areas such as runtime options, turbine/model specifications, meteorological boundary conditions, coherent turbulence scaling parameters and spectral modes.

Runtime options allow the user to select a random seed and type of random number generator [80]. The next eight lines of the input file include options for the type of output file and the final line selects whether the turbine rotates clockwise or counterclockwise.

Turbine/model specifications allows the user to specify the number of points in the rectangular grid, the size of time step, the size of grid, the hub height of the turbine being modeled, the desired analysis time and also angles of wind flow [80]. Figure 3.5shows three different scenarios about how the rotor is placed in the grid. It is automatically centered at the top of the grid. The grid needs to be large enough so that no part of any blade lies outside the grid. AeroDyn automatically checks these criteria before running. The number of grid points is determined by the user. Adding more points requires larger size of memory to construct the matrix of wind data. The default size is thirteen by thirteen grid points[80].

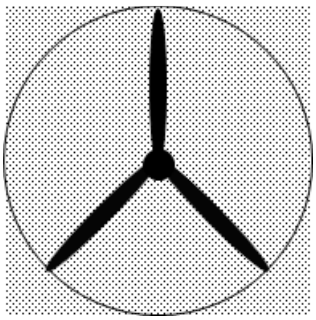

Figure 3.5a: Grid and Rotor Placement when Height equal to Width

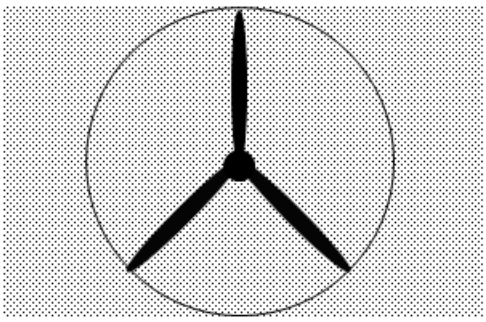

Figure 3.5b: Grid and Rotor Placement when Height smaller than Width

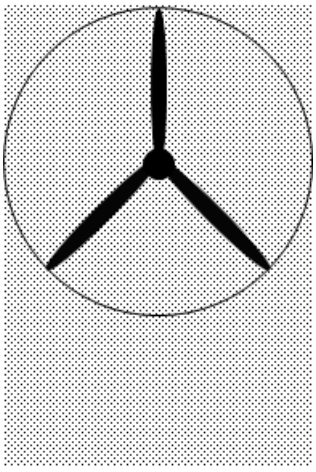

Figure 3.5c: Grid and Rotor Placement when Height larger than Width

Figure 3.5 Grid and Rotor Placement in Different Scenarios

Meteorological boundary conditions define the turbulence spectrum model such as von Karman, and Kaimal among others. It defines the turbulence intensity, the mean wind speed, the reference height, the power law exponent and the surface roughness. Non-IEC meteorological boundary conditions are used when turbulence models other than von Karman or Kaimal are used. Parameters such as latitude, gradient Richardson number, shear velocity, mixing layer depth and component coherence can be selected here. Many these parameters are chosen to be the default values in this study except the Richardson number.

When the gradient Richardson number is greater than -0.05 and the option of creating coherent turbulence time-step files is set to be true, the coherent turbulence scaling parameters will be used with non-IEC spectral models. Empirical values are used to calculate when and how coherent events should be added to the background turbulence. These values create a coherent turbulence time step file that sends to AeroDyn.

When the output file is created, a summary file is also created. AeroDyn needs both files because the summary file provides the interpretation of the data in the output file. Setup of a TurbSim wind file is described in the next section. The version of TurbSim used in this thesis work is v1.30.

## 3.4 Summary

In this chapter, the basics of the simulation packages used in this research are described. The dynamic modeling and simulation is essential for control study and design. Simulation packages for wind turbine are developed by NREL. FAST takes the loading information which calculated with TurbSim and applies it to the nonlinear wind turbine model to solve for the relevant equations of motion. TurbSim is used for aerodynamic load analysis on the turbine. AeroDyn is used for generating wind profile which will be the input of TurbSim.

# 4. Modeling of DFIG Based Wind Power System

As described in Chapter 1, one research problem for this thesis study is to develop a self-optimizing robust control for maximizing the energy capture for a DFIG based wind turbine. To realize the proposed controller design, it is critical to have a control oriented dynamic model for the DFIG wind energy system. In this chapter, a DFIG model is derived with moderate simplification, following the work by Belfedal *et al*. **[49]**.

## 4.1. DFIG Modeling

Figure 4.1 shows the schematic of a DFIG system with a back-to-back converter and its equivalent circuit. From the reviews in Chapter 2, the dynamics of a DFIG system can be typically modeled in the field synchronous reference frame [48, 49, 97] by

$$V_{ds} = R_s I_{ds} + \frac{d\Phi_{ds}}{dt} - \omega_s \Phi_{qs} \tag{4.1}$$

$$V_{qs} = R_s I_{qs} + \frac{d\Phi_{qs}}{dt} + \omega_s \Phi_{ds} \tag{4.2}$$

$$V_{dr} = R_r I_{dr} + \frac{d\Phi_{dr}}{dt} - \omega_r \Phi_{qr} \tag{4.3}$$

$$V_{qr} = R_r I_{qr} + \frac{d\Phi_{qr}}{dt} + \omega_r \Phi_{dr} \tag{4.4}$$

where the flux is calculated as

$$\Phi_{ds} = L_s I_{ds} + M I_{dr} \tag{4.5}$$

$$\Phi_{qs} = L_s I_{qs} + M I_{qr} \tag{4.6}$$

$$\Phi_{dr} = L_r I_{dr} + M I_{ds} \tag{4.7}$$

$$\Phi_{qr} = L_r I_{qr} + M I_{qs} \tag{4.8}$$

where subscripts *'d', 'q', 's', 'r'* denote the *d*-axis component, *q*-axis component, stator and rotor, respectively, $I, \Phi, V, R, L$ and $M$ represent the current, flux, voltages, phase resistance, cyclic inductance and cyclic mutual inductance, respectively. The electrical rotor frequency $\omega_r$ should be the difference between the synchronous speed $\omega_s$ and the rotor speed $\omega$. The leakage inductances are not considered.

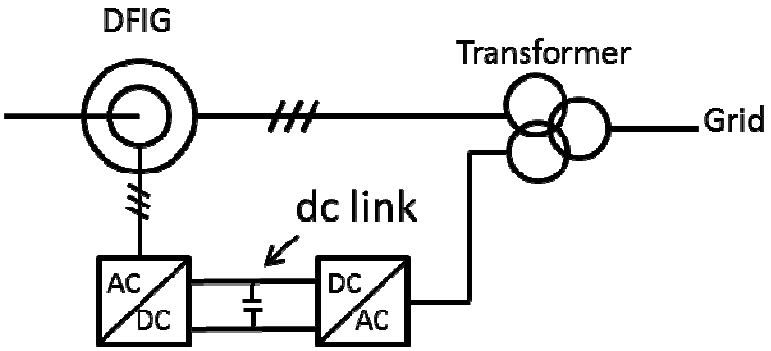


a) Schematic Diagram

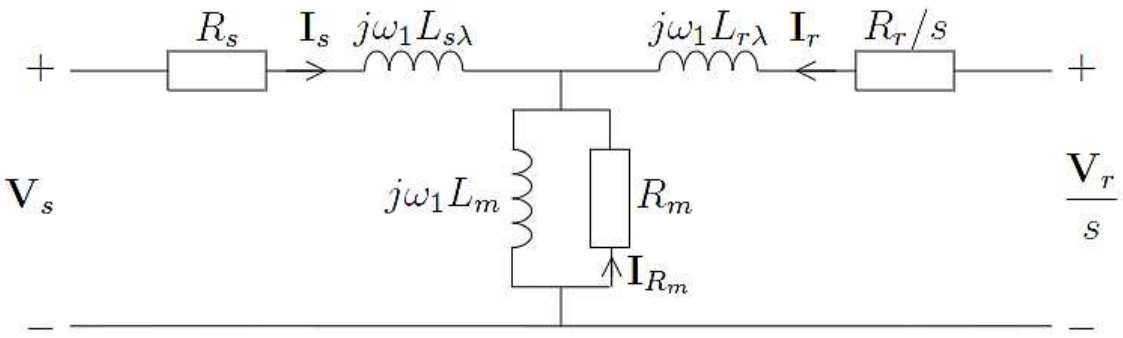


b) Equivalent Circuit

Figure 4.1 Description for DFIG System in WECS

The DFIG model in a state-space representation[49] can be simplified as

$$\begin{bmatrix} \dot{\Phi}_{dr} \\ \dot{\Phi}_{qr} \end{bmatrix} = [A_s] \begin{bmatrix} \Phi_{dr} \\ \Phi_{qr} \end{bmatrix} + [B_{s1}] \begin{bmatrix} I_{ds} \\ I_{qs} \end{bmatrix} + [B_{s2}] \begin{bmatrix} V_{dr} \\ V_{qr} \end{bmatrix} \tag{4.9a}$$

$$\begin{bmatrix} V_{ds} \\ V_{qs} \end{bmatrix} = [C_s] \begin{bmatrix} \Phi_{dr} \\ \Phi_{qr} \end{bmatrix} + [D_{s1}] \begin{bmatrix} I_{ds} \\ I_{qs} \end{bmatrix} + [D_{s2}] \begin{bmatrix} V_{dr} \\ V_{qr} \end{bmatrix} \tag{4.9b}$$

where,

$$[A_s] = \begin{bmatrix} -\frac{R_r}{L_r} & \omega_r \\ -\omega_r & -\frac{R_r}{L_r} \end{bmatrix} \tag{4.10 a}$$

$$[B_{s1}] = \begin{bmatrix} \frac{R_r M}{L_r} & 0 \\ 0 & \frac{R_r M}{L_r} \end{bmatrix}, [B_{s2}] = \begin{bmatrix} 1 & 0 \\ 0 & 1 \end{bmatrix} \tag{4.10c}$$

$$[C_s] = \begin{bmatrix} -\frac{MR_r}{L_r^2} & -\frac{M}{L_r}\omega \\ -\frac{M}{L_r}\omega & \frac{MR_r}{L_r^2} \end{bmatrix} \tag{4.10d}$$

$$[D_{s1}] = \begin{bmatrix} R_s + (\frac{\mathrm{M}^2 R_r}{L_r^2}) & -\sigma L_s \omega_s \\ \sigma L_s \omega_s & R_s + (\frac{\mathrm{M}^2 R_r}{L_r^2}) \end{bmatrix}, [D_{s2}] = \begin{bmatrix} 1 & 0 \\ 0 & 1 \end{bmatrix} \tag{4.10e}$$

This state-space model of DFIG is derived by forcing the derivatives of stator currents to zero, i.e. assuming that $I_{ds}$ and $I_{qs}$ are constant in the field synchronous reference frame. The stator transients are neglected with the following assumptions: 1) the magnetic saturation is neglected, 2) the flux distribution is sinusoidal, and 3) losses except copper losses are all neglected and stator voltages and currents are sinusoids of the fundamental frequency. Also, the voltage source converters at the rotor side are modeled as current sources and rotor voltages and currents are sinusoids of the slip frequency. These assumptions avoid the elaboration of dealing with the insignificant fast dynamics in a full converter model simulation for better computational efficiency, meanwhile achieving acceptable simulation accuracy. The resultant state-space model [49] is then

$$[\dot{X}] = [A_s]X + [B_s]U \tag{4.11a}$$

$$[Y] = [C_s]X + [D_s]U \tag{4.11b}$$

where $[B_s] = \begin{bmatrix}[B_{s1}] & [B_{s2}]\end{bmatrix}$, $[D_s] = \begin{bmatrix}[D_{s1}] & [D_{s2}]\end{bmatrix}$, $X = [\Phi_{dr} \quad \Phi_{qr}]^T$ is the state vector, $Y = [V_{ds} \quad V_{qs}]^T$, is the output vector, and $U = \begin{bmatrix} I_{ds} & I_{qs} & V_{dr} & V_{qr} \end{bmatrix}^T$ is the control input vector.

## 4.2. Modeling of Power Electronics Converters

The power converters used in DFIG based wind power systems consist of a back-to-back converter connecting the rotor circuit and the grid, as shown in Fig. 4.2. The converters are typically made up of voltage/current regulating inverters to realize bidirectional power flow. The two power electronic converters are connected through the so-called DC link capacitor in order to keep the voltage variations in the dc-link voltage small.

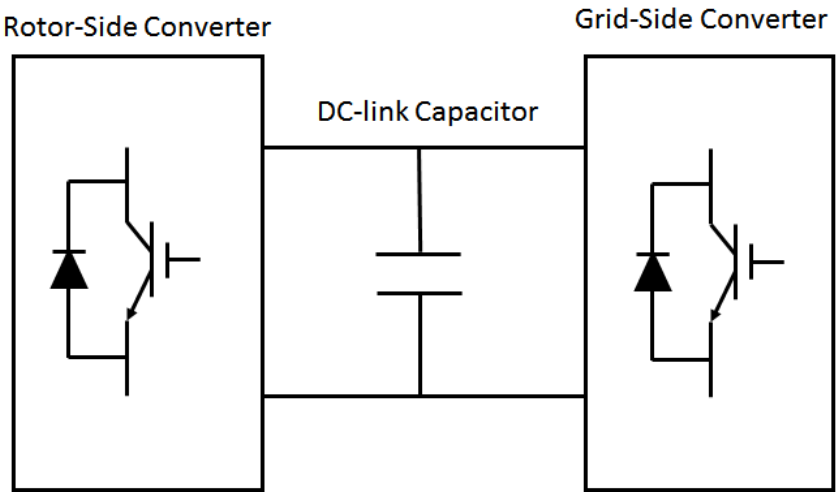


Figure 4.2 Power Converters in DFIG Wind Turbine

### 4.2.1 Rotor-side Converter

One characteristic of DFIG is that the power rating of the rotor-side converter is selected to meet the requirement of the maximum slip power and the reactive power control capability. The rotor-side converter is treated as a current controlled voltage-source converter. The most general adopted rotor current control scheme for the rotor-side converter is proposed in [32, 36] . The actuation and control of rotor-side converter are dependent on the measurement of the stator and the rotor currents, the stator voltage and the rotor position.

A typical rotor-side converter controller can be a Proportional-Integral (PI) controller to eliminate the power error in steady state. The output of the PI regulator is the reference rotor current that should be injected into the rotor by the rotor-side converter and used to produce the electromagnetic torque. The actual rotor current measured is project onto the *d-q* components. The *q* component current is compared to the reference value and sent to current PI regulator. The output is the *q* component voltage generated by the rotor-side converter.

### 4.2.2 Grid-side Converter

The control objective of the grid-side converter is to maintain the dc link voltage at a predefined value despite the magnitude and direction of the rotor power [36]. The power rating of the grid-side converter is decided by the maximum slip power for the reason that it typically operates at a unity power factor. The grid-side converter also allows grid reactive power support during a grid fault.

For the grid-side converter, applying the Kirkhoff Voltage Law for the *d-q* components yields

$$V_{gd} = R_g i_{gd} + L_g \frac{di_{gd}}{dt} - \omega_e L_g i_{gq} + V_{cd} \tag{4.12a}$$

$$V_{gq} = R i_{gq} + L_g \frac{di_{gq}}{dt} + \omega_e L_g i_{gd} + V_{cq} \tag{4.12b}$$

where $R_g$ and $L_g$ are the grid filter resistance and reactance, respectively; $i_{gd}$ and $i_{gq}$ are the grid currents for *d* and *q* coordinates, respectively; $V_{gd}$ and $V_{gq}$ are the grid voltages for *d* and *q* coordinates, respectively; $V_{cd}$ and $V_{cq}$ are the converter voltages for *d* and *q* coordinates, respectively, and $\omega_e$ is the grid frequency.

The control scheme of the grid-side converter is shown as Fig. 4.3. There are two control loops: the *d* component current regulation consisting of the dc voltage regulator and the current regulator. The dc capacitor voltage is measured and compared with the reference dc voltage, and their difference is sent to the dc voltage regulator. The output is the *d* component reference current. The *d-q* current regulation is implemented to apply a current regulator. The *d* and *q* components of the grid-side current is measured and compared with the *d* component of the current reference produced by the dc voltage regulation, and specified *q* component reference current. From this, the current regulator controls the magnitude and phase of the voltage provided by the grid side converter. Notice that the maximum value of the current is limited to the converter maximum power at the nominal voltage. Under conditions when neither the active nor the reactive power can be reached without exceeding of the current limit, the converter control will make the reactive current to be the priority. Under such circumstance, the *q* component current will be reduced in order to bring back to its maximum value.

Base on the above analysis, the simulation model of the grid-side converter control system can be developed in Simulink®, whose layout is shown in Fig. 4.4 [98]. The bipolar transistor PWM inverters are chosen with the maximum switching frequency of 1 kHz. With the use of IGBT converters, a higher switching frequency is allowed for implementation of the proposed control strategy. The DC-link voltage is regulated with the grid-side converter operating at a modulation depth of 0.75. This will allow sufficient latitude to prevent over modulation during transients.

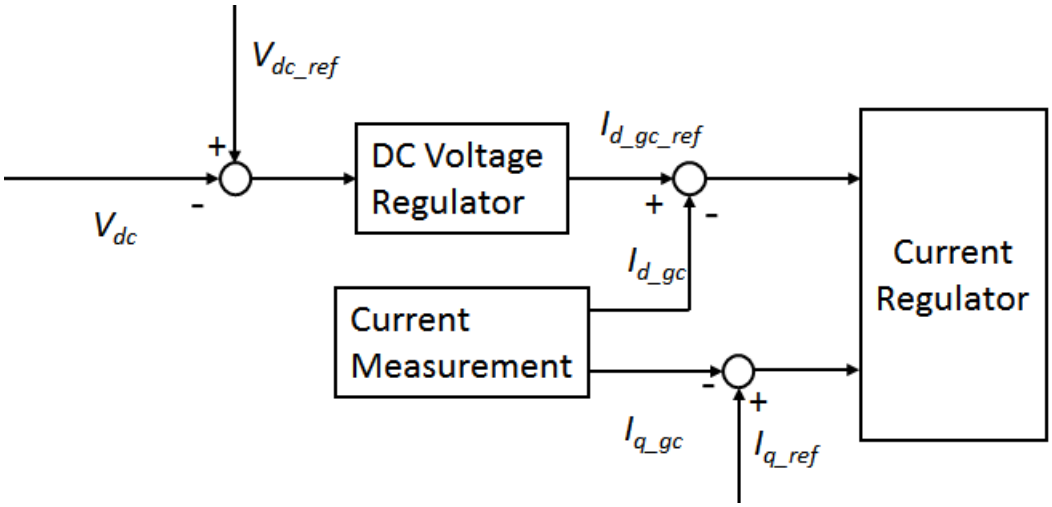


Figure 4.3 Block Diagram of Grid-side Converter Control System

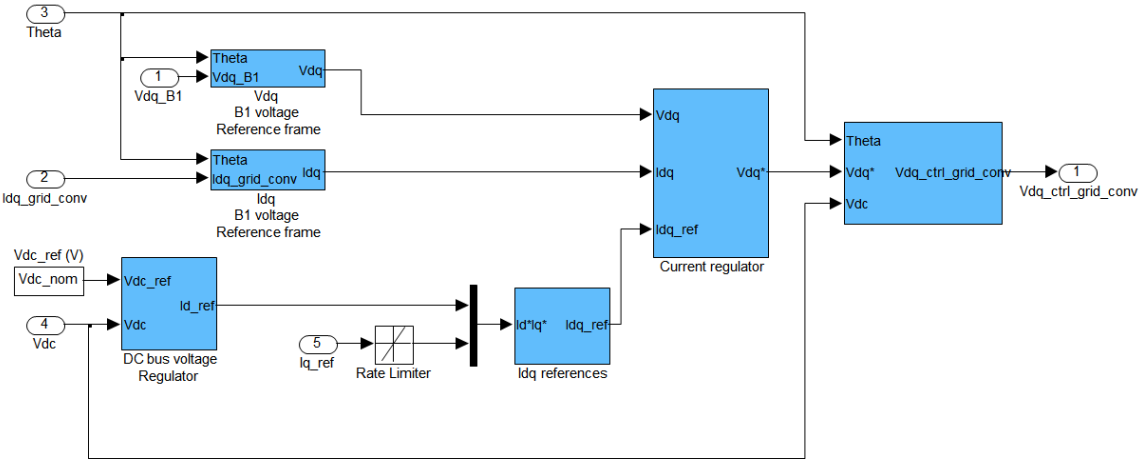


Figure 4.4 Simulink Layout for Grid-side Converter Control System

# 5. Self-Optimizing Robust Control of Power Capture for DFIG Wind Turbines

In this chapter, a self-optimizing scheme based on the previous ESC work is presented for wind power generation for variable speed wind turbines. A two-loop control strategy is proposed to maximize the overall power generation with consideration of uncertainties in power map [98], unreliable wind measurement and uncertainties in generator parameters. The outer loop is an ESC controller that tunes the rotor torque to maximize the mechanical power conversion, while the inner loop is generator controller for maximizing the electrical power conversion.

In particular, the Doubly-Fed Induction Generator (DFIG) is chosen for the variable-speed turbine used to demonstrate the proposed scheme. The DFIG has recently become the dominant choice for utility wind turbines, with intensive work done in its dynamic modeling, stability analysis and control [11, 12, 13, 14, 15]. Design of the DFIG controllers for converting rotor power to electrical power is not independent from the rotor power control. With the broad-spectrum nature of the turbulent wind input, the rotor power obtained from the rotor control is determined by both the wind characteristics and the rotor controllers. Therefore, for the DFIG controller to be designed, the performance specifications for power conversion need to cover appropriate and width so as to capture the dominant frequency components of the rotor power. Meanwhile, the designed controller needs to be robust against the variations in system parameters such as winding resistance/inductance and frequency. The DFIG systems are multi-input-multi-output (MIMO). Such control task can be well dealt with by the $\mathscr{H}_\infty$ control method [49, 99]. In this study, we propose that the performance weight for the $\mathscr{H}_\infty$ DFIG controller can be

selected based on the instantaneous spectrum of the rotor power. In particular, the $\mathcal{H}_\infty$ controller for the DFIG need can be cast into a robust performance design problem. Such control design strategy can fit well variable speed wind turbine operation, as the rotor power frequency components may vary with the rotor speed. The DFIG controller thus designed for maximizing the electric power conversion can be adapted to the speed changes in the wind turbine operation.

The proposed control strategy for the DFIG wind turbine system is sketched in Fig.5.1, where the ESC is applied to optimize the rotor power of the wind turbine, and the $\mathcal{H}_\infty$ DFIG controller can guarantee the optimal conversion of the electrical power into the grid power. The self-optimizing robust control of the DFIG based wind energy system is thus realized.

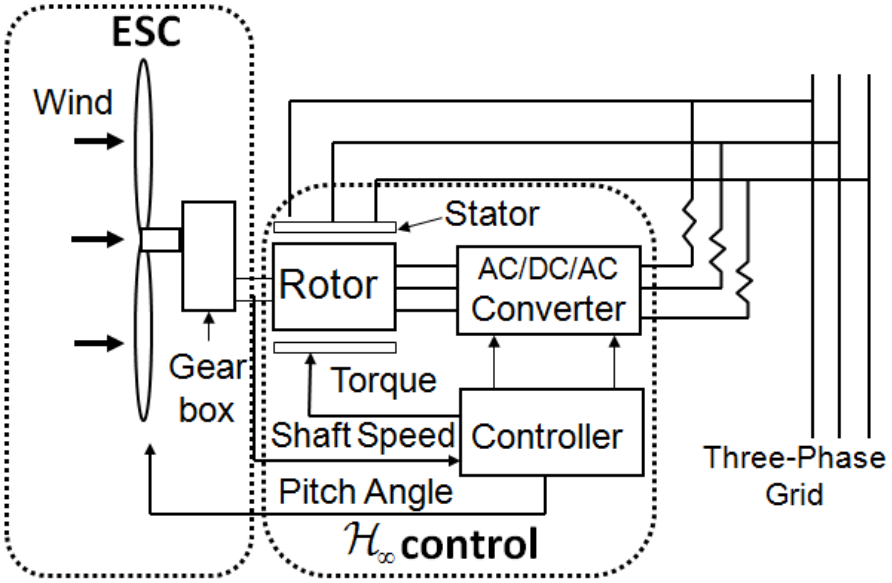


Figure 5.1 Schematic of the Self-optimizing Robust Control of DFIG Wind Energy System

In addition, the robustness of the ESC turbine control is evaluated in this study based on the averaged system of the ESC framework. The variation of the Hessian of the power

map is quantified and the robust stability of the ESC system designed can be evaluated. The control design and simulation involves both the turbine rotor and the generator. The field recorded turbulent wind data are used for the simulation of the DFIG based wind energy system. The fatigue analysis is conducted to evaluate the damage equivalent load (DEL) induced when applying the proposed control scheme. The simulation platform includes multi-physical platforms by integrating TurbSim, FAST, Simulink® and SimPowerSystems™.

The remainder of this chapter is organized as follows. First, the principle and design for ESC are presented, followed by the robust stability conditions derived from the averaging analysis. Then the DFIG modeling is presented. The $\mathscr{H}_\infty$ control design for wind power conversion is described. Simulation results for both ESC and the DFIG control are presented, and the current stage of work is concluded.

## 5.1 Extremum Seeking Control Design

As a nearly model-free and self-optimizing control strategy, the ESC algorithm [57, 58, 100] is used for the torque control to maximize the rotor power output of a variable speed wind turbine. This section reviews the working principle of ESC and the design guidelines, followed by the robustness analysis.

ESC considers finding an optimizing input $u_{opt}(t)$ in an online optimization problem for the generally unknown time varying cost function $l(t,u)$, i.e

$$u_{opt}(t) = \arg\min_{u \in \mathbb{R}^m} l(t,u) \tag{5.1}$$

The block diagram of the most adopted ESC method is shown in Figure5.2, where $y(t)$ is the measurement of the cost function $l(t,u)$ and noise is denoted by $n(t)$. The plant input

dynamics and output (sensor) dynamics denoted by $F_I(s)$, $F_O(s)$ respectively.

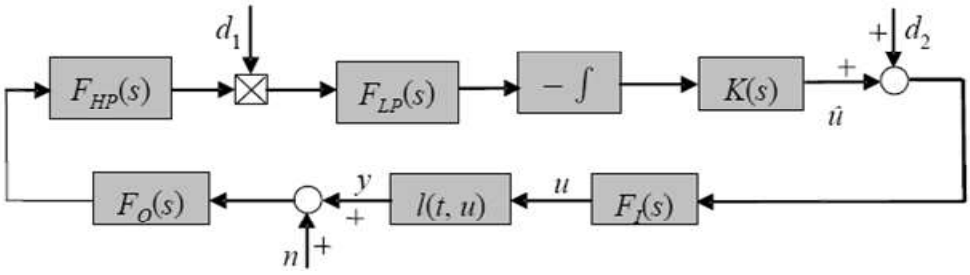


Figure 5.2 Block Diagram for ESC System

The ESC consists of a high-pass filter $F_{HP}(s)$, a low-pass filter $F_{LP}(s)$, integrator and a dynamic compensator $K(s)$. The dither and demodulation signals are $d_1^T(t)=\left[a_1\sin(\omega_1 t),\ldots,a_m\sin(\omega_m t)\right]$ and $d_2^T(t)=\left[\sin(\omega_1 t+\alpha_1),\ldots,\sin(\omega_m t+\alpha_m)\right]$, respectively, where $\omega_1,...,\omega_{\mathrm{m}}$ are the dither frequencies and $\alpha_1,...,\alpha_m$ are the phase angles. The dither and demodulating signals, in junction with the high-pass and low-pass filters, are used to extract a signal that is proportional to the gradient of the performance index with respect to the input. With the closed-loop stability secured, the integrator drives the gradient to zero and thus achieve the optimality. The dynamic compensator *K(s)* is used to improve the transient performance of the ESC loops.ESC design includes the selection of the dither amplitudes, dither frequencies, phase angles, the low-pass filter, the high-pass filter and the dynamic compensator. Our study follows the guidelines of ESC design in [100].

The dither frequencies should be distinct, and all be in the pass band of the high-pass filter and the stop band of the low-pass filter. The dither frequencies should be high but below the cut-off frequency of the dynamics of the tuning mechanism. The dither phase angles should satisfy

$$-\frac{\pi}{2} < \angle F_{Ii}(j\omega_i) + \alpha_i < \frac{\pi}{2} \tag{5.2}$$

The angle $\theta_i = \alpha_i + \angle \mathrm{F}_{Ii}(j\omega)$ should be close to zero to improve steady state tracking of optimal parameters. The dither amplitude should large enough so that the dithered output harmonics stands out in the noisy measurement.

The stability properties of the ESC could be determined form the characteristic equation

$$\det\left[I - G(s)RQ\right] = 0 \tag{5.3}$$

where,

$$G(s) = \frac{-F_I(s)K(s)F_{LP}(s)}{s} \tag{5.4}$$

$$R = \frac{1}{2}\begin{pmatrix} a_1\left|F_{I,1}(j\omega_1)\right|\cos(\theta_1) & 0 & 0 \\ 0 & \ddots & 0 \\ 0 & 0 & a_m\left|F_{I,m}(j\omega_m)\right|\cos(\theta_m) \end{pmatrix} \tag{5.5}$$

$G(s)$ denotes the series of the input dynamics, the dynamic compensator, the integrator and the low-pass filter. $Q > 0$ is the Hessian of the cost function near the optimality, i.e.

$$l(t,u) \approx l_{opt} + \frac{1}{2}\left(u - u_{opt}\right)^T Q(u - u_{opt}) \tag{5.6}$$

where $u_{opt}$ and $l_{opt}$ are optimal input and optimal performance index, respectively, and $u$ is assumed within a reasonable neighborhood of $u_{opt}$ such that Eq. (5.6) holds. The stability and transient performance can be assessed by Eq. (5.3) with the knowledge of the loop transfer matrix $G(s)RQ$.

## 5.2. Robustness Stability Condition of ESC

When uncertainty is present for the performance map, it is important to guarantee the robust stability of the ESC. For the case of wind turbine control, the profile of the power

map varies with wind speed and other factors. It is desirable to guarantee the robustness of the ESC controller, at least for the reasonable neighborhood of the maximum power point. This subsection gives the robust stability condition of the ESC method. Without loss of generality, and especially for some neighborhood of the optimality, we can consider the quadratic cost function in Eq. (5.6). Following the averaging analysis for the closed-loop ESC system[100], we reach the averaged system, shown as a typical tracking problem in Fig. 5.3, where

$$G_2(s) = F_2(s)C(s) = -F_2(s)K(s)\mu s^{-1}F_{LP}(s) \tag{5.7a}$$

$$R_{12} = \lim_{T\to\infty}\frac{1}{T}\int_0^T d_1(t)\omega_2(t)dt \tag{5.7b}$$

$$r_{122} = \lim_{T\to\infty}\int_0^T d_1(t)\omega_2^T Q\omega_2(t)dt \tag{5.7c}$$

$$r_{1n} = \lim_{T\to\infty}\frac{1}{T}\int_0^T d_1(t)n(t)dt \tag{5.7d}$$

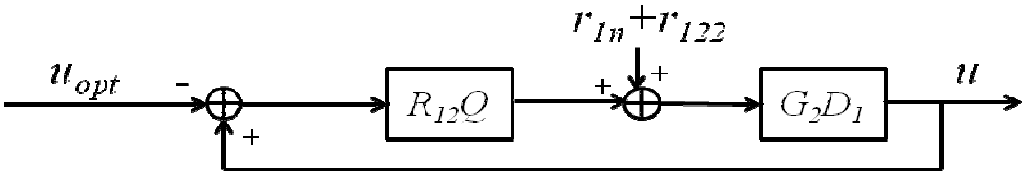


Figure 5.3 The Averaged Model for ESC System

The ESC is thus equivalent to tracking the unknown reference $u_{opt}$, while rejecting the disturbance due to measurement noise and the phase difference between dither and demodulation signals. The uncertainty in performance map shape is simplified as an additive uncertainty in the Hessian matrix $Q$, i.e. $Q = Q_0 + W_Q \cdot \Delta_Q$, as shown in Fig. 5.4, where $D_1$ and $D_2$ are the direct feed-through term in the state-space realization of

$G_1 = F_{HP}(s)F_o(s)$ and $G_2 = F_l(s)K(s)\left(-1/s\right)F_{LP}(s)$ respectively $Q_0$is the nominal Hessian matrix, $W_Q$ is the uncertainty weight matrix, and $\left\|\Delta_Q\right\|_\infty \le 1$.

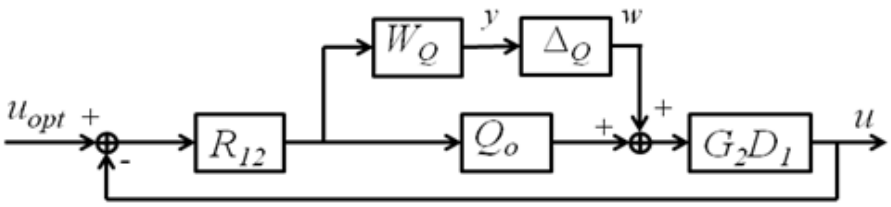


Figure 5.4 Robust Stability Analysis of the Averaged ESC System with Parametric Uncertainty in Hessian Matrix

Based on the Small Gain Theorem[101], as illustrated in Fig. 5.4, the closed-loop system is stable, if and only if

$$\left\|W_Q N_{yw}(j\omega)\right\|_\infty < 1 \tag{5.8a}$$

where,

$$N_{yw}(s) = \frac{W_Q R_{12} G_2 D_1}{1 + Q_o R_{12} G_2 D_1} \tag{5.8b}$$

is the transfer matrix from perturbation input *w* to perturbation output *y*.

## 5.3 $\mathcal{H}_\infty$ Control of DFIG Power Conversion

The DFIG power conversion controller needs to be designed such that the performance of conversion is satisfactory within the bandwidth where most of the rotor power resides. Also, such performance should be robust to system uncertainties. In this study, the uncertainty in resistance and inductance of the rotor and stator is considered. Such variations are due to manufacturing inconsistency, change in operation temperature and component degradation. To achieve such robust performance as expected, the $\mathcal{H}_\infty$ control

design is a suitable framework. The $\mathcal{H}_\infty$ DFIG power conversion control strategy is shown in Fig. 5.5.

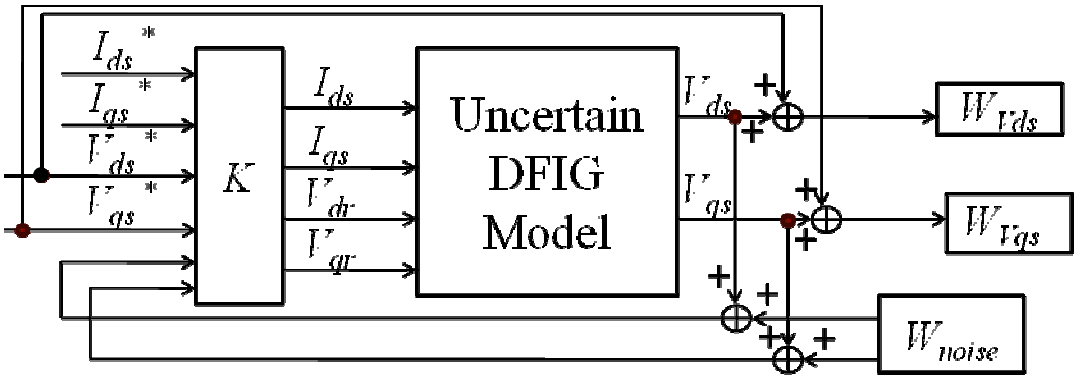


Figure 5.5 Block Diagram of $\mathcal{H}_\infty$ DFIG Power Conversion Controller

Recall the DFIG model discussed in Chapter 4, the state-space representation of DFIG can be described as follows,

$$\begin{bmatrix} \dot{\Phi}_{dr} \\ \dot{\Phi}_{qr} \end{bmatrix} = [A_s] \begin{bmatrix} \Phi_{dr} \\ \Phi_{qr} \end{bmatrix} + [B_{s1}] \begin{bmatrix} I_{ds} \\ I_{qs} \end{bmatrix} + [B_{s2}] \begin{bmatrix} V_{dr} \\ V_{qr} \end{bmatrix} \tag{5.9a}$$

$$\begin{bmatrix} V_{ds} \\ V_{qs} \end{bmatrix} = [C_s] \begin{bmatrix} \Phi_{dr} \\ \Phi_{qr} \end{bmatrix} + [D_{s1}] \begin{bmatrix} I_{ds} \\ I_{qs} \end{bmatrix} + [D_{s2}] \begin{bmatrix} V_{dr} \\ V_{qr} \end{bmatrix} \tag{5.9b}$$

Equation (5.9) is deemed as the nominal model of DFIG for the $\mathcal{H}_\infty$ control design in this chapter. As stator current depend on the mechanical load from wind turbine, the reference signals $I_{ds}^*$ and $I_{qs}$* are used for the input of the $\mathcal{H}_\infty$ controller. $W_{noise}(s)$ is used to model magnitude uncertainty of the sensor noise in the stator voltage. The variations in the rotor/stator resistance and inductance ($R_s$, $R_r$, $L_s$, $L_r$) are modeled as multiplicative parametric uncertainties, i.e.

$$R_s = R_{sn} \cdot (I + W_\delta \cdot \delta_{Rs}) \tag{5.10a}$$

$$R_r = R_{rn} \cdot (I + W_\delta \cdot \delta_{Rr}) \tag{5.10b}$$

$$L_s = L_{sn} \cdot (I + W_\delta \cdot \delta_{Ls}) \tag{5.10c}$$

$$L_r = L_{rn} \cdot (I + W_\delta \cdot \delta_{Lr}) \tag{5.10d}$$

Where $R_{sn}$, $R_{rn}$, $L_{sn}$, and $L_{rn}$ are the nominal values, $W_\delta$ is the weight for the uncertainty and $\delta$ is the unit-norm variation for resistances and inductances. The weighting functions $W_{Vds}(s)$ and $W_{Vqs}(s)$ are designed to weight the tracking error of the stator voltages $V_{ds}$ and $V_{qs}$ with the emphasis of the desired frequency ranges.

The robust performance controller design can be shown in Fig. 5.6, where $\Delta$ is the structured perturbation from the uncertainty we assumed in the system above, *d* and *e* are the generalized disturbance and error. The performance of the MIMO DFIG control system we studied is characterized by $\mathcal{H}_\infty$ norms in (5.11), where the *T* is weighted, uncertain transfer function matrix from *d* to *e*.

$$\|\mathrm{T}\|_\infty = \max_{\omega \in R} \bar{\sigma}[T(j\omega)] \le 1 \tag{5.11}$$

where $\bar{\sigma}(\cdot)$ is the maximum singular value. The $\mathcal{H}_\infty$ controller is synthesized with the Matlab Robust Control Toolbox Version3.4.1 [85].

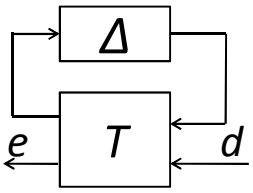


Figure 5.6 Robust Performance Control Design

## 5.4 Simulation Results

The proposed control strategy is evaluated via simulation study. The turbine model studied for simulation is the CART (Controls Advanced Research Turbine) facility located at the National Renewable Energy Laboratory in Golden, Colorado. The CAET

facility is a two-blade, active-yaw 600 kW variable-speed variable-pitch turbine [27], and extensively modified for a test bed to study wind turbine controls. The generator model used in this study is a 600 kW, 4-pole DFIG, as listed in Table 5.1. The simulation platforms includes FASTv7.0, TurbSim v1.50, AeroDynv13 developed by NREL for wind turbine simulation, interfaced with Simulink® 7.5 and SimPowerSystems™ 5.2.1 developed by Mathworks. More details of CART and FAST based simulation is given in Appendix.

Table 5.1 Parameters of the Simulated DFIG

| | |
|---|---|
| Rated power | 650 kW |
| Stator voltage | 220V |
| Frequency | 60 Hz |
| Stator resistance, $R_s$ | 5 Ω |
| Rotor resistance, $R_r$ | 1.01 Ω |
| Stator cyclic inductance, $L_s$ | 0.341 H |
| Rotor cyclic inductance, $L_r$ | 0.060 H |
| Mutual cyclic inductance, $M$ | 0.135 H |

This study presents highly multi-physical domains of simulation, ranging from aerodynamics to power electronics. The block diagram of the code interaction used in simulation is given in Fig. 5.7.TurbSim creates turbulent wind files (the input file of TurbSim is given in Appendix A.3). AeroDyn takes the wind data from TurbSim and then calculate the aerodynamic loads of the turbine. FAST takes the aerodynamic loads and applies it to the nonlinear wind turbine model to calculate the equations of motion.

AeroDyn in turn takes information about the turbine and recalculates the aerodynamic loads. The control algorithm takes measurements form FAST produce the control signals send to the generator model in SimPowerSystems™. The $\mathcal{H}_\infty$ DFIG controller controls the generator torque which is then sent back to FAST.

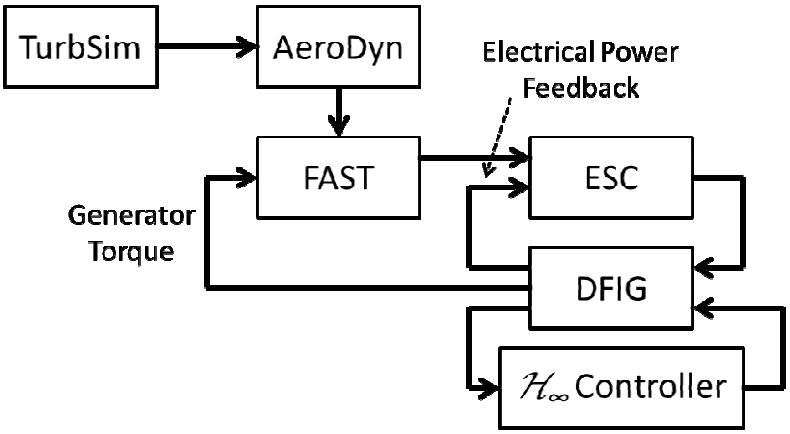


Figure 5.7Block Diagram of Simulation Platform

The torque controller is used to regulate the speed of the turbine to the optimum tip speed ratio so that to capture the maximize power from the wind. The reference torque is calculated as proportional to the square of the rotor speed with torque gain *k*. The power capture is maximized when the torque gain *k* is regulated to optimum value. ESC is used to search for the optimal *k* under different wind speeds. The electrical torque command is obtained from ESC and will then send to the DFIG model. For the torque ESC controller, the dithering frequency was chosen to be 0.07 rad/s. The high-pass and low-pass filters are designed as

$$\mathrm{F}_{HP}(s) = \frac{s^2}{s^2 + 2*0.58*0.06s + 0.06^2} \tag{5.12a}$$

$$F_{LP}(\mathrm{s}) = \frac{0.02^2}{s^2 + 2*0.6*0.02s + 0.02^2} \tag{5.12b}$$

### 5.4.1. ESC Robust Stability Test

An initial robust analysis of the ESC is based on the data obtained from the CART turbine operating in a smooth 10m/s wind with various combinations of blade pitch angle and generator torque. The power capture was recorded for each combination once the turbine outputs reached the steady state.

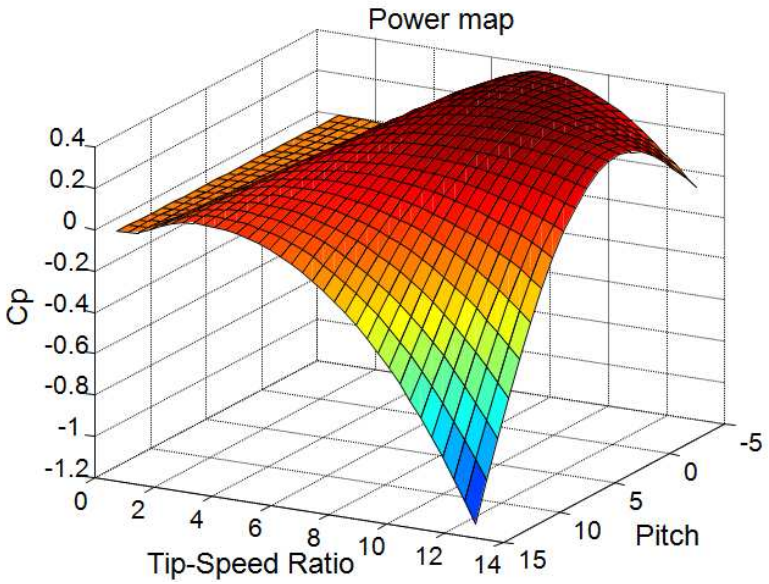


Figure 5.8 $C_p$ Surface in TSR and Pitch Angle

The $Q$ matrix is developed corresponding to the Region 2 operation with the wind speed is between the cut-in and the rated, the control objective is to maximize the power output. Figure5.8 shows the $C_p$ surface simulated for the CART turbine model. Maximum energy capture can be achieved if the turbine is operated at the maximum power coefficient point $C_{pmax}$. For the average model of ESC, the $Q$ matrix could be calculated from

$$l(t,u) \approx l_{opt} + \frac{1}{2}\begin{bmatrix} q_1(u_1 - u_{1opt})^2 + 2q_3(u_1 - u_{1opt})(u_2 - u_{2opt}) + \\ q_2(u_2 - u_{2opt}) \end{bmatrix} \quad (5.13)$$

where $u_1$ is the pitch angle, $u_{1opt}$ is the optimum pitch angle, $u_2$ is the torque gain $k$, $u_{2opt}$ is the optimum torque gain $k$, $l(t,u)$ is the power at the chosen point and $l_{opt}$ is the optimum

power at the optimum parameter setting. The $Q$ matrix can be found and the uncertainty in $Q$ matrix is bounded. Nominal value of $Q$ matrix, $Q_0$is

$$\mathrm{Q}_o = \begin{bmatrix} q_{1o} & q_{3o} \\ q_{3o} & q_{2o} \end{bmatrix} = \begin{bmatrix} -3.7864 & -0.0073 \\ -0.0073 & -0.0429 \end{bmatrix} \tag{5.14}$$

The elements of the $Q$ matrix have the following variations according to Region 2 operation: $q_1 \in [-4.9223, -3.4078]$ , $q_2 \in [-0.0514, -0.0386]$ , $q_3 \in [-0.0080, -0.0066]$ . The weight matrix $W_Q$ is thus

$$W_Q = \begin{bmatrix} 0.7572 & 0.0073 \\ 0.0073 & 0.0064 \end{bmatrix} \tag{5.15}$$

As shown in Fig. 5.9, the profile of the maximum singular value of $W_Q N_{yw}(j\omega)$ validates the robust stability of the ESC system.

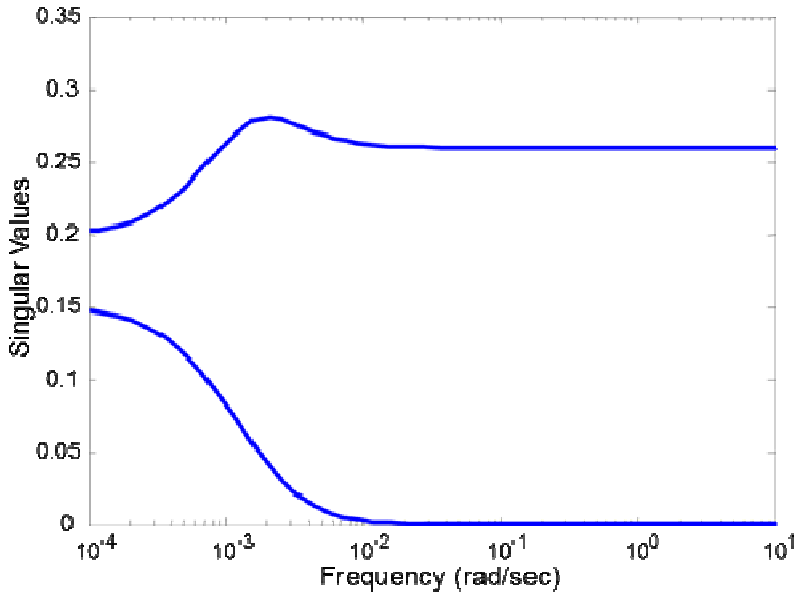


Figure 5.9 Bode Plot for Robust Stability Test

### 5.4.2. Simulation Results for ESC Wind Power Generation

Simulation study was conducted using the ESC control scheme for the CART wind turbine model (more details can be found in Appendix A.5). First, the smooth wind input

of 10m/s mean speed is provided, with the results shown in Fig. 5.10. The simulation time is 1 hour and the ESC control is turned on at 200second. The initial torque gain is set at 168 kg·m$^3$/rad$^3$. Per-unit (p.u.) power is 650kW and p.u. torque (low speed side) is 148kN-m. After the ESC is turned on, the torque gain keeps reducing until it reaches the optimal value at about 100 kg·m$^3$/rad$^3$. The energy capture improvement is 2.92%. Figure 5.10(a) shows the profiles of the key mechanical variables, while Figure 5.10(b) plots the DFIG electrical variables. Similar results have also been obtained for 8m/s and 6m/s steady winds. The simulation is then repeated with field recorded turbulent wind data with 2% turbulence intensity, with the results shown in Fig. 5.11(a). For smooth 10m/s wind case as shown in Fig. 5.11(b), the ESC starts at 200s and the torque gain converges on its optimal value 110 kg·m$^3$/rad$^3$in about 200 seconds. The torque gain converges on the optimum and thus the rotor power conversion is maximized.

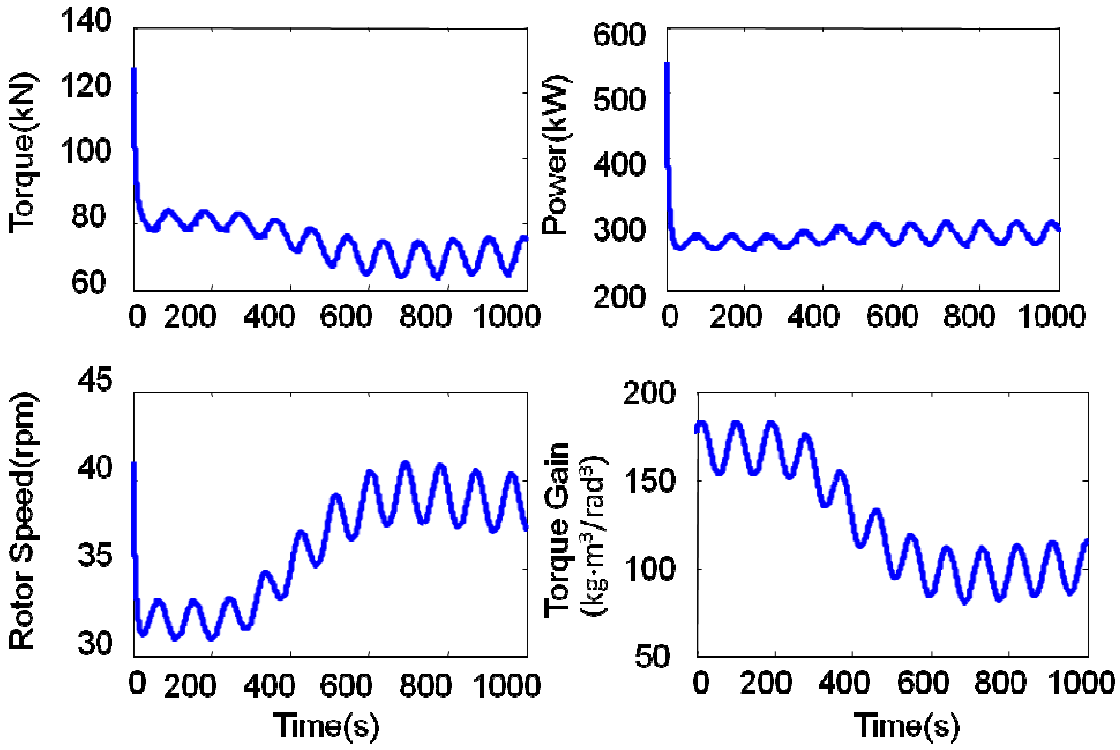


(a) Rotor Variables

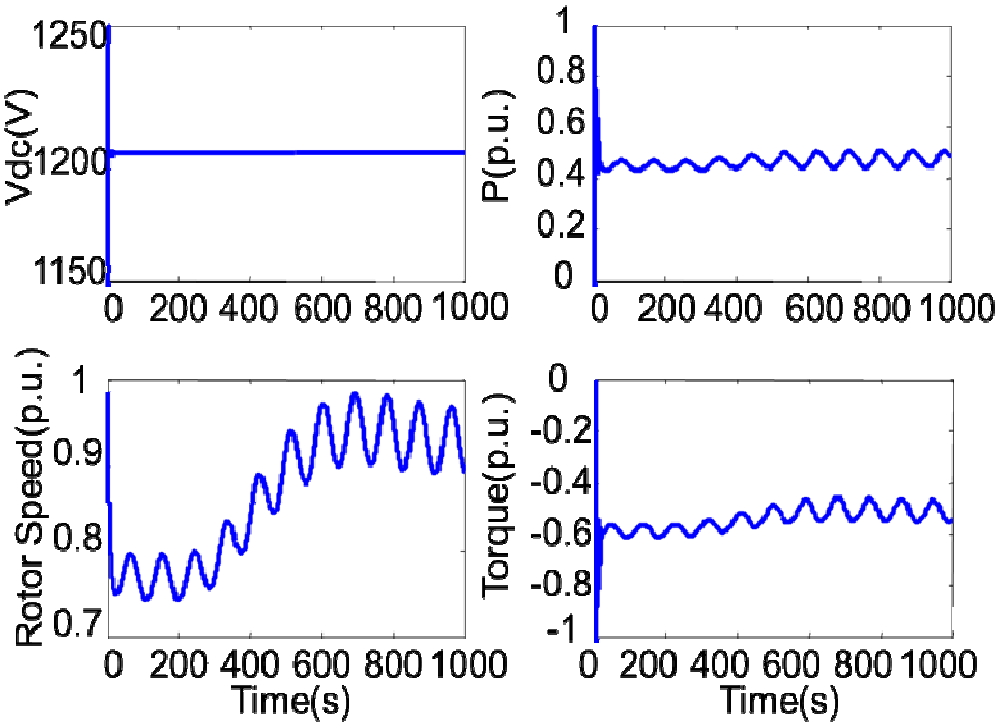


(b) Generator Variables

Figure 5.10 Simulation Result of ESC Control for DFIG Wind Turbine

Based on the simulations at different wind speeds, the energy capture improvement, compared to the standard wind turbine control method with constant torque gain of 168 $kg{\cdot}m^3/rad^3$ is shown in Table 5.2.

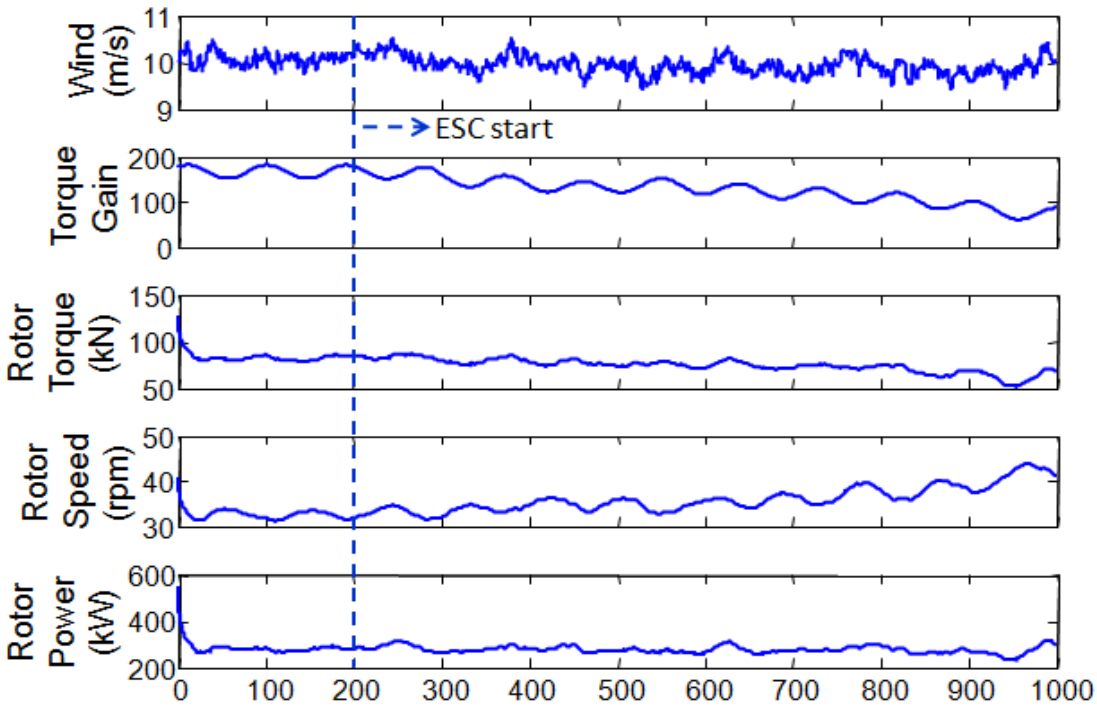


(a) Turbulent wind simulation

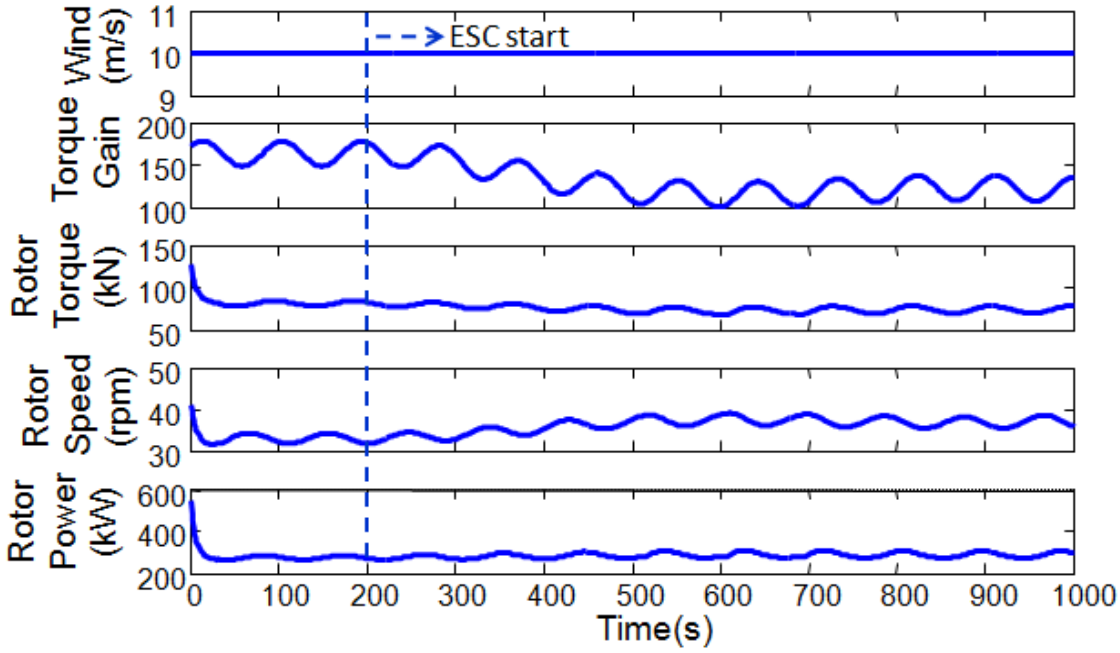


(b) Smooth wind simulation

Figure 5.11 Simulation Results under Field Recorded Turbulent Wind 10m/s

Table 5.2 Energy Capture Improvements by ESC under Several Wind Speeds

| Wind Input | Proposed (kWh) | Standard (kWh) | Energy Increase (%) |
|---|---|---|---|
| 10m/s Steady Wind | 284.35 | 276.27 | 2.92% |
| 10m/s Turbulent Wind | 283.45 | 275.47 | 2.90% |
| 8m/s Turbulent Wind | 146 | 142.02 | 2.80% |
| 6m/s Turbulent Wind | 61.91 | 60.89 | 1.68% |

### 5.4.3 Fatigue Analysis for Proposed Control Scheme

As fatigue loading is critical for the reliability of wind turbines, it is important to inspect the effect on wind turbine load change due to the use of ESC. In this study, NREL's MCrunch[102] was used to analyze the fatigue load change associated with the ESC (the input file for MCrunch is given in Appendix A.4). The S-N slope was set at 10 for blades with composite material. The damage equivalent loads (DEL) were calculated for both the flap-wise and edge-wise blade-root bending moments. The DEL between the ESC and the standard control under different wind speed with 2% turbulence are compared in Table 5.3, where RootMyb1 is the flapwise moment at the blade root and RootMxb1 is the edgewise moment, both for blade 1. For most cases, the load change by ESC is not apparent. A remarkable increase in DEL was observed for10m/s wind, for the flap-wise moment increased significantly, which deserves more study in future.

Table 5.3 Damage Equivalent Loads Comparison for ESC Turbine Control

| Mean Wind Speed | Turbulence Intensity | Channel | Standard | Proposed | Increase |
|---|---|---|---|---|---|

| | | | | | |
|---|---|---|---|---|---|
| 10 m/s | 1.91% | RootMyb1 | 42.58 | 75.98 | 78.4% |
| | | RootMxb1 | 155.3 | 161.7 | 4.12% |
| 8 m/s | 2.39% | RootMyb1 | 54.22 | 53.26 | -1.77% |
| | | RootMxb1 | 162.4 | 153.9 | -5.23% |
| 6m/s | 3.19% | RootMyb1 | 55.52 | 53.33 | -3.94% |
| | | RootMxb1 | 158.8 | 158.7 | -0.06% |

### 5.4.4 Robust Performance $\mathcal{H}_\infty$ Controller Synthesis

The DFIG control system is then tested under the 10m/s turbulent wind. As shown in Fig. 5.12, $T_m$ is the mechanical torque reference from ESC, and $T_e$ is the electrical torque output of the DFIG. The generator quickly follows the optimal rotor torque command. For the step response as shown in Fig. 5.12(a), the settling time is 0.2086 second. In Fig. 5.12(b), the torque following control is simulated for ESC simulation with 10 m/s field recorded turbulent wind data.

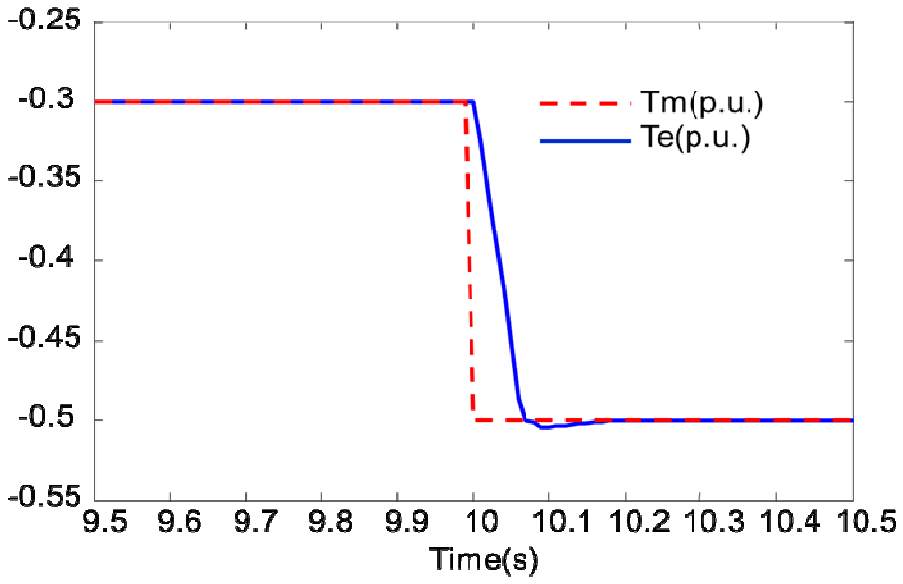

(a) Step Response of DFIG

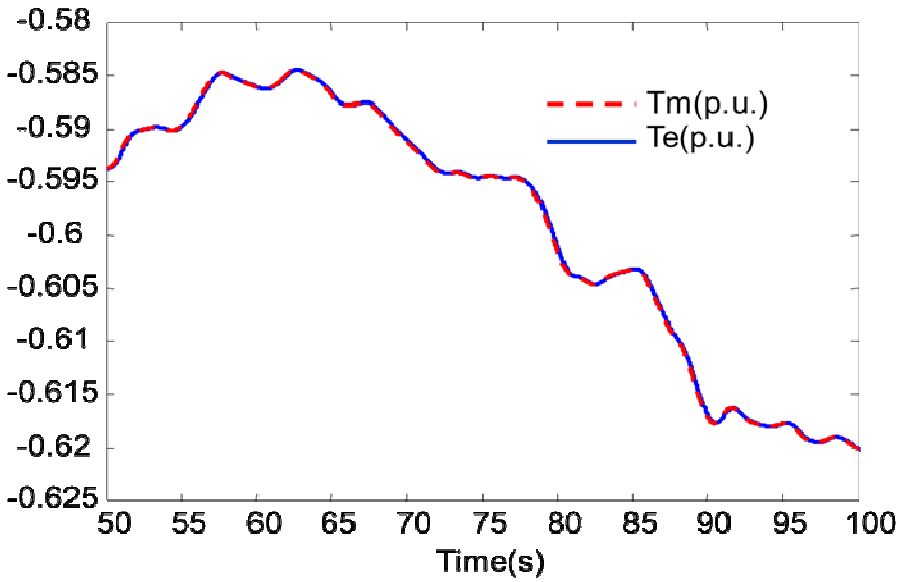


(b) Simulation Result for Turbulent 10m/s Wind

Figure 5.12 DFIG Model Simulation Results

The $\mathcal{H}_\infty$ controller for DFIG power conversion is designed by first choosing the relevant weight functions. Regarding to the parameter uncertainty, as an initial trial, 20% variation is considered for the values of $R_s$, $R_r$, $L_s$, and $L_r$. The block $W_{noise}(s)$ in Fig. 5.6 which serves to model sensor noise is set to be 0.01.

The weighting functions $W_{Vds}(s)$ and $W_{Vqs}(s)$ are designed to keep the tracking error for stator voltages $V_{sd}$ and $V_{sq}$ small in the desired frequency ranges. The cut-off frequency is chosen based on the spectra of the rotor speed and rotor power in the ESC results as shown in Fig. 5.13(a). Notice that the rotor power has quite a few higher frequency components that do not appear in the rotor speed spectrum. These frequency components shift with the change of the wind speed. These harmonics are due to the generator torque and do not have to be considered for the tracking control for the DFIG power conversion control. As an initial attempt, the following performance weights are selected:

$$W_{Vds}(s) = W_{Vqs}(s) = \frac{0.1s + 10}{s + 2.5} \tag{22}$$

The magnitude responses of the weighting functions $W_{Vds}(s)$ and $W_{Vqs}(s)$ are shown in Fig. 5.14(a). The weight magnitude rolls off at 16 rad/s, the second peak of the spectrum plot of the rotor speed, in order to maximize the rotor power conversion and reject the high frequency component of the turbulence as well. In the rotor power spectrum under 10 m/s turbulent wind, the power from 0 to 5Hz takes about 99.76% of the total; and for 4m/s wind, it is 99.97%. Therefore, neglecting higher frequency components in the $\mathcal{H}_\infty$ robust performance controller design would lead only trivial power loss.

The spectrum of the rotor power will changes due to the wind speed variation. When considering a 4m/s turbulent wind case, the weighting function should track the change of the frequency in rotor power. As shown in Fig. 5.13(b), the select frequency is shifted to 3.282Hz, and the weighting function can be synthesized as

$$W_{Vds}(s) = W_{Vqs}(s) = \frac{0.1s + 23.8}{s + 4.5} \tag{23}$$

The magnitude response of the selected weight is shown as Fig. 5.15(b).

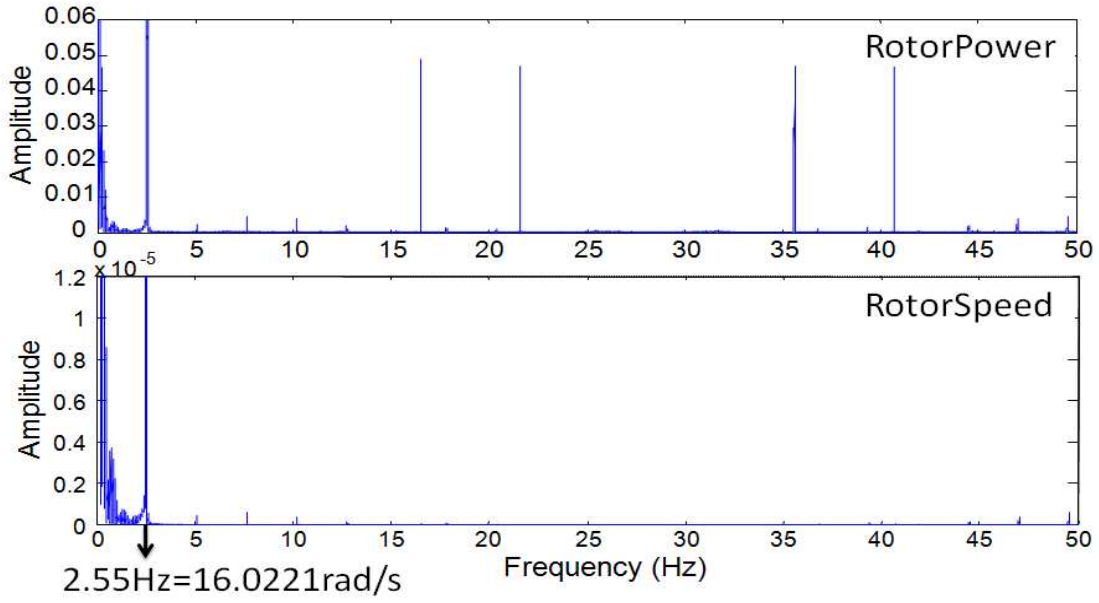


(a) 10m/s Wind

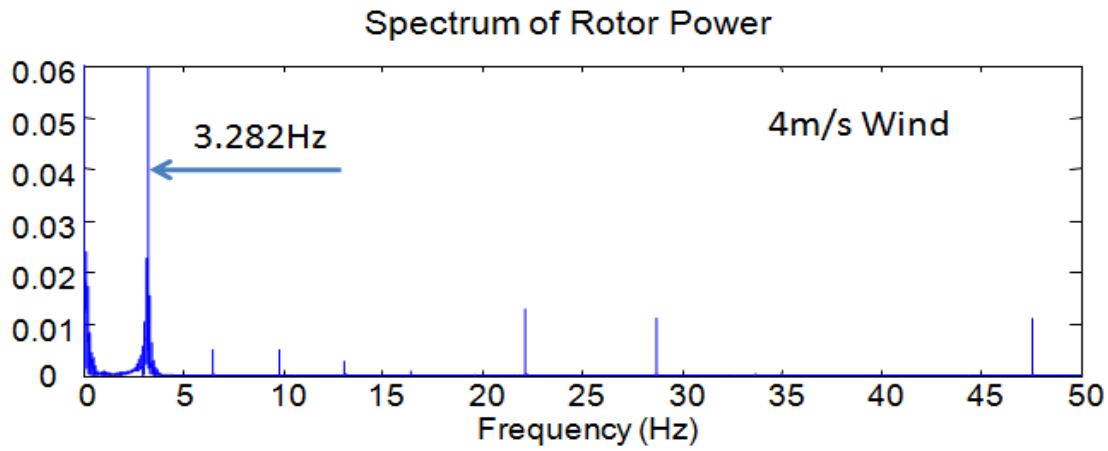


(b) 4m/s Wind

Figure 5.13 Spectra of Rotor Power and Rotor Speed under Different Mean Wind Speeds

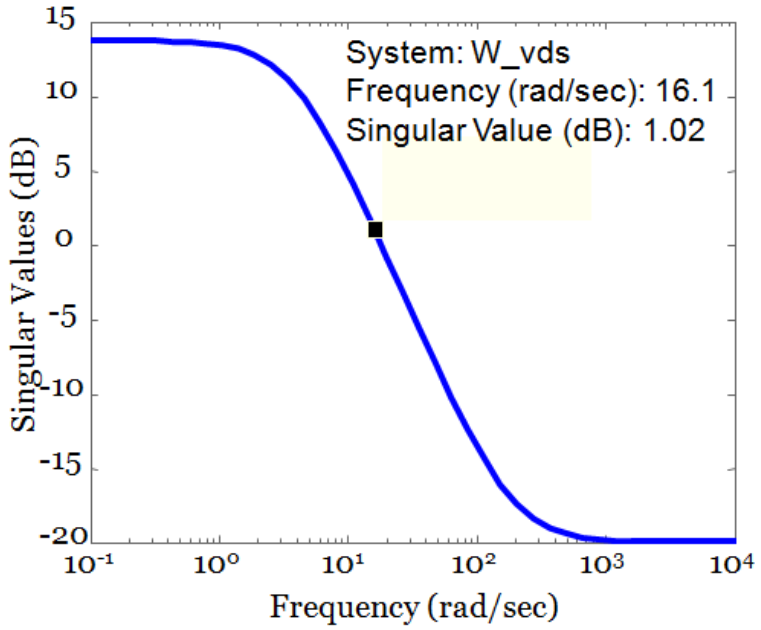


(a) 10m/s wind case

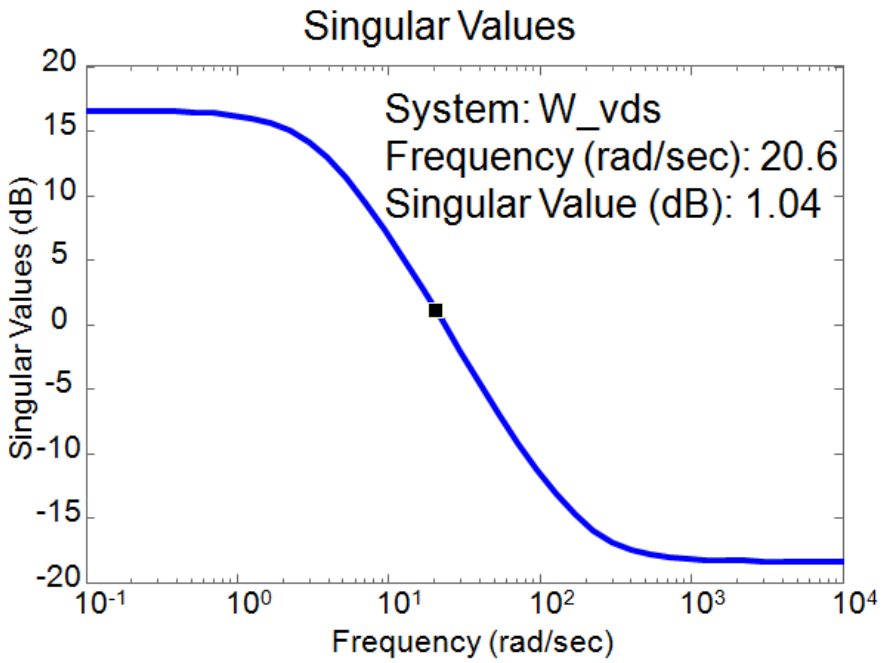


(b) 4m/s wind case

Figure 5.14 Magnitude Responses of the Two Performance Weights

The controller is designed via μ-synthesis to meet the specified robust performance requirement. With the *D-K* iteration process, the obtained controller has 4 outputs, 6

inputs, and 92 states. The robust performance bound for the closed-loop DFIG system is 0.7411, indicating that the requirements can be met for the specified performance requirement and model uncertainties. Controller order reduction was performed based on the Hankel singular values shown in Fig. 5.15. For the 8$^{th}$ order controller, the robust performance bound was 0.9324. When the controller is reduced to the 14$^{rd}$ order, the robust bound is increased to 0.8436. Figure 5.18 compares the singular-value plots of the full-order and the reduced-order controllers with 8 states.

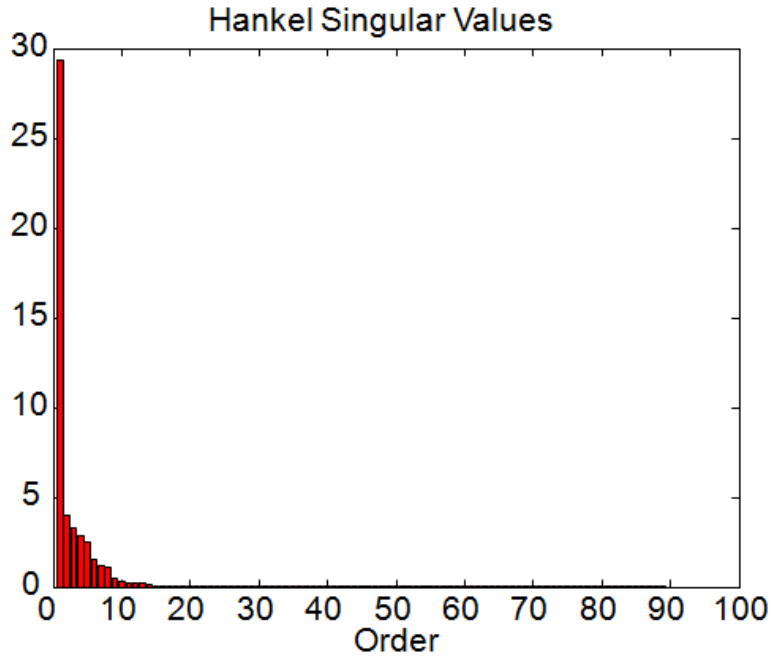


Figure 5.15 Hankel Singular Value Plot for DFIG Controller

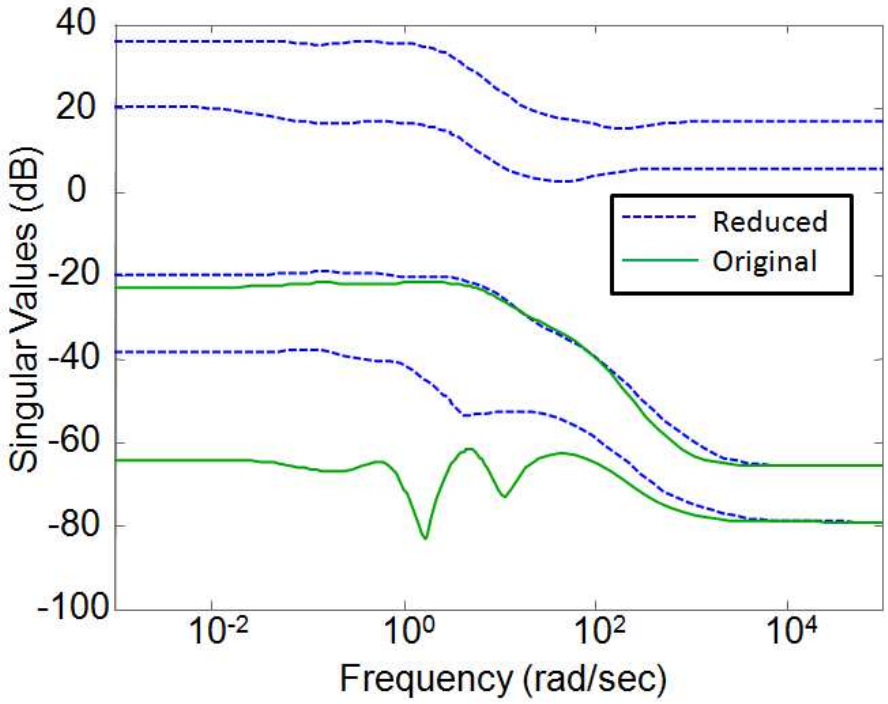


Figure 5.16 Singular Value Comparison of the Original and Reduced Controller

Figure 5.17 gives the spectra of the grid power conversion with the synthesized controller. The rotor power conversion is improved via the main frequency component of the power is conversed with $\mathcal{H}_\infty$ controller. In field wind data simulation, the grid power converted from the PI controller is 74.55% of the available power from the wind, which based on the optimal $C_P$ is 0.4 for CART model as shown in Fig. 5.8. Compared to the PI controller, the $\mathcal{H}_\infty$ controller improved power conversion by 9.89%, i.e. 81.92% of the wind power is converted to grid.

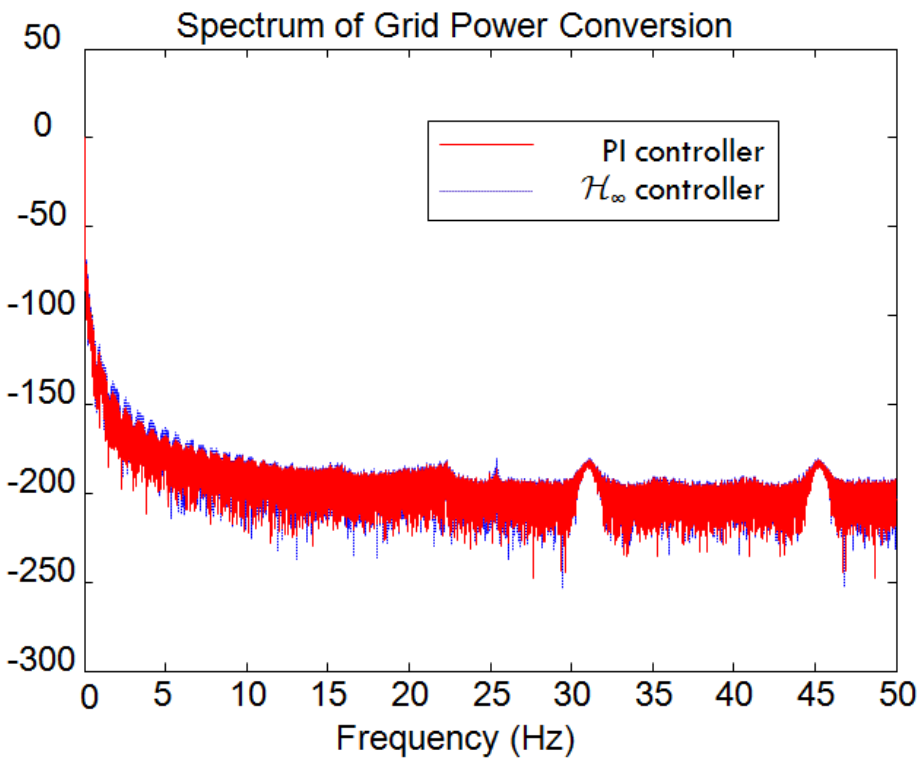


Figure 5.17 Comparison of Spectra of Rotor Power and Grid Power

## 5.5 Summary

This chapter proposes a two-loop self-optimizing robust control scheme for maximizing the power generation for the region-2 operation for a variable speed wind turbine with DFIG. The outer loop is an Extremum Seeking Control (ESC) based generator torque regulation via the rotor power feedback. The ESC can search for the optimal generator torque to maximize the rotor power under variation of the power map. The robust stability of the ESC controller near the optimum is evaluated. The damage equivalent load is also evaluated for the ESC control results. The inner loop is an electrical control using PWM converters via vector control schemes. A robust performance $\mathcal{H}_\infty$ controller is synthesized for maximizing the conversion from the rotor power to grid power. The performance weights are defined based on the rotor power spectrum from the ESC outer

loop, and the controller is designed to be robust against the variations of some key parameters of the DFIG system. Simulation results have sustained the proposed scheme. The proposed control scheme incorporates both rotor and generator control, and provides a solution of adaptively maximizing the wind power generation for region 2 operation.

# 6. Bumpless Transfer based Inter-Region Controller Switching

For wind energy systems, both power quality and structural loads are strongly affected by the fluctuating nature of wind source. Recall that the Region-2 control, generator torque control is normally used for the variable-speed operation for maximizing the power output, while for the Region-3 control, blade pitch control is used to regulate the rotor speed around the rated speed and reduce the load. When the turbine operates in wind fluctuating around the rated wind speed, the rotor speed will vary around the reference RPM, which may result in (frequent) switching between the Region-2 controller and the Region-3 controller. As to be shown later in this chapter, such controller switching involves switching in control references, and thus induces significant flicker emissions[24] in the electric power fed into the grid and also fatigue loads for the turbine structure. Therefore, from the perspective of power quality and load reduction, it is beneficial to design appropriate controller switching scheme during such inter-region controller switching. In controls area, the stability and transient improvement of reference and controller switching have been dealt with by developing various bumpless transfer techniques. In this thesis study, two existing bumpless transfer schemes are applied to the switching between Region-2 and Region-3 operations for variable speed wind turbines.

The two bumpless transfer techniques are reviewed first, and then their application to the wind turbine inter-region switching is presented. Finally, the simulation results are presented to validate the effectiveness of the proposed schemes.

## 6.1 Brief Overview of Bumpless Transfer

Use of multiple controllers is often needed for practical control systems, e.g. due to piecewise linearization of nonlinear systems [73]. When switching between different controllers, there are often undesirable transients presented in the system outputs and states due to the discontinuities involved. In most malicious situations, the bumps produced by controller switching may even destabilize the system. Therefore, various bumpless transfer techniques have been investigated [67, 68, 70, 75, 77], as described in Chapter 2.

In this study, two well-received bumpless transfer techniques have been adopted for the inter-region control switching for wind turbine operation. One is the so-called Conditioning Technique proposed by Hanus [77], which is designed to improve the tracking performance of system output while achieving the desired bumpless transfer. The Conditioning Technique has been widely applied as an anti-windup strategy for general applications to reduce the deterioration of the control performance under actuator saturation [70], and meanwhile this scheme is also very effective in handling the bumpless transfer situation. The second approach is a linear quadratic (LQ)control technique for bumpless transfer proposed by Turner and Walker [69, 75]. This LQ bumpless transfer scheme frames the bumpless transfer design task into an optimal control problem, which lends nice convenience in compromising between bumpless transfer and output tracking. These two techniques will be described in the following two sections.

## 6.2 Linear Quadratic Bumpless Transfer

The linear quadratic bumpless transfer (LQBT) technique treats the problem of switching between two linear controllers as an LQ optimal control problem [69, 75, 103]. As shown in Figure 6.1 [103], the LQBT scheme proposed in [69] is concerned about the scenario of switching from an Online Controller to an Offline Controller. As desired by bumpless transfer, in order to minimize the transient at the switching instant, it is desirable to minimize both the difference between the two controller outputs and the difference between the signals driving the two controllers. A static feedback matrix *F*, known as the 'bumpless transfer compensator', is designed to achieve this goal. The inputs to matrix *F* include the states *x* of the Offline Controller, the control input $\tilde{u}(t)$ from the Online Controller, the plant output *y*, and the reference signal *r*. The output of matrix *F*, i.e. $\alpha(t)$, becomes $\tilde{\alpha}(t)$ after passing through a low-pass filter, and the sum of $\tilde{\alpha}(t)$ and $r(t)$ is then the input to the Offline Controller. The low-pass filter is introduced by [8] in order to smooth the bump of $\tilde{\alpha}(t)$ during controller switching.

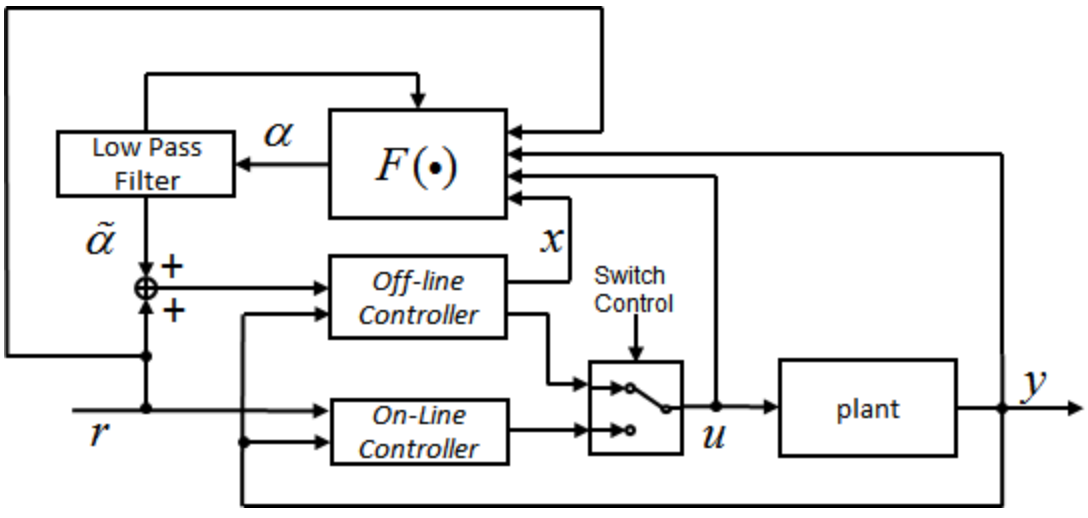


Figure 6.1 Illustrative Block Diagram for the LQ Bumpless Transfer

The derivation of the LQ bumpless transfer design is briefly reviewed next, following the description by Turner et al. [9]. For the case of finite time horizon, the associated LQ optimal control problem aims to minimize the following quadratic cost function,

$$J(u,\alpha,T)=\frac{1}{2}\int_0^T z_u(t)'W_u z_u(t)+z_e(t)'W_e z_e(t)+\frac{1}{2}z_u(T)'Pz_u(T) \tag{6.1}$$

where

$$z_u(t)=u(t)-\tilde{u}(t) \tag{6.2}$$

$$z_e(t)=\alpha(t) \tag{6.3}$$

Notice $\alpha(t)$ is chosen to be minimized instead of low pass filter output $\tilde{\alpha}(t)$. The purpose of the low-pass filter is to enable the input to the controller to evolve gradually towards $r(t)$ when the Offline controller is connected, thus avoiding a large jump. Due to the use of the low-pass filter, the input to the Offline Controller is actually $r(t)+\tilde{\alpha}(t)$, instead of the $\alpha(t)$ included in Eq. (6.3). $W_u$ and $W_e$ are positive definite weight matrices, which are sized to compromise between tracking the control-input signal (i.e. forcing $u(t)\approx\tilde{u}(t)$) and limiting the deviation of $\alpha(t)$ from $r(t)$. $P$ is the positive-definite terminal weighting matrix for penalizing the deviation of the control input signal at the final time $T$.

To synthesize the bumpless transfer compensator $F$, one needs to solve the problem of minimizing the quadratic performance index in Eq. (6.1). Assume that the Offline controller $K_{off}(s)$ is stabilizable and detectable[103], and its state space representation is

$$\begin{cases}\dot{x}=Ax+B_1(r+\tilde{\alpha})+B_2y\\ u=Cx+D_1(r+\tilde{\alpha})+D_2y\end{cases} \tag{6.4}$$

The low-pass filter $L(s)$, also assumed to be stabilizable and detectable, has the state space realization

$$\begin{cases} \dot{x}_l = A_l x_l + B_l \alpha \\ \tilde{\alpha} = C_l x_l \end{cases} \tag{6.5}$$

Combining the dynamics of the Offline controller and low-pass filter, we have the augmented system as

$$\begin{aligned} \dot{\tilde{x}} &= \tilde{A}\tilde{x} + \tilde{B}_1 w + \tilde{B}_2 \alpha \\ u &= \tilde{C}\tilde{x} + \tilde{D}w \end{aligned} \tag{6.6}$$

where,

$$\tilde{A} = \begin{bmatrix} A & B_1 C_l \\ 0 & A_l \end{bmatrix},\ \tilde{B}_1 = \begin{bmatrix} B_1 & B_2 \\ 0 & 0 \end{bmatrix},\ \tilde{B}_2 = \begin{bmatrix} 0 \\ B_l \end{bmatrix}$$

$$\tilde{C} = \begin{bmatrix} C & 0 \end{bmatrix},\ \tilde{D} = \begin{bmatrix} D_1 & D_2 \end{bmatrix}$$

$$\tilde{x} = \begin{bmatrix} x \\ x_l \end{bmatrix},\ w = \begin{bmatrix} r \\ y \end{bmatrix}$$

Substitute these into the quadratic performance index and then formulate the Hamiltonian,

$$H = \frac{1}{2}\left\{\left(\tilde{C}\tilde{x} + \tilde{D}\ w - \tilde{u}\right)' W_u \left(\tilde{C}\tilde{x} + \tilde{D}\ w - \tilde{u}\right) + \alpha' W_e \alpha\right\} + \lambda'\left(\tilde{A}\tilde{x} + \tilde{B}_1 w + \tilde{B}_2 \alpha\right) \tag{6.7}$$

With Eq.(6.7), standard procedure of LQ optimal control derivation can be applied. Applying the first-order necessary condition to the Hamiltonian in Eq. (6.7) yields

$$\dot{\tilde{x}} = \tilde{A}\tilde{x} + \tilde{B}_1 w + \tilde{B}_2 \alpha \tag{6.8a}$$

$$\dot{\lambda} = -\tilde{C}' W_u \tilde{C}\tilde{x} - \tilde{A}'\lambda - \tilde{C}' W_u \tilde{D}\ w + \tilde{C}' W_u \tilde{u} \tag{6.8b}$$

$$\alpha = -W_e^{-1} \tilde{B}_2' \lambda \tag{6.8c}$$

Substituting (6.8c) into (6.8a) yields the corresponding homogeneous Hamiltonian system can thus be formulated as

$$\begin{bmatrix} \dot{\tilde{x}} \\ \dot{\lambda} \end{bmatrix} = \begin{bmatrix} \tilde{A} & -\tilde{R} \\ -\tilde{Q} & -\tilde{A}' \end{bmatrix} \begin{bmatrix} \tilde{x} \\ \lambda \end{bmatrix} + \begin{bmatrix} \tilde{B}_1 & 0 \\ -\tilde{C}'W_u\tilde{D} & \tilde{C}'W_u \end{bmatrix} \begin{bmatrix} w \\ \tilde{u} \end{bmatrix} \tag{6.9}$$

where in the Hamiltonian matrix

$$\tilde{R} = \tilde{B}_2 W_e^{-1} \tilde{B}_2' \tag{6.10a}$$

$$\tilde{Q} = \tilde{C}'W_u\tilde{C} \, . \tag{6.10b}$$

Then following the typical sweep method for the time-varying LQ design, one can assume the relation between co-state and state follows

$$\lambda(t) = \Pi(t)\tilde{x}(t) - g(t) \tag{6.11a}$$

Differentiation of the co-state in Eq. (6.11) yields an expression for $\dot{\lambda}$ , and in turn leads to the Riccatti differential equation as

$$\dot{\Pi}(t) + \Pi(t)\tilde{A} + \tilde{A}'\Pi(t) - \Pi(t)\tilde{R}\Pi(t) + \tilde{Q} = 0 \tag{6.11b}$$

$$\left[\tilde{A} - \tilde{R}\Pi(t)\right]'\mathrm{g} - \left[\tilde{C}'W_u\tilde{D}\Pi(t)\tilde{B}_1\right]w + \tilde{C}'W_u\tilde{u} = -\dot{g} \tag{6.11c}$$

with two equations for terminal points

$$\Pi(T) = C'PC \tag{6.11d}$$

$$-g(T) = \tilde{C}'PD_1w(T) - \tilde{C}'P\tilde{u}(T) \tag{6.11e}$$

Eventually, $\alpha$ can be obtained as

$$\alpha = -W_e^{-1}\tilde{B}_2'\lambda \tag{6.12}$$

Equation (6.11a) is used to find co-state trajectory $\lambda(t)$, with which the optimal $\alpha(t)$can be obtained.

The foregoing results give the finite horizon solution of LQBT which is usually tedious and difficult for practical use. More often, the steady-state solution is much easier for practical implementation, which can be obtained by solving an algebraic Riccatti equation (ARE)[103].In order to get steady-state LQ solution, converge to the positive semi-definite stabilizing solution of the following equation,

$$\tilde{A}'\Pi + \Pi\tilde{A} - \Pi\tilde{R}\Pi + \tilde{Q} = 0 \tag{6.13}$$

When T→∞, $\left(\tilde{A}, \tilde{R}, \tilde{Q}^{1/2}\right)$ is stabilizable and detectable. This is easy to achieve due to the strict positive definiteness of $W_u$ and $W_e$ and also the assumption of stabilizable and detectable controller.

The steady-state solution of $\alpha$ can be expressed as

$$\alpha = F\left[\tilde{x}' \quad w' \quad \tilde{u}'\right] \tag{6.14a}$$

And the constant matrix $F$ can be computed from reference [103], equation (6.10) and (6.11)

$$F = -W_e^{-1}\tilde{B}_2'\begin{bmatrix} \Pi \\ -\left[(\tilde{A}-\tilde{R}\Pi)^{-T}(\Pi\tilde{B}_1+\tilde{C}'W_u\tilde{D}_1)\right]' \\ \left[(\tilde{A}-\tilde{R}\Pi)^{-T})\tilde{C}'W_u\right]' \end{bmatrix}' \tag{6.14b}$$

## 6.3 Conditioned Transfer Techniques

The conditioned transfer techniques [77] is a classic bumpless transfer technique introduced to minimize the bump at the system input while at the same time guarantee a good tracking performance .

The conditioned transfer framework in [6] is followed in this study. As shown in

Figure 6.2, a proportional-integral-derivation (PID) feedback controller is considered, with input saturation included. The control input is thus

$$U(s) = K\left[E(s) + \frac{1}{sT_i}E(s) - \frac{sT_d}{1+s\frac{T_d}{N}}Y(s)\right] \tag{6.15}$$

where the proportional gain is denoted by $K$, $T_i$ and $T_d$ are the integral time constant and the derivative time constant respectively. The value of the high frequency gain N is typically set in the range of 7-15.

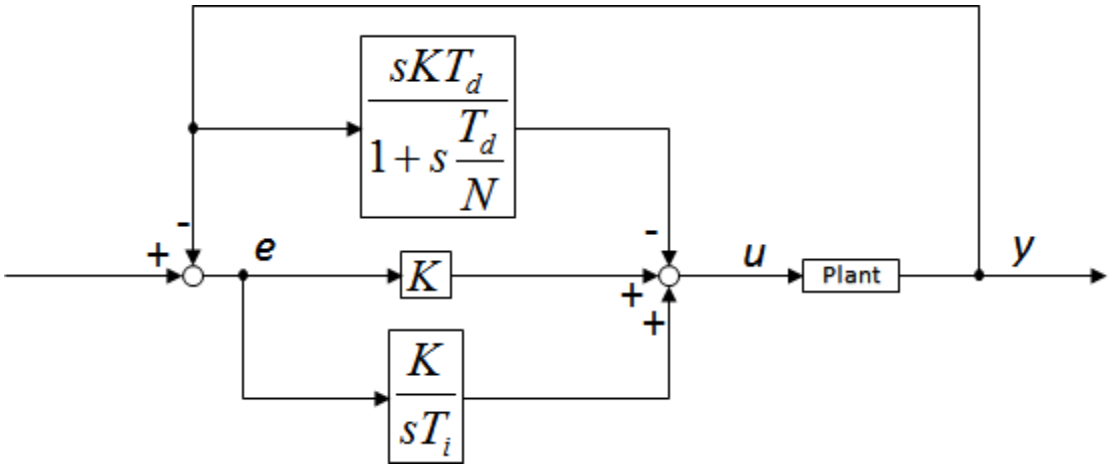


Figure 6.2 Configuration of PID Closed Loop System

The state-space realization of (6.15) can be formulated as

$$\dot{x} = w - y = e \tag{6.16a}$$

$$u = \frac{K}{T_i}x + Ke - y_d \tag{6.16b}$$

where,

$$Y_d(s) = \frac{sKT_d}{1+s\frac{T_d}{N}}Y(s) \tag{6.17}$$

Figure 6.3 shows the architecture of conditioning technique scheme. To apply conditioning technique approach, we use the so-called *realizable reference* $w^r$ instead of $w$. The realizable reference refers to the reference input such that if it were applied to the controller instead of the reference $w$, the controller output $u$ would be the same as the real plant input $u^r$ resulted from using reference $w$. If $w^r$ is applied to the controller instead of $w$, we can obtain

$$\dot{x}_c = w^r - y \tag{6.18a}$$

$$u^r = \frac{K}{T_i} x_c + K(w^r - y) - y_d \tag{6.18b}$$

where $x_c$ is the new controller state when using $w^r$.

As $w^r$ is not available in advance, $w$ is used to update $u$. Then $w^r$ can be obtained by

$$w^r = w + \frac{u^r - u}{K} \tag{6.19}$$

Substituting (6.19) to the state-space realization of the PID controller, the conditioning technique controller can be obtained as

$$\dot{x}_c = w - y + \frac{u^r - u}{K} \tag{6.20a}$$

$$u = \frac{K}{T_i} x_c + K(w - y) - y_d \tag{6.20b}$$

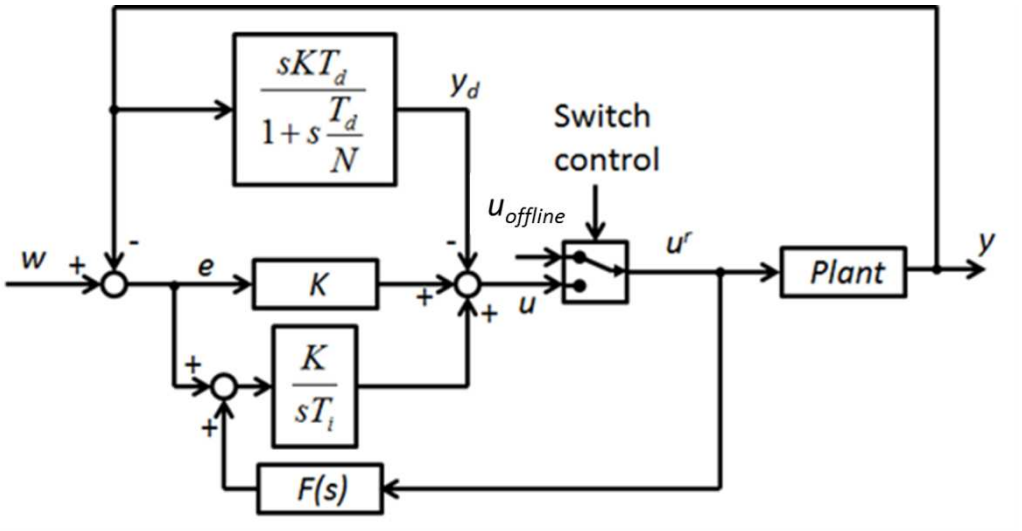


Figure 6.3 Configuration of Conditioning Technique based Bumpless Transfer

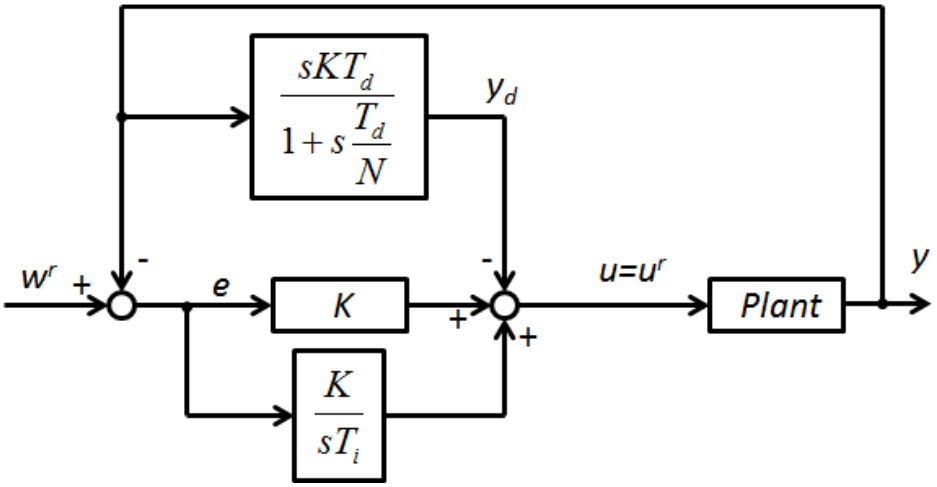


Figure 6.4 Equivalent Scheme of Realizable Reference

Introduce the realizable reference $w^r$, as shown in Figure 6.4, defined as when applied to the controller at the switching moment, the controller output $u$ would be equal to the offline controller $u_{offline}$. After offline controller is active, $u^r = u_{offline}$, output $y$ track realizable reference $w^r$. After controller is switched, $u^r = u$ and $y$ will track $w$ with the same dynamics as closed-loop step response if $w^r = w$. The equivalent scheme of realizable reference $w^r$ is shown in Fig 6.3b. From this assumption, $u^r$ can be given as

$$u^r = K\left(1+\frac{1}{sT_i}\right)w^r - K\left(1+\frac{1}{sT_i}+\frac{sT_d}{1+\frac{sT_d}{N}}\right) \tag{6.21}$$

When the compensator *F(s)* is defined as

$$F(s) = \frac{1}{K_a} \tag{6.22}$$

with $K_a$ is a prescribed constant, this configuration can be referred to as linear feedback anti-windup methodology. From Fig 6.3a, *u* can be obtained as

$$u = K\left(1+\frac{1}{sT_i}\right)w - K\left(1+\frac{1}{sT_i}+\frac{sT_d}{1+\frac{sT_d}{N}}\right)y + \frac{K}{sT_i}\left(\frac{u^r-u}{K_a}\right) \tag{6.23}$$

Subtracting (6.23) from (6.21), $w^r$ has the expression as

$$w^r = w + \frac{K+sK_aT_i}{KK_a(1+sT_i)}\left(u^r-u\right) \tag{6.24}$$

When $K_a = K$, the above equation can be written as

$$w^r = w + \frac{1}{K}\left(u^r-u\right) \tag{6.25}$$

The offline controller is connected to the online controller's output based on the conditioning technique, in order to make plant output *y* track the reference input *w* with the same dynamics as the closed loop response. This switching method is called conditioned transfer (CT)[77].

Notice that, if the controller output *u* is made as close as possible to the controller output before switching, without explicitly considering the tracking performance, the

mode switching is called *bumpless transfer* (BT). A special case of linear feedback anti-windup algorithm when $K_a$ approaches to zero in Equ.6.22, also called Incremental algorithm[77], is a solution for BT. BT method can minimize the bump produced by the controller switching, however, the tracking performance cannot be guaranteed at the same time. According to [77], the settling time of closed-loop system is longer than CT.

Compared to BT, the CT method is designed to have a better tracking performance with a small but not minimized bump during the switching. Based on above analysis, the configuration of CT and BT scheme can be obtained as Fig. 6.3.

Thus after controller is switched, $u^r = u$, realized reference $w^r$ will be equal to actual reference $w$. Therefore, the best tracking performance is achieved by CT method. From the standpoint of minimizing the bump to zero during the switch (BT), the $K_a$ should be chosen as $K_a \to 0$ [70, 77, 104].

## 6.4 Bumpless Transfer based Switching of Inter-Region Controllers

For the variable speed generator, the load torque can be regulated via generator control directly, thus the rotor speed can vary between certain ranges. The advantage of variable speed turbine is that, in Region 2 operation, the rotor speed can be adjusted in proportion to the wind speed in order to operate at the tip speed ratio (TSR) of maximum power coefficient, i.e. $C_{p,\max}$ (Fig.6.5).The turbine can thus capture maximum energy from wind. Notice that, under the variable speed operation, the optimal pitch corresponding to the maximum power yield would not change that much. Therefore, in this study, the pitch tuning is omitted, assuming that the optimum pitch is known *a priori* through other procedure.

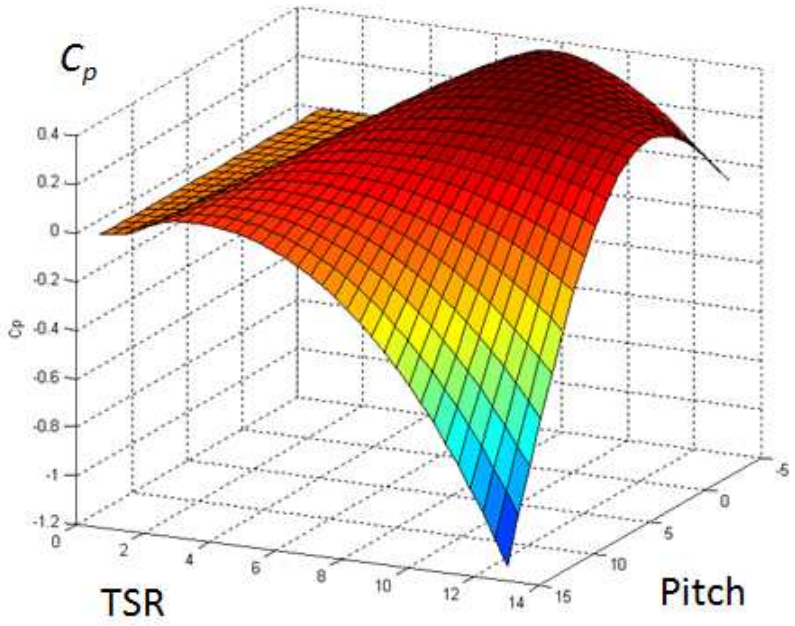


Figure 6.5 Relationships between Power Coefficient, TSR and Pitch Angle

Once the rated torque is reached, turbine will start to accelerate, as the load torque will not increase any more. The pitch control is then used to regulate the rotor speed, with the load torque held constant. Thus, the turbine control is switched from Region 2 generator control to Region 3 pitch control.

To bridge the Region 2 to Region 3 control, the so-called *Region 2.5* operation has been developed[105]. Observation of Region-2 and Region-3 controllers tells that a jump occurs for the generator toque reference. The Region-2.5 control law is generally designed to increase the generator torque in order to regulate the rotor speed instead of maintaining the torque at the optimal power point operation. Regarding the switching between the Region-2, Region-3 and Region-2.5 controllers, there are transition jumps for the generator torque reference. The switching point between the Region 2 to Region 2.5 can be determined by the rotor speed. The controllers provide optimal TSR control under the rated rotor speed and regulate the rotor speed with generator torque to maintain

the rated rotor speed. The switching point between Region 2.5 and Region 3 is set where the generator torque reaches the rated value, thus the controller will be switched from the torque control to the pitch control. The schematics of the different region controllers are shown in Fig. 6.6.

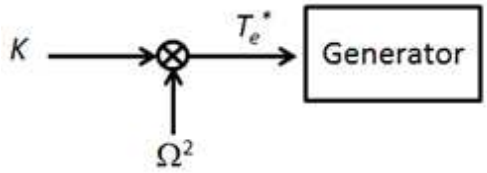


(a) Region 2 Control

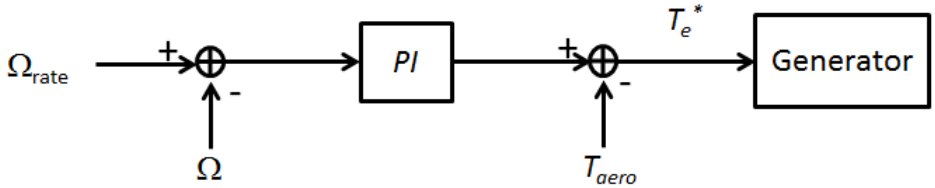


(b) Region 2.5 Control

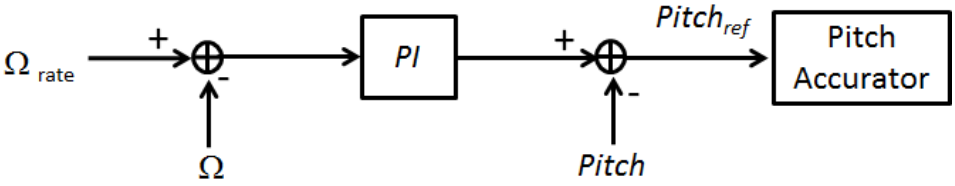


(c) Region 3 Control

Figure 6.6 Control Schemes for Three Regions of Wind Turbine Operation

Plots (a) and (b) in Fig. 6.6 show that switching between Region 2 and Region 2.5 is merely switching between two torque controllers without change of the system dynamics. Therefore, the condition transfer method is adopted for this case. For the switch from Region 2.5 to Region 3, the torque controller become off-line and the pitch controller becomes online. Whereas, from Region 3 back to Region 2.5, the pitch controller becomes off-line, and the torque controller is switched back on. The LQ bumpless transfer is chosen to handle this switching.

Following the LQ bumpless transfer and conditioned transfer methods described in Sections6.2 and 6.3, the inter-region control switching schemes are developed as shown in the following figures. Figure 6.7 shows the block diagram for the torque controller switching between Region 2 and Region 2.5. The output *y* in this case is the rotor speed feedback. After the rotor speed reaches the Region-2.5 set-point, operation will switch from the Region-2 torque controller (the optimal torque-gain control) to the Region-2.5 torque controller to limit the rotor speed. In next section, both the BT and CT techniques are applied to evaluate their respective performance. Figure 6.8 shows the torque-pitch controller switching from Region 2.5 to Region 3. In this case, the online controller is the fine pitch, while $\Omega_{ref}$ refers to the speed reference, output *y* is the turbine rotor speed, and *u* refers to the pitch angle command. When the speed set-point of Region 3 is reached, the pitch control will switch from fine pitch to pitch controller to regulate the rotor speed.

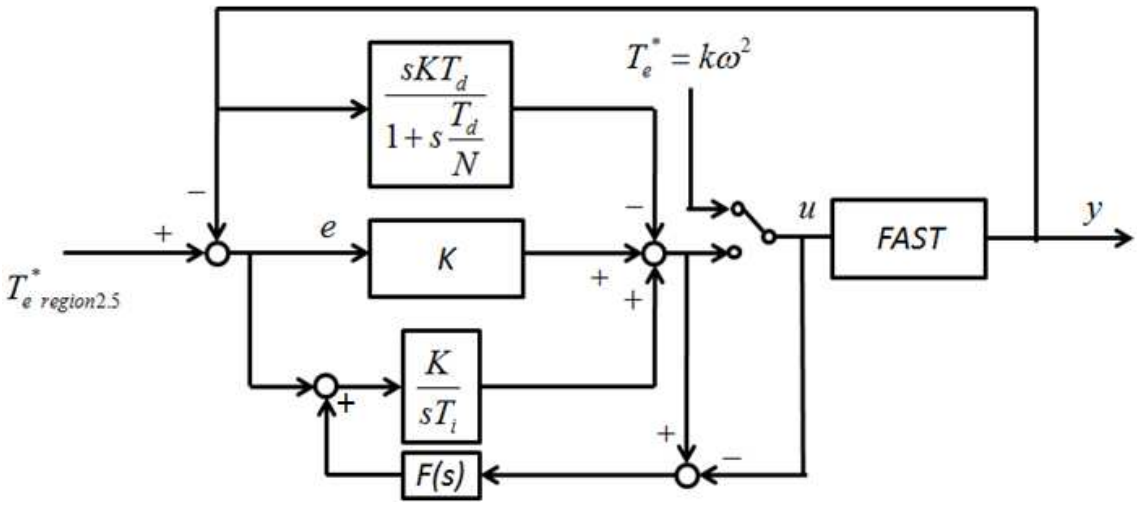


Figure 6.7 Bumpless Transfer Torque Control Switching from Region 2 to Region 2.5

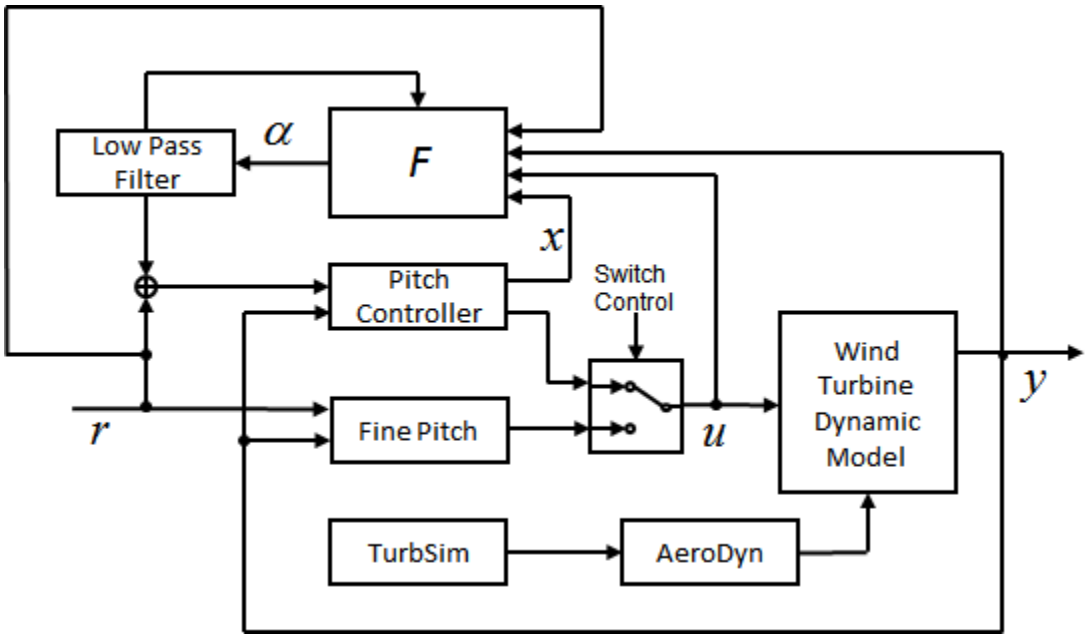


Figure 6.8 Torque-Pitch Controller Switching from Region 2.5 to Region 3

## 6.5 Simulation Study

The proposed bumpless transfer control strategy is evaluated via simulation study (more details is given in Appendix A.6, A.7). The turbine model studied for simulation the CART (Control advanced Research Turbine) facility located at the National Renewable Energy Laboratory in Golden, Colorado. The CART facility is a two-blade, active-yaw 600kW variable speed variable pitch turbine [27], and extensively modified for a test bed to study wind turbine controls. The generator model used in this study is a 600kW, 4-pole Doubly Fed Induction Generator (DFIG) as listed in Table 6.1.

Table 6.1 Parameters of the Simulated DFIG

| | |
|---|---|
| Rated power | 600 kW |
| Stator voltage | 220V |
| Frequency | 60 Hz |
| Stator resistance, $R_s$ | 5 Ω |

| | |
|---|---|
| Rotor resistance, $R_r$ | 1.01 Ω |
| Stator cyclic inductance, $L_s$ | 0.341 H |
| Rotor cyclic inductance, $L_r$ | 0.060 H |
| Mutual cyclic inductance, $M$ | 0.135 H |

The simulation platforms includes FAST v7.0[78], TurbSim V1.50[80], AeroDyn v13[79] developed by NREL for wind turbine simulation, interfaced with Matlab®2009a, Simulink® 7.5 and SimPowerSystems™ 5.2.1 developed by Mathworks. TurbSim creates wind files while AeroDyn takes the wind files data from TurbSim and calculate the aerodynamic loads of the turbine. FAST takes the aerodynamic loads and applies it to the nonlinear wind turbine model to calculate the equation of motion. AeroDyn in turn takes information about the turbine and recalculates the aerodynamic loads. The controller takes measurements from FAST produce the control signals send to generator model and connect to the grid in SimPowerSystems. The generator torque and pitch actuator output is then sent back to FAST.

First, a scenario of switching from Region 2 to Region 2.5 is simulated to evaluate the effectiveness of the conditioned transfer and bumpless transfer described in the previous section. In this simulation, the PID controller parameters in Fig. 6.4 are set as follows: $K$ = 200, $N$ = 10, $T_i$ = 10 and $T_d$ = 0.1. Figure 6.7 shows the ramp change of wind speed from 10 m/s to 12m/s in 50 seconds starting at $t$ = 100second. The control switches from Region 2 to Region 2.5 when the rotor speed exceeds the rated value (41.7 rpm). Transient of the rotor speed in Fig. 6.9is quite smooth due to the large inertia of the turbine rotor. In comparison, as shown in Fig. 6.10, the rotor torque and rotor power

demonstrate significant chattering, and thus large power flicker emission can be expected.

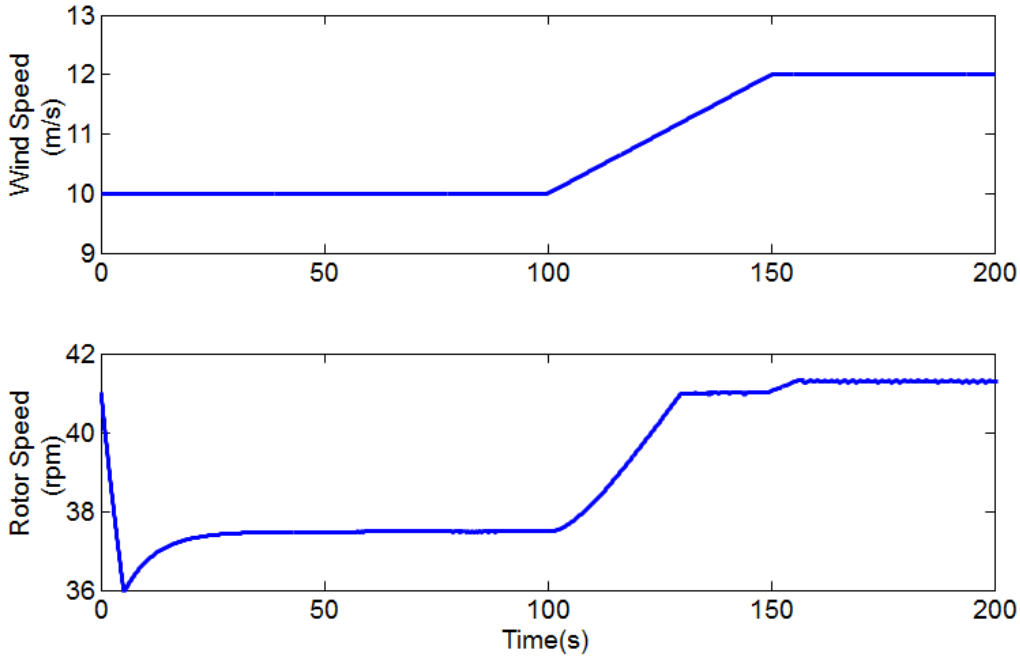


Figure 6.9 Ramp Wind Input and Rotor Speed for Simulating Controller Switching

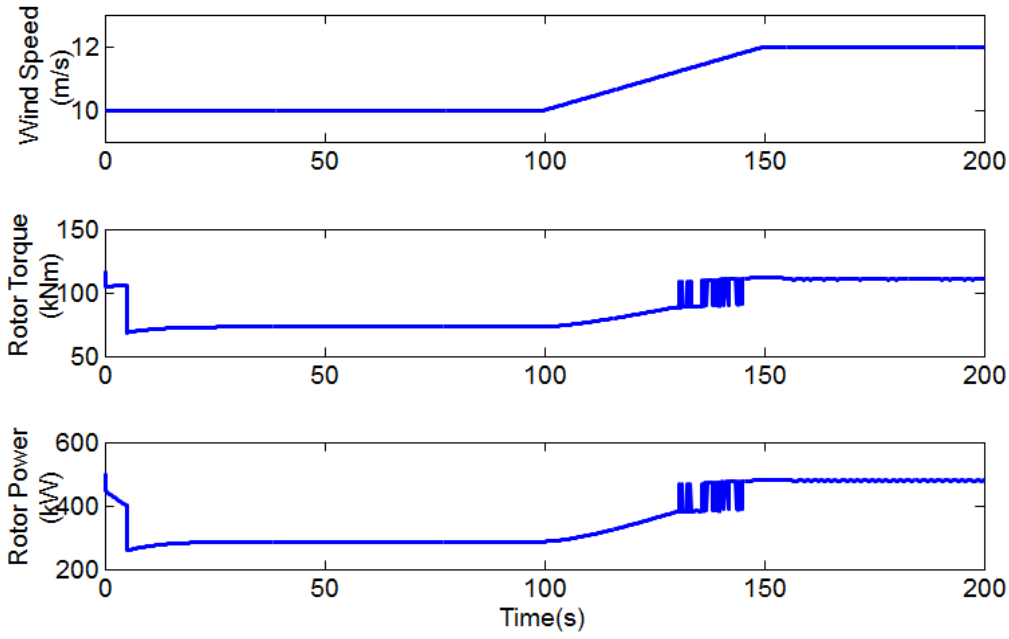


Figure 6.10 Rotor Torque and Power Fluctuation during Ramp Wind

Then the conditioned transfer and bumpless transfer scheme are applied to the

controller switch, with the compensator (in equation 6.23) is set to $K_a$ = 200 for CT method and $K_a$ = 0.1 for BT method. Significant improvement is observed for the switching transient in the rotor torque and rotor power, as shown in Fig. 6.11. Also, the differences between CT and BT are revealed. The CT method will track the reference input with the same dynamics as the off-line controller closed loop response. In this case, the rotor speed setpoint (41 rpm) for switching is a little bit smaller than Region-2.5 control setpoint (41.7 rpm). The dip observed for both rotor torque and power is due to the rotor speed at the switching is less than the setpoint. This descent also helped turbine to pass the switching point and avoid frequent switching between the two regions. In contrast, the BT method shows a better transient with much less overshoot. This is because the BT controller directly drives the torque to the corresponding torque for 12 m/s wind without the interregional dynamics.

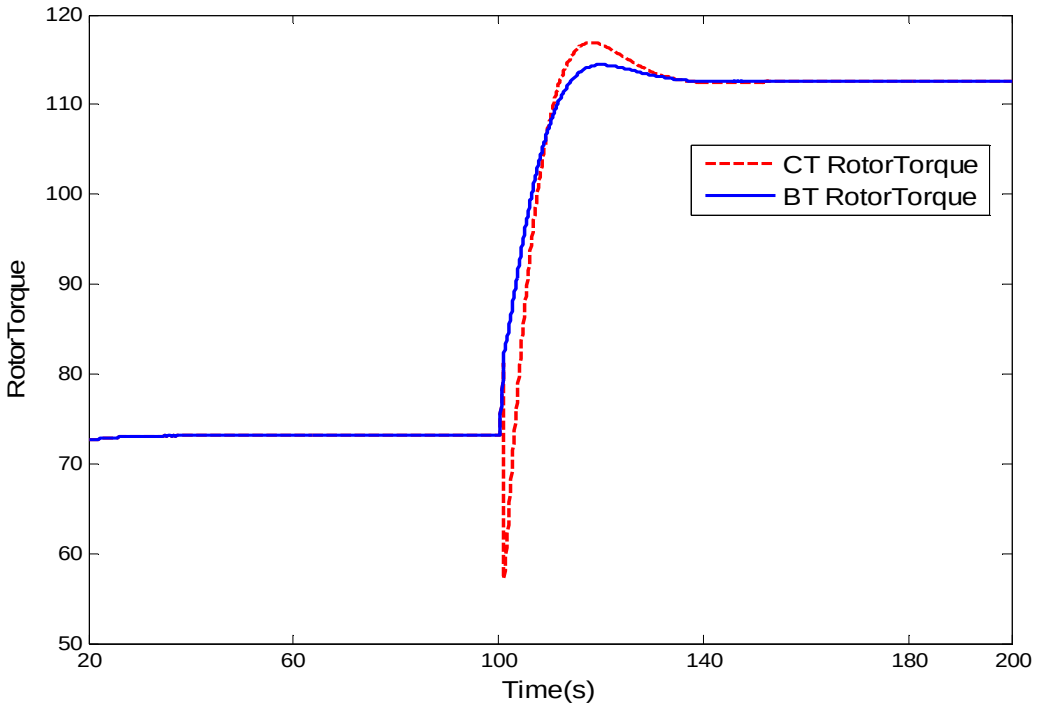


(a) Rotor Torque Profile

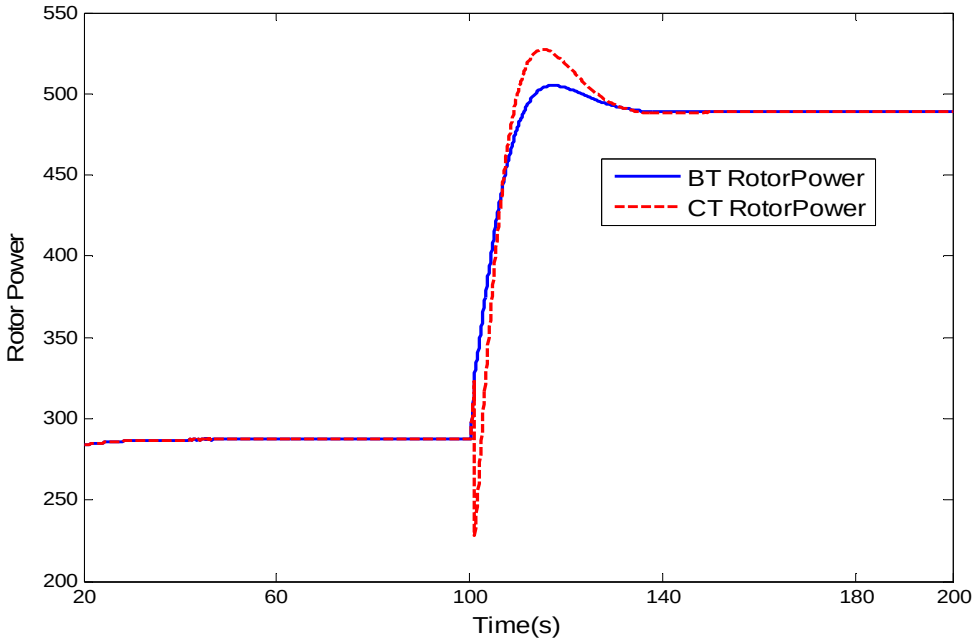


(b) Rotor Power Profile

Figure 6.11 Simulation Results for Switching From Region 2 to Region 2.5

Then, a scenario of switching from Region 2.5 to 3 is simulated. The illustrative wind ramps up from 10m /s up to 14 m/s in 1 second, starting at $t$ = 100 second, as shown in Fig. 6.10. Following the LQ bumpless transfer design described in the previous section, the compensator matrix solved by Eq. (6.21) is

$$F = \begin{bmatrix} -0.027 & 0.0058 & 0.0229 & 0.1321 & -0.1321 & -0.3333 \end{bmatrix}' \tag{6.21}$$

$W_e$ and $W_u$ are chosen to be 5 and 0.5, respectively.

A unity gain first-order low-pass filter is adopted for the LQ bumpless transfer design. The effect of the low-pass filter bandwidth is evaluated as shown in Fig.6.12. Plot (a) shows the Bode plots of the low-pass filter with different time constants. The corresponding profiles of pitch angle and pitch rate are shown in plot (b). The time constant of the first-order low-pass filter should be carefully chosen. As can be seen from

Fig. 6.12(b), relatively smaller time constant will result in oscillating transient after the switch. When the LQBT compensator is switched off, a step change will be introduced in the reference of the controller, if the low-pass filter were not applied, or if the time constant of the low-pass filter is too small, significant transient would appear in the controller output. On the other hand, a too large time constant of low-pass filter will introduce delay in response, as shown in Fig. 6.10(b).

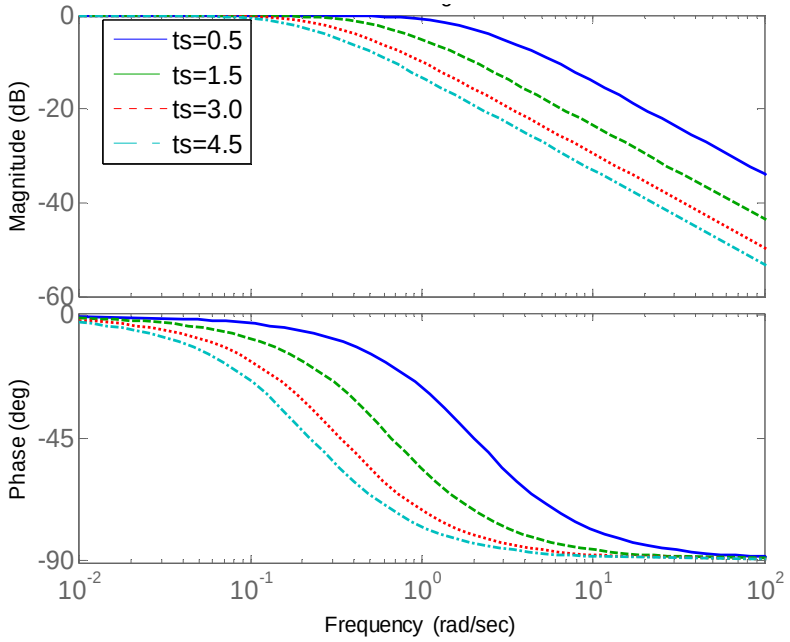


(a) Bode Plot of the Designed Low-pass Filter (ts = 1.5)

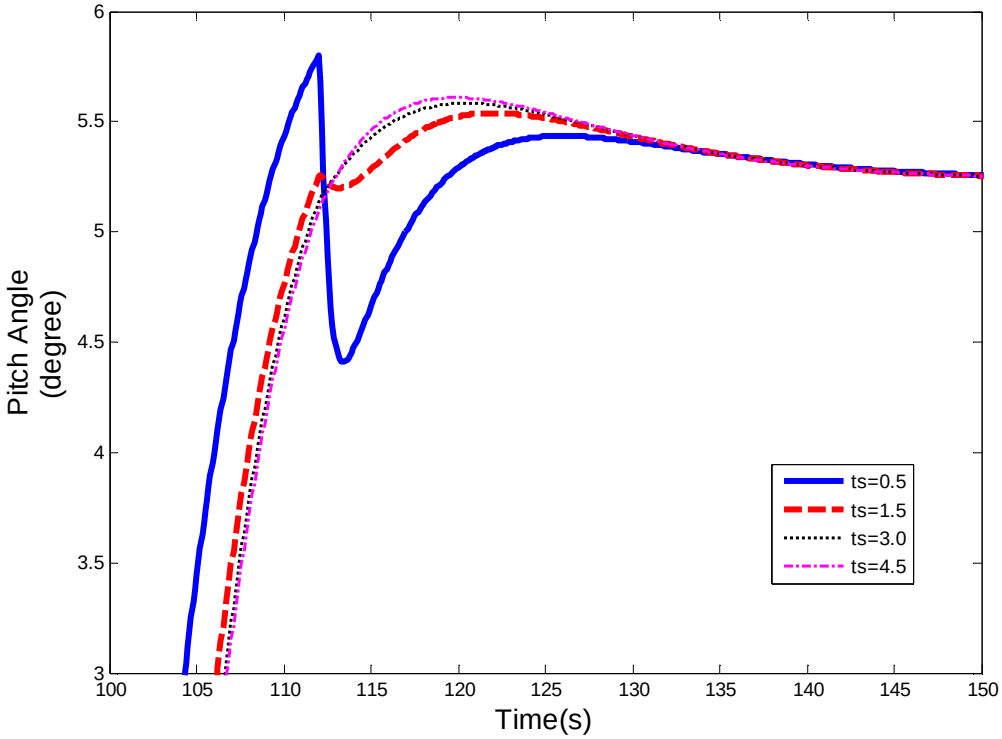


(b) Comparison of Different Low-pass Filter Design

Figure 6.12 Low-Pass Filter Design in LQ Bumpless Transfer

After considering the results in Fig. 6.10, ts = 3.0 second is chosen as the time constant of the low-pass filter, which leads to the simulation results in Fig. 6.11. The overshoot of the pitch angle is reduced by14.77%, from 6.5° to 5.54°. Meanwhile, the system has a quicker response to the wind variation. Compared to the simulation without bumpless transfer, the pitch control is triggered from 119.3 second, the LQBT pitch angle start to increase from 102.5 second on, which will result in a lower structure load during the region switching operation.

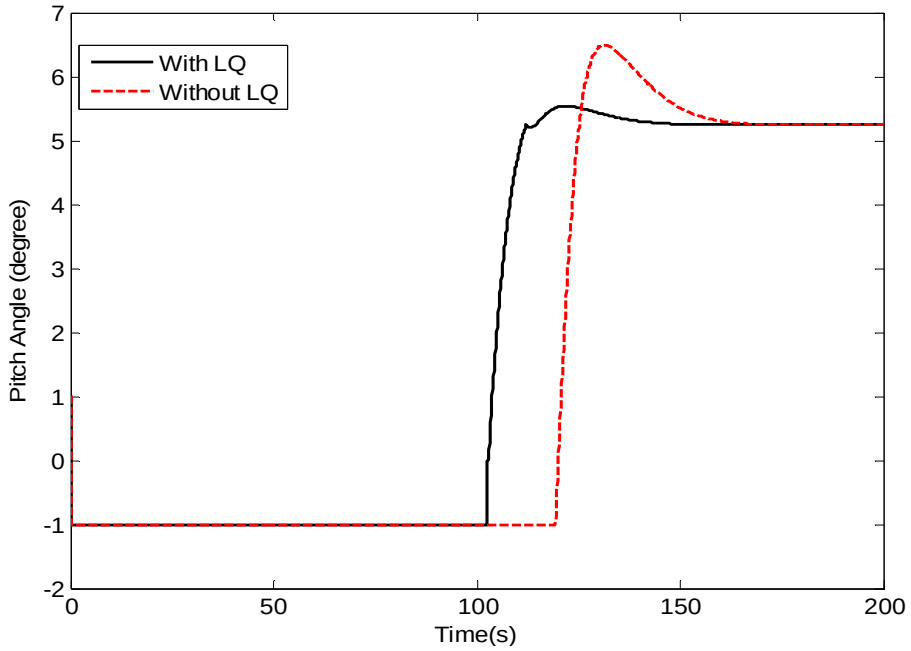


(a) Pitch Angle Signal Comparison

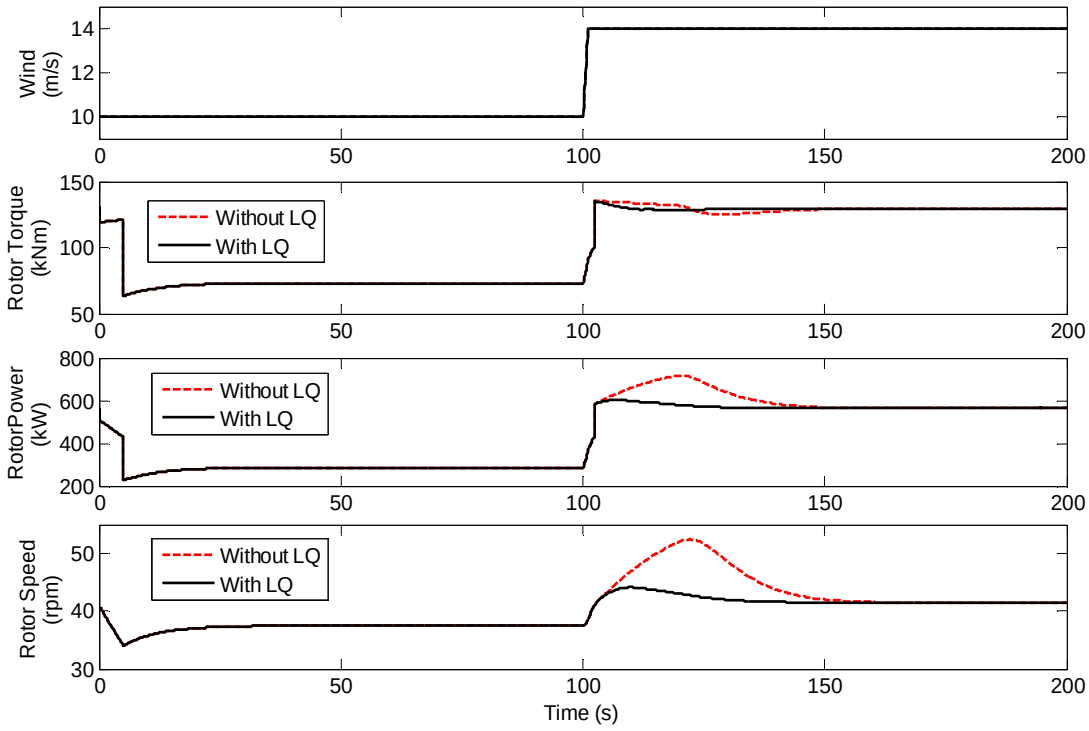


(b) Rotor Speed and Power of LQBT Simulation with Smooth Step Wind

Figure 6.13 LQ Bumpless Transfer for Switching from Region 2 to Region 2.5

The flicker emission of the turbine during the controller switching was then evaluated based on voltage fluctuation. The flicker level measures the annoyance level a human eye perceives when the reference lamp is powered by fluctuating voltage source [9, 10]. A high flicker level will affect the lighting system and cause a flicker that affects eye perception. The flicker level is computed by feeding the voltage time series into the flickermeter calculation from the IEC 61000-4-15. The flicker level is evaluated by calculating the short-term flicker severity $P_{st}$. For this case study, the short-term flicker severity for smooth and turbulent wind is shown in Fig. 6.13.

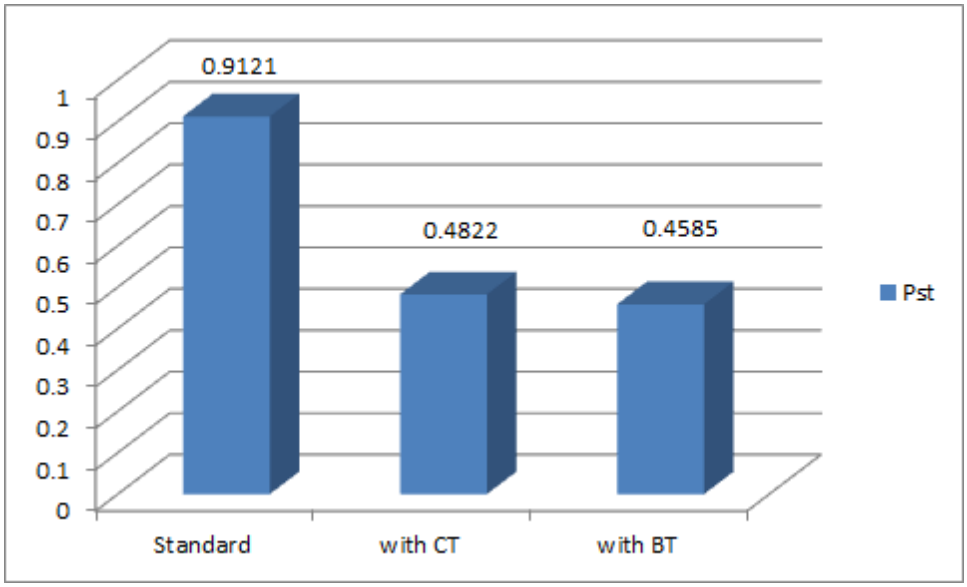


(a) Smooth Wind Simulation

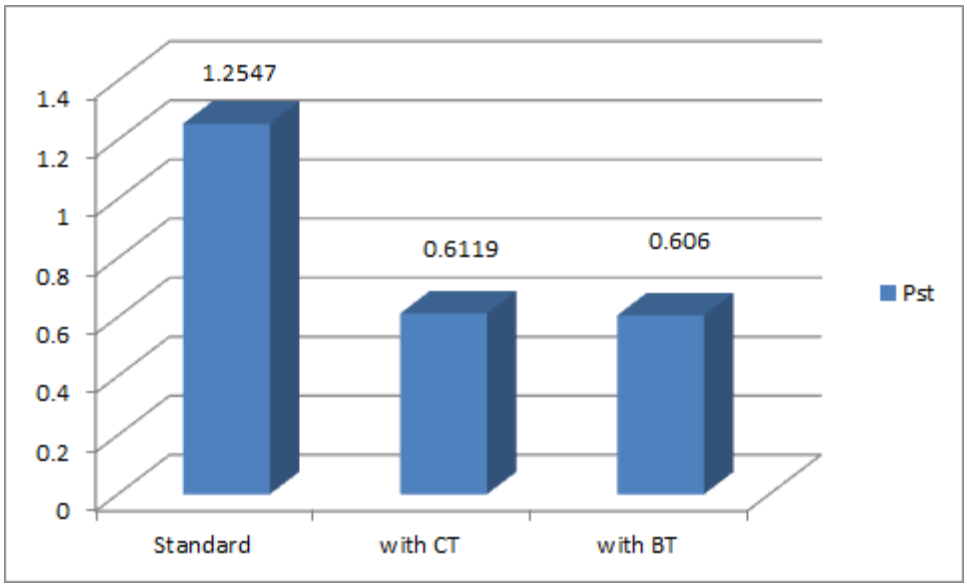


(b)Turbulent Wind Simulation

Figure 6.14 Short-term Flicker Severity $P_{st}$ with Smooth Ramp Wind Simulation

From Fig. 6.14(a), with BT method, the short-term flicker severity can be reduced by 49.73% compared to the standard control method. Also, the short-term flicker severity can also be reduced by 47.13% using the CT method. The BT method shows a better performance although not much in short-term flicker severity test than the CT method. This is due to BT method designed to passing the controller output as close as possible to the controller output before switching thus deliver a bumpless controller switching. The simulation is then evaluated for the same ramp wind, but with2% turbulence intensity added. The simulation result shows both methods will dramatically reduce the short-term flicker severity. Similar to smooth wind case, BT can reduce the short-term flicker severity by 51.70%, a little bit higher than CT method which reduces the flicker by 51.23%.

With proposed switching control method the transient can be minimized during the switching operation base on the above power fluctuation analysis. As fatigue loading is

critical for the reliability of wind turbines, it is important to inspect the load variation comparison of standard control method and the switching control method. In this study, NREL's MCrunch [102] was used to analyze the fatigue load change associated with switching control method of wind turbine. The S-N slope was set at 10 for blades with composite material. The damage equivalent loads (DEL) were calculated for the blade-root flap-wise and edge-wise bending moments, and also tower-base side-to-side and fore-after bending moments. The DELs using the standard control method and the proposed switching control methods are compared in Fig. 6.15. Compared to the standard control method, the CT and BT methods can reduce the blade-root flap-wise bending moment by 52.99%, while for the edge-wise moment, there is only slight improvement. For the tower-base load analysis, the CT and BT method can reduce the fore-aft moment by 53.03% while the reduction of the side-to-side moment is small.

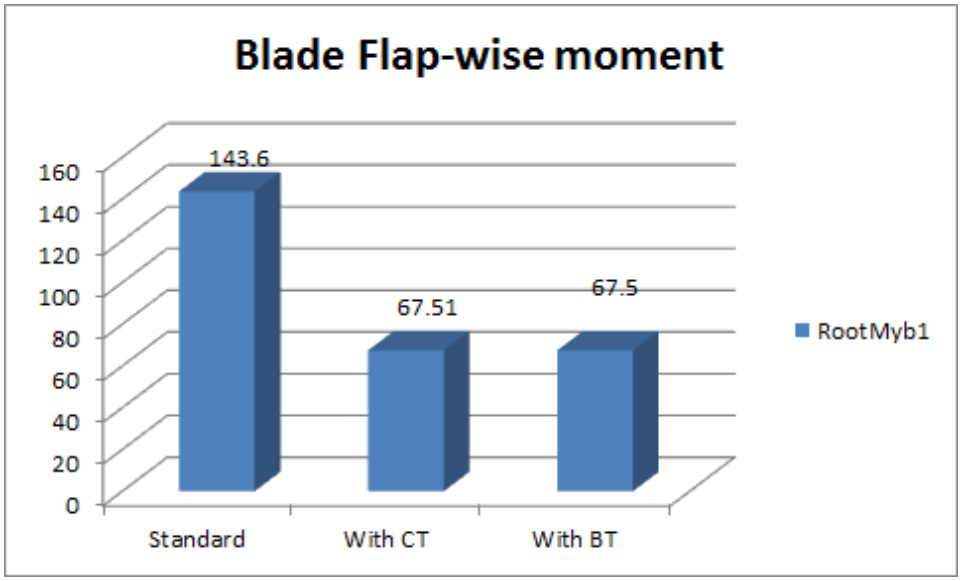


(a) DEL Comparision for Blade-root Flap-Wise Bending Moment

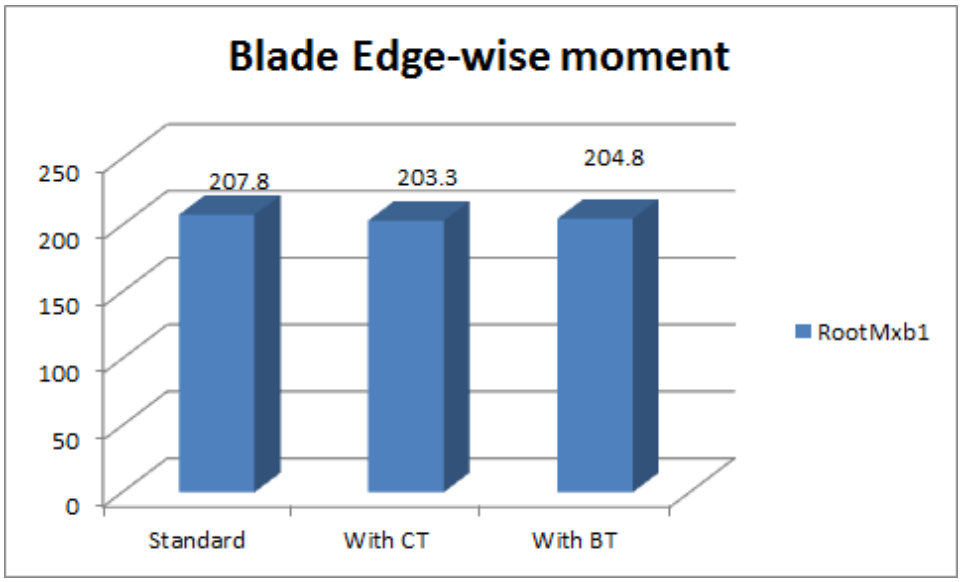


(b) DEL Comparisions for Blade-root Edge-wise Bending Moment

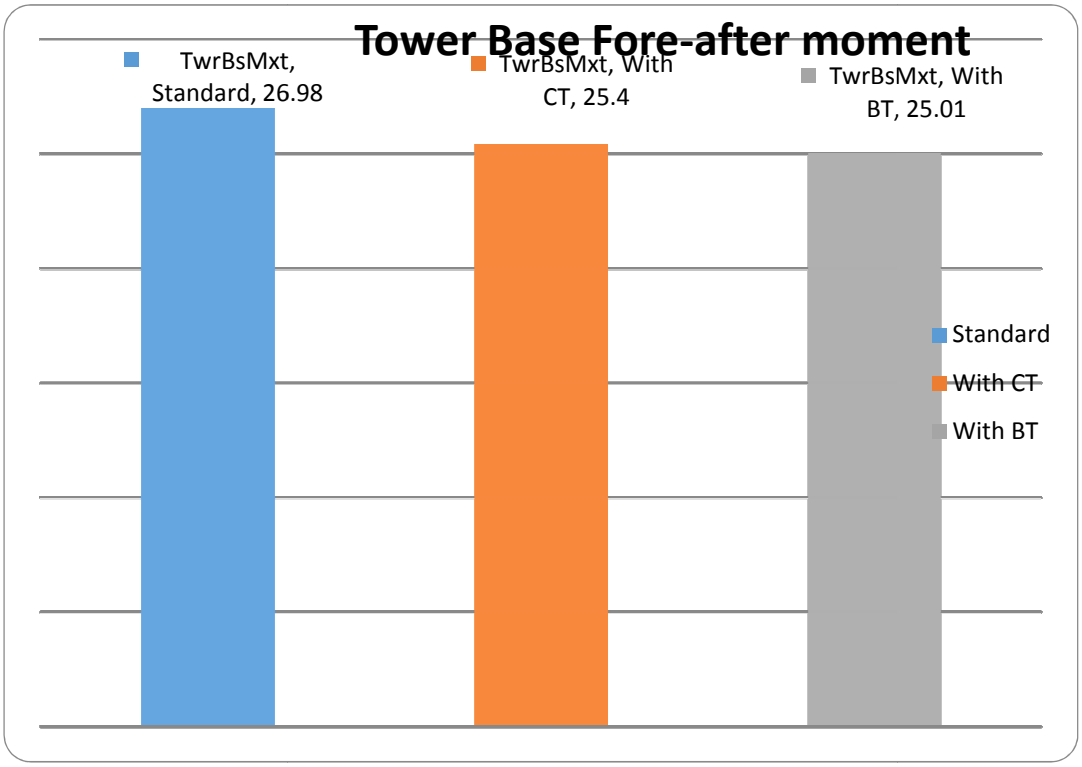


(c) DEL Comparisions for Tower-base Fore-aft Bending Moment

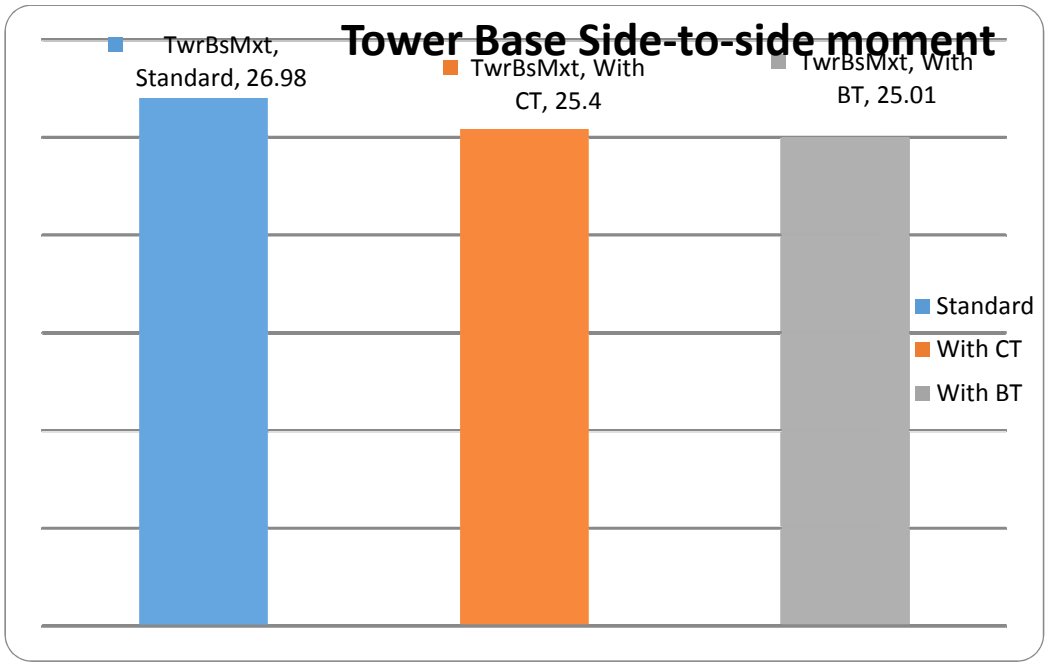


(d) DEL Comparision for Tower-base Side-to-side Bending Moment

Figure 6.15 Damage Equivalent Loads (DEL) with and without Bumpless Transfer

## 6.6 Summary

In this chapter, an inter-region controller switching scheme is developed for variable speed wind turbine based on two types of bumpless transfer techniques. The conditioning technique is applied to drive a bumpless transfer during the switch from Region 2 maximum power capture control to Region 2.5 generator torque control. The LQBT technique is used to reduce the transient at the switch between torque controller in Region 2.5 and the pitch controller in Region 3.

The simulation results have validated the effectiveness of the proposed controller switching scheme. The power fluctuation is significantly reduced by the proposed inter-region switching approach. The flicker level is evaluated and the results indicate the proposed method can minimize the flicker emission during the switching operation of

wind turbine. The damage equivalent load analysis shows the CT and BT method can largely reduce the flap-wise blade root moment and the fore-after tower base moment.

# 7. Conclusions and Future Work

This chapter concludes the contribution of this thesis research and points out the possible future work.

## 7.1 Summary of Research Contribution

Wind power draw a great attention in recent decades and become the most promising renewable energy source in the U.S and worldwide. Modeling and simulation of wind energy conversion system is an important topic both for advanced control system design and validation. The multi-physical nature of the wind energy system, the uncertainties in the model and unpredictable wind fluctuation require the development of advanced control methods to deal with. In this research study, the main contribution can be concluded as the following three sub-topics. This thesis studied the synergy of a multi-domain simulation platform for wind energy system controls. The simulation studies of wind turbine control system have been based on the program codes provided by NREL. The simulation modeling covers from wind turbine aerodynamics, wind turbine aeroelastics and drivetrain dynamics, to power generation of a doubly-fed induction generator. The generator control simulation is developed with Simulink SimPowerSystems™ and Robust Control Toolbox™, developed by Mathworks©. The wind data are field wind measurements provided by NREL. Multi-physical simulation capability from aerodynamics to power electronics is very valuable for control oriented study of wind energy conversion system.

### 7.1.1 Self-optimizing Robust Control of Power Capture for DFIG Wind Turbines

The second contribution of this study is to apply a self-optimizing robust control scheme for maximizing the power generation for a variable speed wind turbine with DFIG. The control system consists of two control loops. The outer loop is generator torque regulation for maximum wind power capture via the rotor power feedback based on ESC method. Compared with previous torque control methods, ESC based torque control is less dependent on the accuracy of the wind turbine model and wind speed measurement. The benefit of the ESC algorithm is that it searches for the optimal generator torque to maximize the rotor power considering the variation of the power map. The inner loop is vector control schemes of generator control via PWM converters. An $\mathscr{H}_\infty$ controller is synthesized with performance weight defined with the spectrum of the rotor power obtained by the ESC. Therefore, the $\mathscr{H}_\infty$ controller maximizes the energy conversion from the rotor power to grid power. At same time, this controller is robust against the variations of associated uncertainties in the generator system. Simulation results have initially sustained the proposed scheme. The simulation based on the synergy of multiphysical simulation convinces the proposed method performs better energy conversion efficiency under various wind condition.

### 7.1.2BumplessTransfer based Inter-Region Controller Switching

The third contribution of this study is to the design of the inter-region switching control for variable speed wind turbine. This method focuses on improving the power quality of wind energy within Region 2 and 3 operation, which is strongly affected by the fluctuated wind. Two different bumpless transfer methods are presented to deal with different switch scenarios during the region operation. The conditioning technique is posed to

drive a bumpless transfer during the switch from Region 2 maximum power capture control to Region 2.5 generator torque control. The LQ bumpless transfer technique is used to reduce the transient at the switch between torque controller in Region 2.5 and pitch controller in Region 3.The simulation results validate the effectiveness of the presented switching control method. The power fluctuation is greatly reduced by the proposed inter-region switching approach compared other control methods without switching control procedure.

## 7.2 Suggested Future Work

In this thesis research, ESC based self-optimizing scheme is developed for maximizing power capture for DFIG based wind turbine. DFIG based wind energy conversion system are popular for its highly controllable characteristic and allowing large range power capture operation as well as decoupled control of active and reactive power. Beyond doubly-fed induction generator, permanent-magnet synchronous generator (PMSG) has also drawn a lot of attention in wind energy practice, as a promising solution to direct drive wind energy systems [1]. A major advantage of PMSG based wind turbine is the gearbox can be removed, due to the salient pole of PMSG operating at low speeds. Thus not only can the cost be reduced, but also the whole system becomes more reliable. Although its operation is similar to that of DFIG based wind turbine, the AC-DC-AC power inverter of PMSG is rated to the generator power, compared to the case of DFIG where the inverter is rated to only a fraction of the rated power [106].

In this study, Extremum seeking control method is presented for torque control to maximize the rotor power output of a variable speed wind turbine. In our ESC application, sinusoidal perturbations are injected into the system to drive it to an

extremum operating point. Other than sinusoidal perturbations, there are other perturbation methods can be considered for ESC especially for wind energy conversion system. Ripple correlation control (RCC) [107] is a real-time optimization technique utilized high-frequency ripple in the power electronics system to searching for optimization of the dynamic system. Compared to sinusoidal perturbations injection of classic ESC approach, the RCC technique makes use of inherent high-frequency ripple in the converter system of wind turbine. Also, there are several other self-optimizing control strategies that deserve further investigation their application into the wind turbine energy capture control, e.g. switching ESC, sliding mode ESC, adaptive ESC, simultaneous perturbation stochastic approximation, among others.

This thesis study has been simulation based. Success of the proposed control schemes indicated that it is worthwhile to pursue experimental study to further evaluate and improve the control algorithms so as to push the relevant technology towards practice.

# References


[1] I. Munteanu, A.I. Bratcu, N.A. Cutululis, and E. Ceanga, *Optimal Control of Wind Energy Systems: Towards A Global Approach*: Springer Verlag, 2008.

[2] R. Pernick, C. Wilder, and T. Winnie, "Clean Energy Trends," March 2012. Available: http://www.cleanedge.com/sites/default/files/CETrends2012_Final_Web.pdf.

[3] Global Wind Energy Council, "Global Wind Report Annual Market Update," 2012. Available: http://www.gwec.net/wp-content/uploads/2012/06/Annual_report_2012_LowRes.pdf.

[4] Office of Energy Efficiency and Renewable Energy U.S. DOE. (2008). 20% Wind Energy by 2030. [Online]. Available: http://www1.eere.energy.gov/windandhydro/pdfs/41869.pdf.

[5] NREL, "Big Horn Wind Farm," Bickelton, Washington. Available: http://images.nrel.gov/viewphoto.php?&albumId=207429&imageId=6327792&page=6&imagepos=60&sort=&sortorder=.

[6] K.E. Johnson, "Adaptive Torque Control of Variable Speed Wind Turbines," National Renewable Energy Lab, Golden, CO, NREL/TP-500-36265, 2004.

[7] F. Bianchi, H. De Battista, and R. Mantz, *Wind Turbine Control Systems: Principles, Modelling and Gain-scheduling Design (Advances in Industrial Control)*: Springer, 2006.

[8] T. Sun, Z. Chen, and Blaabjerg F., "Flicker Study on Variable Speed Wind Turbines with Doubly Fed Induction Generators," *IEEE Transactions on Energy Conversion*, vol. 20(4), pp. 896-905, 2005.

[9] A. Larsson, "Flicker Emission of Wind Turbines during Continuous Operation," *IEEE Power Engineering Review*, vol. 22(2), p. 59, 2007.

[10] A. Larsson, "Flicker Emission of Wind Turbines Caused by Switching Operations," *IEEE Transactions on Energy Conversion*, vol. 17(1), pp. 119-123, 2002.

[11] N.W. Miller, J.J. Sanchez-Gasca, W.W. Price, and R.W. Delmerico, "Dynamic Modeling of GE 1.5 and 3.6 MW Wind Turbine-Generators for Stability Simulations," in *Proceedings of the 2003 IEEE Power Engineering Society General Meeting*, vol. 3, pp. 1977-1983.

[12] M. A. Poller, "Doubly-Fed Induction Machine Models for Stability Assessment of Wind Farms," in *Proceedings of the 2003 IEEE Power Tech Conference*, Bologna, Italy, vol. 3, p. 6.

[13] Y. Lei, A. Mullane, G. Lightbody, and R. Yacamini, "Modeling of the Wind Turbine with a Doubly Fed Induction Generator for Grid Integration Studies," *IEEE Transaction on Energy Conversion,* vol. 21(1), pp. 257-264, 2006.

[14] F.M. Hughes, O. Anaya-Lara, N. Jenkins, and G. Strbac, "Control of DFIG-based Wind Generation for Power Network Support," *IEEE Transactions on Power Systems,* vol. 20(4), pp. 1958-1966, 2005.

[15] I. Erlich, J. Kretschmann, J. Fortmann, S. Mueller-Engelhardt, and H. Wrede, "Modeling of Wind Turbines Based on Doubly-Fed Induction Generators for Power System Stability Studies," *IEEE Transactions on Power Systems,* vol. 22(3), pp. 909-919, 2007.

[16] W. Leonhard, *Control of Electrical Drives*: Springer Verlag, 2001.

[17] A. Petersson, "*Analysis, Modeling and Control of Doubly-Fed Induction Generators for Wind Turbines*," Ph.D. Dissertation, Department of Energy and Environment, Chalmers University of Technology, 2005.

[18] D. Simms, S. Schreck, M. Hand, and L.J. Fingersh, "NREL Unsteady Aerodynamics Experiment in the NASA-AMES Wind Tunnel: A Comparison of Predictions to Measurements," *National Renewable Energy Laboratory, Golden, CO, Tech. Rep. NREL/TP-500-29494,* 2001.

[19] C. Ishii, H. Hashimoto, and H. Ohmori, "Modeling of Variable Pitch Micro Wind Turbine and Its Output Optimization Control with Adaptive Extremum Control Scheme," *Transactions of the Japan Society of Mechanical Engineers, Part C,* vol. 69(11), pp. 3034–3040, 2003.

[20] J. Creaby, Y. Li, and J.E. Seem, "Maximizing Wind Turbine Energy Capture using Multivariable Extremum Seeking Control," *Wind Engineering,* vol. 33(4), pp. 361-387, 2009.

[21] A.D. Wright, "Modern Control Design for Flexible Wind Turbines," National Renewable Energy Laboratory, Golden, CO, Technical Report NREL/TP-500-35816, 2004.

[22] T. Burton, D. Sharpe, N. Jenkins, and E. Bossanyi, *Wind Energy Handbook*. John Wiley & Sons, 2011.

[23] M.H. Hansen, A. Hansen, T.J. Larsen, S. Øye, P. Sørensen, and P. Fuglsang, "Control Design for a Pitch-Regulated, Variable Speed Wind Turbine," Risø National Laboratory, Denmark, Risø report R-1500, 2005.

[24] International Electrotechnical Commission, "Wind Turbines - Part 21: Measurement and Assessment of Power Quality Characteristics of Grid Connected Wind Turbines," International Standard IEC 61400-21, 2008.

[25] L.J. Fingersh and K.E. Johnson, "Controls Advanced Research Turbine (CART) Commissioning and Baseline Data Collection," National Renewable Energy Laboratory, NREL/TP-500-32879 2002.

[26] R. Gasch and J. Twele, *Wind Power Plants: Fundamentals, Design, Construction and Operation*: Springer, 2002.

[27] M.M. Hand, K.E. Johnson, L.J. Fingersh, and A.D. Wright, "Advanced Control Design and Field Testing for Wind Turbines " National Renewable Energy Laboratory, Golden, CO, NREL/CP-500-36118, Aug. 29 -Sep. 3, 2004.

[28] T. Ackermann, "Wind Power in Power Systems," *Wind Engineering*, vol. 30(5), pp. 447-449, 2006.

[29] V. Akhmatov, *Analysis of Dynamic Behaviour of Electric Power Systems with Large Amount of Wind Power*: Electric Power Engineering, Ørsted-DTU, Technical University of Denmark, 2003.

[30] T. Lund, P. Sørensen, and J. Eek, "Reactive Power Capability of A Wind Turbine with Doubly Fed Induction Generator," *Wind Energy*, vol. 10(4), pp. 379-394, 2007.

[31] M. Heller and W. Schumacher, "Stability Analysis Of Doubly-Fed Induction Machines in Stator Flux Reference Frame," in *Proceedings of the 1997 European Conference on Power Electronics and Applications*, vol. 2, pp. 2707-2710.

[32] R. Pena, R. Cardenas, G.M. Asher, J.C. Clare, J. Rodriguez, and P. Cortes, "Vector Control of a Diesel-driven Doubly Fed Induction Machine for a Stand-alone Variable Speed Energy System," in *the 28th Annual Conference of the IEEE Industrial Electronics Society*, 2003, vol. 2, pp. 985-990.

[33] H. Akagi and H. Sato, "Control and Performance of A Doubly-Fed Induction Machine Intended for a Flywheel Energy Storage System," *IEEE Transactions on Energy Conversion*, vol. 17(1), pp. 109-116, 2002.

[34] S. Li, R. Challoo, and M. J. Nemmers, "Comparative Study of DFIG Power Control Using Stator-Voltage and Stator-Flux Oriented Frames," in *Proceedings of the 2009 IEEE Power and Energy Society General Meeting*, pp. 1-8.

[35] W. Leonhard, "Field Oriented Control of a Variable Speed Alternator Connected to the Constant Frequency Line," in *Proceedings of the IEEE Conference on Control of Power Systems*, Houston, TX, 1979, pp. 149-153.

[36] R. Pena, J.C. Clare, and G.M. Asher, "Doubly Fed Induction Generator Using Back-to-back PWM Converters and Its Application to Variable-speed Wind-energy Generation," in *Proceedings of the IEE-Electric Power Applications*, 1996, vol. 143, pp. 231-241.

[37] Y. Tang and L. Xu, "A Flexible Active and Reactive Power Control Strategy for a Variable Speed Constant Frequency Generating System," in *Proceedings of the 24th Annual IEEE Power Electronics Specialists Conference*, 1993, pp. 568-573.

[38] B. Hopfensperger, D.J. Atkinson, and R.A. Lakin, "Stator-Flux-Oriented Control of a Doubly-Fed Induction Machine with and without Position Encoder," *IEE Proceedings of Electric Power Applications*, vol. 147(4), pp. 241-250, 2000.

[39] B.H. Chowdhury and S. Chellapilla, "Double-Fed Induction Generator Control for Variable Speed Wind Power Generation," *Electric Power Systems Research*, vol. 76(9–10), pp. 786-800, June, 2006.

[40] B. Hopfensperger, D.J. Atkinson, and R.A. Lakin, "Stator Flux Oriented Control of a Cascaded Doubly-Fed Induction Machine," *IEE Proceedings of Electric Power Applications*, vol. 146(6), pp. 597-605, 1999.

[41] L. Morel, H. Godfroid, A. Mirzaian, and J.M. Kauffmann, "Double-Fed Induction Machine: Converter Optimisation and Field Oriented Control without Position Sensor," in *Proceedings of the 1998 IEE-Electric Power Applications*, vol. 145, pp. 360-368.

[42] S. Wang and Y. Ding, "Stability Analysis of Field Oriented Doubly-Fed Induction Machine Drive based on Computer Simulation," *Electric Machines and Power Systems*, vol. 21(1), pp. 11-24, 1993.

[43] L. Xu and W. Cheng, "Torque and Reactive Power Control of a Doubly Fed Induction Machine by Position Sensorless Scheme," *IEEE Transactions on Industry Applications*, vol. 31(3), pp. 636-642, 1995.

[44] L. Xu and P. Cartwright, "Direct Active and Reactive Power Control of DFIG for Wind Energy Generation," *IEEE Transactions on Energy Conversion,*, vol. 21(3), pp. 750-758, 2006.

[45] D. Zhi and L. Xu, "Direct Power Control of DFIG with Constant Switching Frequency and Improved Transient Performance," *IEEE Transactions on Energy Conversion,*, vol. 22(1), pp. 110-118, 2007.

[46] L. Xu and Y. Wang, "Dynamic Modeling and Control of DFIG-Based Wind Turbines Under Unbalanced Network Conditions," *IEEE Transactions on Energy Conversion*, vol. 22(1), pp. 314-323, 2007.

[47] T. Brekken, N. Mohan, and T. Undeland, "Control of a Doubly-Fed Induction Wind Generator under Unbalanced Grid Voltage Conditions," in *Proceedings of the 2005 European Conference on Power Electronics and Applications*, 2005, pp. 1-10.

[48] F. Khatounian, E. Monmasson, F. Berthereau, E. Delaleau, and J.P. Louis, "Control of a Doubly Fed Induction Generator for Aircraft Application," in

*Proceedings of the 29th Annual Conference of the IEEE Industrial Electronics Society*, 2003, vol. 3, pp. 2711 - 2716.

[49] C. Belfedal, S. Gherbi, M. Sedraoui, S. Moreau, G. Champenois, T. Allaoui, and M.A. Dena, "Robust Control of Doubly Fed Induction Generator for Stand-alone Applications," *Electric Power Systems Research*, vol. 80(2), pp. 230–239, 2009.

[50] L.C. Kramer and K.W. Jenkins, "A New Technique for Preventing Direct Digital Control Windup," in *Proceedings of the 1971 Joint Automatic Control Conference*, St. Louis, MO, pp. 571-577.

[51] C.S. Draper and Y.T. Li, *Principles of Optimalizing Control Systems and An Application to The Internal Combustion Engine*. New York: American Society of Mechanical Engineers, 1951.

[52] K.J. Åström and B. Wittenmark, *Computer-Controlled Systems: Theory and Design, 3rd Edition*: Dover Publications, 2011.

[53] Y. Tan, W.H. Moase, C. Manzie, D. Nesic, and I.M.Y Mareels, "Extremum Seeking from 1922 to 2010," in *Proceedings of the 29th Chinese Control Conference* 2010, pp. 14-26.

[54] F.D. Bianchi, R.J. Mantz, and C.F. Christiansen, "Power Regulation in Pitch-Controlled Variable-Speed WECS above Rated Wind Speed," *Renewable Energy*, vol. 29(11), pp. 1911-1922, 2004.

[55] R.J.L. Hanus, "The Conditioned Control: A New Technique for Preventing Windup Nuisances," *Automatica*, vol. 21(1), pp. 15-20, 1980.

[56] K.J. Åström and B. Wittenmark, *Adaptive Control, 2nd edition*: Addison-Wesley, 1995.

[57] M. Krstić and H.H. Wang, "Stability of Extremum Seeking Feedback for General Nonlinear Dynamic Systems," *Automatica*, vol. 36(4), pp. 595-601, 2000.

[58] M. Krstić, "Performance Improvement and Limitations in Extremum Seeking Control," *Systems and Control Letters*, vol. 39(5), pp. 313-326, 2000.

[59] F.G. Shinskey, "Process-control Systems: Application, Design, Adjustment," Instrument Society of America, 67 Alexander Drive, Research Triangle Park, NC 27709, 1967.

[60] H.A. Fertik and C.W. Ross, "Direct Digital Control Algorithm with Anti-Windup Feature," *ISA Transactions*, vol. 6(4), pp. 317-328, 1967.

[61] R. Rocha, L.S.M. Filho, and M.V. Bortolus, "Optimal Multivariable Control for Wind Energy Conversion System A Comparison between $H_2$ and $H_\infty$ Controllers,"

in *Proceedings of the 44th IEEE Conference on Decision and Control and the European Control Conference*, 2005, pp. 7906-7911.

[62] R. Rocha and L.S.M. Filho, "A Multivariable $H_\infty$Control for Wind Energy Conversion System," in*Proceedings of the 2003 IEEE Conference on Control Applications*, vol. 1, pp. 206-211.

[63] B. Connor, S. N. Iyer, W.E. Leithead, and M.J. Grimble, "Control of a Horizontal Axis Wind Turbine using H Infinity Control," in *Proceedings of the 1992 IEEE Conference on Control Applications*, 1992, vol. 1, pp. 117-122

[64] L.Y. Pao and K. E. Johnson, "Control of Wind Turbines," *IEEE Control Systems Magazine*, vol. 31(2), pp. 44-62, 2011.

[65] L.J. Fingersh and K.E. Johnson, "Baseline Results and Future Plans for The NREL Controls Advanced Research Turbine," in *Proceedings of the 23rd ASME Wind Energy Symposium*, 2004, pp. 87-93.

[66] J. Aho, L.Y. Pao, and J. Hauser, "Optimal Trajectory Tracking Control for Wind Turbines During Operating Region Transitions," in *Proceedings of the 2013 American Control Conference*, pp. 1424-1429.

[67] P.J. Campo, M. Morari, and C.N. Nett, "Multivariable Anti-Windup and Bumpless Transfer: A General Theory," in *Proceedings of the 1989 American Control Conference*, pp. 1706-1711.

[68] C. Edwards and I. Postlethwaite, "Anti-Windup and Bumpless-Transfer Schemes," *Automatica*, vol. 34(2), pp. 199-210, 1998.

[69] M.C. Turner and D.J. Walker, "Modified Linear Quadratic Bumpless Transfer," in *Proceedings of the 1999 American Control Conference*, vol. 4, pp. 2285-2289.

[70] R. Hanus, M. Kinnaert, and J.L. Henrotte, "Conditioning Technique, a General Anti-Windup and Bumpless Transfer Method," *Automatica*, vol. 23(6), pp. 729-739, 1987.

[71] P.S. Buckley, "Override Controls for Distillation Columns," *Instrumentation Technology*, vol. 15(8), pp. 51-58, 1968.

[72] R. Hanus, "Anti-Windup and Bumpless Transfer: A Survey," *Computing and Computers for Control Systems*, vol. 4, pp. 3-9, 1989.

[73] K.J. Åström and B. Wittenmark, *Computer-Controlled Systems : Theory and Design, 3rd Edition*. Mineola, N.Y.: Dover Publications, 2011.

[74] K.S. Walgama, S. Ronnback, and J. Sternby, "Generalisation of Conditioning Technique for Anti-Windup Compensators," in *Proceedings of the IEE Control Theory and Applications*, 1992, vol. 139, pp. 109-118.

[75] M.C. Turner and D.J. Walker, "Linear Quadratic Bumpless Transfer," *Automatica*, vol. 36(8), pp. 1089-1101, August 2000.

[76] M.C. Turner and D.J. Walker, "Modified Linear Quadratic Bumpless Transfer," in *Proceedings of the 2002 American Control Conference*, vol. 4, pp. 2285-2289.

[77] Y. Peng, D. Vrancic, and R.J.L. Hanus, "Anti-Windup, Bumpless, and Conditioned Transfer Techniques for PID Controllers," *IEEE Control Systems Magazine*, vol. 16(4), pp. 48-57, 2002.

[78] J.M. Jonkman and M.L. Buhl, Jr., "FAST User's Guide," National Renewable Energy Laboratory, Golden, CO, NREL/EL-500-38230

[79] P.J. Moriarty and A.C. Hansen, "AeroDyn Theory Manual " National Renewable Energy Laboratory, Golden, CO, NREL/TP-500-36881 Jan. 2005.

[80] B.J. Jonkman and M.L. Buhl, Jr, "TurbSim User's Guide," National Renewable Energy Laboratory Golden, CO, NREL/TP-500-39797 Sept. 2006.

[81] T.R. Kane and D.A. Levinson, *Dynamics, Theory and Applications*: McGraw Hill, 1985.

[82] T.R. Kane and D.A. Levinson, "Engineering Mechanics Online Parts 1 & 2 " *Statics & Dynamics, Online Dynamics, Sunnyvale, CA, available from www.autolev.com*, 1997.

[83] P.C. Mitiguy and T.R. Kane, "Motion Variables Leading to Efficient Equations of Motion," *The International Journal of Robotics Research*, vol. 15(5), p. 522, 1996.

[84] The MathWorks. Simulink Documentation. [Online]. Available: http://www.mathworks.com/products/simulink/.

[85] The MathWorks. MATLAB Documentation [Online]. Available: http://www.mathworks.com/help/matlab/.

[86] National Renewable Energy Laboratory. NREL Wind Turbine Design Codes Certified. [Online]. Available: http://www.nrel.gov/news/press/2005/357.html?print.

[87] R.R. Ryan, "ADAMS—Multibody System Analysis Software," in *Multibody Systems Handbook*: Springer, 1990, pp. 361-402.

[88] M.L. Buhl, Jr and A. Manjock, "A Comparison of Wind Turbine Aeroelastic Codes Used for Certification," in *Proceedings of the 44th AIAA Aerospace Sciences Meeting and Exhibit*, Reno, NV, 2006, pp. 2006-2786.

[89] Patrick J Moriarty and A Craig Hansen, *AeroDyn theory manual*: National Renewable Energy Laboratory Golden, Colorado, USA, 2005.

[90] J.G. Leishman, *Principles of Helicopter Aerodynamics*: Cambridge University Press, 2006.

[91] J. Creaby, "*Maximizing Wind Power Capture Using Multi-variable Extremum Seeking Control*," M.Sc. Theis, Department of Mechanical Engineering, University of Wisconsin--Milwaukee, 2008.

[92] D.A. Peters and C.J. He, "Correlation of Measured Induced Velocities with a Finite State Wake Model," *Journal of the American Helicopter Society*, vol. 36, p. 59, 1991.

[93] C. He, "*Development and Application of a Generalized Dynamic Wake Theory for Lifting Rotors*," Ph.D. Dissertation, Department of Aeronautical Engineering, Georgia Institute of Technology, 1989.

[94] A. Suzuki, "*Application of Dynamic Inflow Theory to Wind Turbine Rotors*," Ph.D Dissertation, Department of Mechanical Engineering, University of Utah, 2000.

[95] A. Suzuki and A.C. Hansen, "Generalized Dynamic Wake Model for YawDyn," in *the 37th Aerospace Sciences Meeting and Exhibit, Wind Energy Symposium*, Paper No. AIAA-99-0041, Reno, NV, 1999.

[96] D.M. Pitt and D.A. Peters, "Theoretical Prediction of Dynamic-Inflow Derivatives," *Vertica*, vol. 5(1), pp. 21-34, 1981.

[97] J.B. Ekanayake, L. Holdsworth, X. Wu, and N. Jenkins, "Dynamic Modeling of Doubly Fed Induction Generator Wind Turbines," *IEEE Transactions on Power Systems*, vol. 18(2), pp. 803-809, 2003.

[98] Q. Chen, Y. Li, Z. Yang, J.E. Seem, and J. Creaby, "Self-Optimizing Robust Control of Wind Power Generation With Doubly-Fed Induction Generator," in *the ASME 2010 Dynamic Systems and Control Conference*, 2010, pp. 929-936.

[99] M.R. Rathi, P.P. Jose, and N. Mohan, "A Novel $H_\infty$ based Controller for Wind Turbine Applications Operating under Unbalanced Voltage Conditions," in *the 13th International Conference on Intelligent Systems Application to Power Systems*, Arlington, VA, 2005, pp. 355-360.

[100] M.A. Rotea, "Analysis of Multivariable Extremum Seeking Algorithms," in *Proceedings of the 2000 American Control Conference*, Chicago, IL, vol. 1, pp. 433-437.

[101] C.A. Desoer and M. Vidyasagar, *Feedback Systems: Input-output Properties*: Society for Industrial Mathematics, 2009.

[102] M.L. Buhl, Jr, "MCrunch User Guide for Version 1.00," NREL/TP-500-43139, May 2008.

[103] M.C. Turner, N. Aouf, D.G. Bates, I. Postlethwaite, and B. Boulet, "Switched Control of a Vertical/Short Take-off Land Aircraft: An Application of Linear Quadratic Bumpless Transfer," *Proceedings of the Institution of Mechanical Engineers. Part I: Journal of Systems and Control Engineering*, vol. 220, pp. 157-170, 2006.

[104] K. J. Åström and L. Rundqwist, "Integrator Windup and How to Avoid It," in *Proceedings of the 1989 American Control Conference*, pp. 1693-1698.

[105] A.D. Wright and L.J. Fingersh, "Advanced Control Design for Wind Turbines Part I : Control Design , Implementation , and Initial Tests," National Renewable Energy Laboratory, Golden, CO., Technical Report NREL/TP-500-42437, 2008.

[106] M. Alatalo, "*Permanent Magnet Machines with Air Gap Windings and Integrated Teeth Windings*," Ph.D. Dissertation, Department of Electric Power Engineering, Chalmers University of Technology, 1996.

[107] A.M. Bazzi and P.T. Krein, "Ripple Correlation Control: An Extremum Seeking Control Perspective for Real-Time Optimization," *IEEE Transactions on Power Electronics*, vol. 29(2), pp. 988-995, 2014.

# APPENDICES

## Appendix A: FAST Input File

```
------------------------------------------------------------------------
------
------- FAST INPUT FILE -------------------------------------------------
------
FAST certification test #1 for AWT-27CR2 with many DOFs.
Compatible with FAST v4.3   !JASON:v3.6.
---------------------- SIMULATION CONTROL ----------------------------
------
False       Echo        - Echo input data to "echo.out" (switch)
   1        ADAMSPrep   - ADAMS preprocessor mode  (switch)
   1        AnalMode    - Analysis mode  (switch)
   2        NumBl       - Number of blades (-)
 300.0      TMax        - Total run time (s)
 0.006      DT          - Integration time step (s)
---------------------- TURBINE CONTROL -------------------------------
------
   2        YCMode      - Yaw control mode  (switch)
   0      TYCOn       - Time to enable active yaw control (s)
   2        PCMode      - Pitch control mode  (switch)
   0.      TPCOn       - Time to enable active pitch control (s)
   3        VSContrl    - Variable-speed control mode  (switch)
 1781.98     VS_RtGnSp    - Rated generator speed for simple variable-
speed generator control (HSS side) (rpm) [used only when VSContrl=1]
3524.36       VS_RtTq     - Rated generator torque/constant generator
torque in Region 3 for simple variable-speed generator control (HSS
side) (N-m) [used only when VSContrl=1]
.0008992     VS_Rgn2K    - Torque constant for simple variable-speed
generator control in Region 2 (HSS side) (N-m/rpm^2) [used only when
VSContrl=1]
 23.05       VS_SlPc     - Rated generator slip percentage in Region 2
1/2 for simple variable-speed generator control (%) [used only when
VSContrl=1]
   1        GenModel    - Generator model  (-)
True        GenTiStr    - Method to start the generator  (switch)
True        GenTiStp    - Method to stop the generator  (switch)
 900.0      SpdGenOn    - Generator speed to turn on the generator for
a startup (HSS speed) (rpm)
   0.0      TimGenOn    - Time to turn on the generator for a startup
(s)
99999.9      TimGenOf    - Time to turn off the generator (s)
   1        HSSBrMode   - HSS brake model  (switch)
99999.9      THSSBrDp    - Time to initiate deployment of the HSS brake
(s)
99999.9      TiDynBrk    - Time to initiate deployment of the dynamic
generator brake [CURRENTLY IGNORED] (s)
99999.9      TTpBrDp(1)  - Time to initiate deployment of tip brake 1
(s)
99999.9      TTpBrDp(2)  - Time to initiate deployment of tip brake 2
(s)
```

```
99999.9      TTpBrDp(3)  - Time to initiate deployment of tip brake 3
(s) [unused for 2 blades]
99999.9      TBDepISp(1) - Deployment-initiation speed for the tip
brake on blade 1 (rpm)
99999.9      TBDepISp(2) - Deployment-initiation speed for the tip
brake on blade 2 (rpm)
99999.9      TBDepISp(3) - Deployment-initiation speed for the tip
brake on blade 3 (rpm) [unused for 2 blades]
99999.9      TYawManS    - Time to start override yaw maneuver and end
standard yaw control (s)
99999.9      TYawManE    - Time at which override yaw maneuver reaches
final yaw angle (s)
   0.0      NacYawF     - Final yaw angle for yaw maneuvers (degrees)
99999.9      TPitManS(1) - Time to start override pitch maneuver for
blade 1 and end standard pitch control (s)
99999.9      TPitManS(2) - Time to start override pitch maneuver for
blade 2 and end standard pitch control (s)
99999.9      TPitManS(3) - Time to start override pitch maneuver for
blade 3 and end standard pitch control (s) [unused for 2 blades]
99999.9      TPitManE(1) - Time at which override pitch maneuver for
blade 1 reaches final pitch (s)
99999.9      TPitManE(2) - Time at which override pitch maneuver for
blade 2 reaches final pitch (s)
99999.9      TPitManE(3) - Time at which override pitch maneuver for
blade 3 reaches final pitch (s) [unused for 2 blades]
 1.       B1Pitch(1)  - Blade 1 initial pitch (degrees)
 1.        B1Pitch(2)  - Blade 2 initial pitch (degrees)
 1.        B1Pitch(3)  - Blade 3 initial pitch (degrees) [unused for 2
blades]
 5.3        B1PitchF(1) - Blade 1 final pitch for pitch maneuvers
(degrees)
 5.3        B1PitchF(2) - Blade 2 final pitch for pitch maneuvers
(degrees)
 5.3        B1PitchF(3) - Blade 3 final pitch for pitch maneuvers
(degrees) [unused for 2 blades]
---------------------- ENVIRONMENTAL CONDITIONS ----------------------
---------
9.80665 !JASON:  9.80665  Gravity     - Gravitational acceleration
(m/s^2)
---------------------- FEATURE SWITCHES ------------------------------
---------
False  FlapDOF1    - First flapwise blade mode DOF (switch)
False   FlapDOF2    - Second flapwise blade mode DOF (switch)
False   EdgeDOF     - First edgewise blade mode DOF (switch)
False  TeetDOF     - Rotor-teeter DOF (switch) [unused for 3 blades]
False  DrTrDOF     - Drivetrain rotational-flexibility DOF (switch)
True    GenDOF      - Generator DOF (switch)
False   YawDOF      - Yaw DOF (switch)
False    TwFADOF1    - First fore-aft tower bending-mode DOF (switch)
False    TwFADOF2    - Second fore-aft tower bending-mode DOF (switch)
False  TwSSDOF1    - First side-to-side tower bending-mode DOF (switch)
False    TwSSDOF2    - Second side-to-side tower bending-mode DOF
(switch)
True    CompAero    - Compute aerodynamic forces (switch)
False   CompNoise   - Compute aerodynamic noise (switch)
---------------------- INITIAL CONDITIONS ----------------------------
---------
```

```
   0.0      OoPDefl     - Initial out-of-plane blade-tip displacement,
(meters)
   0.0      IPDefl      - Initial in-plane blade-tip deflection,
(meters)
   0.0      TeetDefl    - Initial or fixed teeter angle (degrees)
[unused for 3 blades]
   0.0      Azimuth     - Initial azimuth angle for blade 1 (degrees)
   41.0     RotSpeed    - Initial or fixed rotor speed (rpm)
  -0.0      NacYaw      - Initial or fixed nacelle-yaw angle (degrees)
   0.      TTDspFA     - Initial fore-aft tower-top displacement
(meters)
   0.0      TTDspSS     - Initial side-to-side tower-top displacement
(meters)
---------------------- TURBINE CONFIGURATION --------------------------
---------
  21.336    TipRad      - The distance from the rotor apex to the blade
tip (meters)
   1.381    HubRad      - The distance from the rotor apex to the blade
root (meters)
   1        PSpnElN     - Number of the innermost blade element which
is still part of the pitchable portion of the blade for partial-span
pitch control [1 to BldNodes] [CURRENTLY IGNORED] (-)
  0.000     UndSling    - Undersling length [distance from teeter pin
to the rotor apex] (meters) [unused for 3 blades]
  0.210     HubCM       - Distance from rotor apex to hub mass
[positive downwind] (meters)
 -3.858     OverHang    - Distance from yaw axis to rotor apex [3
blades] or teeter pin [2 blades] (meters)
  -1.1      NacCMxn     - Downwind distance from the tower-top to the
nacelle CM (meters)
   0.0      NacCMyn     - Lateral  distance from the tower-top to the
nacelle CM (meters)
   1.734    NacCMzn     - Vertical distance from the tower-top to the
nacelle CM (meters)
 34.862     TowerHt     - Height of tower above ground level (meters)
 1.734      Twr2Shft    - Vertical distance from the tower top to the
yaw/shaft intersection (meters)
   0.0      TwrRBHt     - Tower rigid base height (meters)
  -3.77      ShftTilt    - Rotor shaft tilt angle (degrees)
   0.0      Delta3      - Delta-3 angle for teetering rotors (degrees)
[unused for 3 blades]
   0.0      PreCone(1)  - Blade 1 cone angle (degrees)
   0.0      PreCone(2)  - Blade 2 cone angle (degrees)
   0.0      PreCone(3)  - Blade 3 cone angle (degrees) [unused for 2
blades]
 270.0      AzimB1Up    - Azimuth value to use for I/O when blade 1
points up (degrees)
---------------------- MASS AND INERTIA -------------------------------
---------
   0.0      YawBrMass   - Yaw bearing mass (kg)
 29113.     NacMass     - Nacelle mass (kg)
  5852.     HubMass     - Hub mass (kg)
    0.      TipMass(1)  - Tip-brake mass, blade 1 (kg)
    0.      TipMass(2)  - Tip-brake mass, blade 2 (kg)
    0.      TipMass(3)  - Tip-brake mass, blade 3 (kg) [unused for 2
blades]
  71750.     NacYIner    - Nacelle inertia about yaw axis (kg m^2)
```

```
 34.4      ! 64100. GenIner     - Generator inertia about HSS (kg m^2)
  15000.     HubIner     - Hub inertia about teeter axis (kg m^2)
[unused for 3 blades]
---------------------- DRIVETRAIN --------------------------------
---------
 100.0      GBoxEff     - Gearbox efficiency (%)
 100.0      GenEff      - Generator efficiency [ignored by the Thevenin
and user-defined generator models] (%)
 43.165       !43.165     GBRatio     - Gearbox ratio (-)
False       GBRevers    - Gearbox reversal  (switch)
6000.0      HSSBrTqF    - Fully deployed HSS-brake torque (N-m)
   0.5      HSSBrDt     - Time for HSS-brake to reach full deployment
once initiated (sec)
"DynBrk.dat"DynBrkFi    - File containing a mech-gen-torque vs HSS-
speed curve for a dynamic brake [CURRENTLY IGNORED] (quoted string)
 2.691e7    DTTorSpr    - Drivetrain torsional spring (N-m/rad)
 0.e0    DTTorDmp    - Drivetrain torsional damper (N-m/s)
---------------------- SIMPLE INDUCTION GENERATOR ----------------
---------
   0.001   SIG_SlPc    - Rated generator slip percentage [>0] (%)
Now HSS side!
1799.98      SIG_SySp    - Synchronous (zero-torque) generator speed
[>0] (rpm)  Now HSS side!
1799.98      SIG_RtTq    - Rated torque [>0] (N-m)
Now HSS side!
   2      SIG_PORt    - Pull-out ratio (Tpullout/Trated) [>1] (-)
---------------------- THEVENIN-EQUIVALENT INDUCTION GENERATOR --------
---------
  60.0      TEC_Freq    - Line frequency [50 or 60] (Hz)
   6        TEC_NPol    - Number of poles [even integer > 0] (-)
   0.0185   TEC_SRes    - Stator resistance [>0] (ohms)
   0.017    TEC_RRes    - Rotor resistance [>0] (ohms)
 480.0      TEC_VLL     - Line-to-line RMS voltage (volts)
   0.0340   TEC_SLR     - Stator leakage reactance (ohms)
   0.0050   TEC_RLR     - Rotor leakage reactance (ohms)
   0.7750   TEC_MR      - Magnetizing reactance (ohms)
---------------------- PLATFORM MODEL ----------------------------
---------
   0        PtfmModel   - Platform model {0: none, 1: onshore, 2: fixed
bottom offshore, 3: floating offshore} (switch)
PtfmFile    - Name of file containing platform properties (quoted
string) [unused when PtfmModel=0]
---------------------- TOWER -------------------------------------
---------
  15        TwrNodes    - Number of tower nodes used for analysis (-)
"CART_towersoft.dat" TwrFile - Name of file containing tower properties
(quoted string)
---------------------- NACELLE-YAW -------------------------------
---------
   0.0      YawSpr      - Nacelle-yaw spring constant (N-m/rad)
   0.0      YawDamp     - Nacelle-yaw constant (N-m/rad/s)
   0.0      YawNeut     - Neutral yaw position--yaw spring force is
zero at this yaw (degrees)
---------------------- FURLING -----------------------------------
---------
False       Furling     - Read in additional model properties for
furling turbine (flag)
```

```
FurlFile    - Name of file containing furling properties (quoted string)
---------------------- ROTOR-TEETER ---------------------------------
---------
   1        TeetDMod    - Rotor-teeter damper model (0: none, 1: linear,
2: user-defined) (switch) [unused for 3 blades]
   0.0      TeetDmpP    - Rotor-teeter damper position (degrees)
[unused for 3 blades]
  0.0e4    TeetDmp     - Rotor-teeter damping constant (N-m/rad/s)
[unused for 3 blades]
   0.0      TeetCDmp    - Rotor-teeter rate-independent Coulomb-damping
moment (N-m) [unused for 3 blades]
   0.0      TeetSStP    - Rotor-teeter soft-stop position (degrees)
[unused for 3 blades]
 180.0      TeetHStP    - Rotor-teeter hard-stop position (degrees)
[unused for 3 blades]
  0.0e4      TeetSSSp    - Rotor-teeter soft-stop linear-spring
constant (N-m/rad) [unused for 3 blades]
   5.0e6    TeetHSSp    - Rotor-teeter hard-stop linear-spring constant
(N-m/rad) [unused for 3 blades]
---------------------- TIP-BRAKE ------------------------------------
---------
   0.0      TBDrConN    - Tip-brake drag constant during normal
operation, Cd*Area (m^2)
   0.0      TBDrConD    - Tip-brake drag constant during fully-deployed
operation, Cd*Area (m^2)
   0.5      TpBrDT      - Time for tip-brake to reach full deployment
once released (sec)
---------------------- BLADE ----------------------------------------
---------
"CART_blades.dat" "CART_blades1_extramass.dat" BldFile(1) - Name of
file containing properties for blade 1 (quoted string)
"CART_blades.dat" BldFile(2) - Name of file containing properties for
blade 2 (quoted string)
"CART_blades.dat" BldFile(3) - Name of file containing properties for
blade 3 (quoted string) [unused for 2 blades]
---------------------- AERODYN --------------------------------------
---------
"AeroDyn01sim.ipt" ADFile  - Name of file containing AeroDyn input
parameters (quoted string)
---------------------- NOISE ----------------------------------------
---------
"Noise.dat" NoiseFile   - Name of file containing aerodynamic noise
input parameters (quoted string)
---------------------- ADAMS ----------------------------------------
---------
"ADAMS.dat" ADAMSFile   - Name of file containing ADAMS-specific input
parameters (quoted string)
---------------------- LINEARIZATION CONTROL ------------------------
---------
"CART_Linear.dat"   LinFile     - Name of file containing FAST
linearazation parameters (quoted string)
---------------------- OUTPUT ---------------------------------------
---------
True        SumPrint    - Print summary data to "<RootName>.fsm"
(switch)
True        TabDelim    - Generate a tab-delimited tabular output file.
(switch)
```

```
"ES10.3E2"  OutFmt      - Format used for tabular output except time.
Resulting field should be 10 characters. (quoted string)  [not checked
for validity!]
 0         TStart      - Time to begin tabular output (s)
  10         DecFact     - Decimation factor for tabular output [1:
output every time step] (-)
   1.0      SttsTime    - Amount of time between screen status messages
(sec)
   0.0      NcIMUxn     - Downwind distance from the tower-top to the
nacelle IMU (meters)
   0.0      NcIMUyn     - Lateral  distance from the tower-top to the
nacelle IMU (meters)
   0.0      NcIMUzn     - Vertical distance from the tower-top to the
nacelle IMU (meters)
   0.99     ShftGagL    - Distance from rotor apex [3 blades] or teeter
pin [2 blades] to shaft strain gages [positive for upwind rotors]
(meters)
   2        NTwGages    - Number of tower nodes that have strain gages
for output [0 to 5] (-)
  4,7       TwrGagNd    - List of tower nodes that have strain gages [1
to TwrNodes] (-) [unused if NTwGages=0]
   3        NBlGages    - Number of blade nodes that have strain gages
for output [0 to 5] (-)
7,12,15     BldGagNd    - List of blade nodes that have strain gages [1
to BldNodes] (-)
OutList     - The next line(s) contains a list of output parameters.
See OutList.txt for a listing of available output channels, (-)
"Azimuth,LSSGagP"       - Rotor and Gen Azimuth Angles
"WindVxi"               - Hub height windspeed
"LSSGagV,HSShftV,LSSTipVxa"
"LSSGagAxa,HSShftA "      - Low-speed shaft vel. and generator vel.
"blpitch1,BldPitch2"   - Blade 1 and 2 pitch angles
"YawBrTDxt,YawBrTDyt"   - Tower-top fore-aft and side-side displ
"TwHt1MLxt,TwHt1MLyt"
"TipDxb1,TipDxb2"
"TeetPya"
"rotcq"
"rotpwr"
"rotspeed"
"horwnddir"
"TipDxc1, TipDyc1"    - Blade 1 tip out-plane and in-plane defl
"TipDxc2, TipDyc2"    - Blade 2 tip out-plane and in-plane defl
"RotTorq,LSShftTq,HSShftTq"      - Rotor and shaft torque
"GenTq,RotThrust"       - Generator torque and rotor thrust
"RotPwr,GenPwr,HSShftPwr"                - rotor power
"TipSpdRat,RotCp"
"YawBrTAyp"
"YawBrTAxp"
"YawBrTDyp"
"yawpzn"
"LSSTipPxa"
"YawBrMzn"
"NcIMUTVys"
"RootMyb1"
"RootMyb2"
"RootMxb1"
"RootMxb2"
```

```
"RootFxb1"
"RootFxc1"
"LSSTipAxa"
"HSShftA"
"TwrBsMxt"
"YawBrFyp"
"YawBrMxp"
"LSShftFys"
"LSShftFxa"
"RotCt"
END of FAST input file (the word "END" must appear in the first 3
columns of this last line).
---------------------------------------------------------------------
---------
```

**Appendix A.1: Steps for Running FAST based Simulation**

In Matlab:

1. Open Simulink model
2. Direct to FAST installation folder
3. Clear work space
4. Run ’simsetup’, in command window a message will show as follows

   ---

   Enter the name of the FAST input file to read

   ---

5. Enter ‘cart.fst’
6. Start Simulation from Simulink model
7. After simulation finished, make sure record all the data

# Appendix B: CART Aerodynamic Parameters for FAST

**CART aerodynamic parameters for FAST.**

```
SI                      SysUnits - System of units for used for input
and output [must be SI for FAST] (unquoted string)
STEADY                  StallMod - Dynamic stall included [BEDDOES or
STEADY] (unquoted string)
NO_CM                   UseCm    - Use aerodynamic pitching moment
model? [USE_CM or NO_CM] (unquoted string)
EQUIL       !JASON:DYNIN      InfModel - Inflow model [DYNIN or EQUIL]
(unquoted string)
WAKE                    IndModel - Induction-factor model [NONE or WAKE
or SWIRL] (unquoted string)
0.001       !JASON: 0.001     AToler   - Induction-factor tolerance
(convergence criteria) (-)
PRANDTL                  TLModel  - Tip-loss model (EQUIL only) [PRANDtl,
GTECH, or NONE] (unquoted string)
NONE                    HLModel  - Hub-loss model (EQUIL only) [PRANdtl
or NONE] (unquoted string)
"wind2/SmoothSteppedWind4.wnd" Name of file containing wind data
(quoted string)
36.850                  HH       - Wind reference (hub) height
[TowerHt+Twr2Shft+OverHang*SIN(NacTilt)] (m)
0.05    !JASON: 0.3     TwrShad  - Tower-shadow velocity deficit (-)
 3.0                    ShadHWid - Tower-shadow half width (m)
 4.0                    T_Shad_Refpt - Tower-shadow reference point (m)
 1.03                   Rho      - Air density (kg/m^3)
 1.4639e-5              KinVisc  - Kinematic air viscosity [CURRENTLY
IGNORED] (m^2/sec)
 0.002                  DTAero   - Time interval for aerodynamic
calculations (sec)
11                      NumFoil  - Number of airfoil files (-)
"AeroData\art15.air"    FoilNm   - Names of the airfoil files [NumFoil
lines] (quoted strings)
"AeroData\art25.air"
"AeroData\art35.air"
"AeroData\art45.air"
"AeroData\art55.air"
"AeroData\art65.air"
"AeroData\art75.air"
"AeroData\art75-5.air"
"AeroData\art85.air"
"AeroData\art85-5.air"
"AeroData\art95.air"
20                      BldNodes - Number of blade nodes used for
analysis (-)
RNodesAeroTwstDRNodes    Chord  NFoilPrnElm
    1.8799    3.3740         0.998    1.1929    1   PRINT
    2.8777    3.1895         0.998    1.3286    1   PRINT
    3.8754    3.0569         0.998    1.4276    1   PRINT
    4.8731    2.8685         0.998    1.5637    1   PRINT
    5.8709    2.7371         0.998    1.6633    2   PRINT
```

| | | | | | |
|---|---|---|---|---|---|
| 6.8686 | 2.5294 | 0.998 | 1.6575 | 2 | PRINT |
| 7.8663 | 2.3700 | 0.998 | 1.6163 | 3 | PRINT |
| 8.8641 | 2.1379 | 0.998 | 1.5555 | 3 | PRINT |
| 9.8618 | 1.9386 | 0.998 | 1.5017 | 4 | PRINT |
| 10.8595 | 1.6665 | 0.998 | 1.4274 | 4 | PRINT |
| 11.8573 | 1.4339 | 0.998 | 1.3735 | 5 | PRINT |
| 12.8550 | 1.0945 | 0.998 | 1.3000 | 5 | PRINT |
| 13.8528 | 0.8374 | 0.998 | 1.2461 | 6 | PRINT |
| 14.8506 | 0.4020 | 0.998 | 1.1718 | 6 | PRINT |
| 15.8483 | 0.0770 | 0.998 | 1.1179 | 7 | PRINT |
| 16.8460 | -0.4568 | 0.998 | 1.0444 | 7 | PRINT |
| 17.8438 | -0.8951 | 0.998 | 0.9906 | 8 | PRINT |
| 18.8416 | -1.5209 | 0.998 | 0.9171 | 9 | PRINT |
| 19.8393 | -2.1452 | 0.998 | 0.8626 | 10 | PRINT |
| 20.8371 | -2.9979 | 0.998 | 0.7889 | 11 | PRINT |

## Appendix C: TurbSim Input File

```
TurbSim Input File. Valid for TurbSim v1.50, 25-Sep-2009

---------Runtime Options-----------------------------------
2318573             RandSeed1       - First random seed  (-2147483648
to 2147483647)
RANLUX              RandSeed2       - Second random seed (-2147483648
to 2147483647) for intrinsic pRNG, or an alternative pRNG: "RanLux" or
"RNSNLW"
False               WrBHHTP         - Output hub-height turbulence
parameters in binary form?  (Generates RootName.bin)
False               WrFHHTP         - Output hub-height turbulence
parameters in formatted form?  (Generates RootName.dat)
False               WrADHH          - Output hub-height time-series
data in AeroDyn form?  (Generates RootName.hh)
False               WrADFF          - Output full-field time-series
data in TurbSim/AeroDyn form? (Generates Rootname.bts)
True                WrBLFF          - Output full-field time-series
data in BLADED/AeroDyn form?  (Generates RootName.wnd)
False               WrADTWR         - Output tower time-series data?
(Generates RootName.twr)
False               WrFMTFF         - Output full-field time-series
data in formatted (readable) form?  (Generates RootName.u, RootName.v,
RootName.w)
True                WrACT           - Output coherent turbulence time
steps in AeroDyn form? (Generates RootName.cts)
True                Clockwise       - Clockwise rotation looking
downwind? (used only for full-field binary files - not necessary for
AeroDyn)
 0                  ScaleIEC        - Scale IEC turbulence models to
exact target standard deviation? [0=no additional scaling; 1=use hub
scale uniformly; 2=use individual scales]

--------Turbine/Model Specifications-----------------------
13                  NumGrid_Z       - Vertical grid-point matrix
dimension
13                  NumGrid_Y       - Horizontal grid-point matrix
dimension
0.05                TimeStep        - Time step [seconds]
600                 AnalysisTime    - Length of analysis time series
[seconds] (program will add time if necessary: AnalysisTime =
MAX(AnalysisTime, UsableTime+GridWidth/MeanHHWS) )
40                  UsableTime      - Usable length of output time
series [seconds] (program will add GridWidth/MeanHHWS seconds)
84.2876             HubHt           - Hub height [m] (should be >
0.5*GridHeight)
80.00               GridHeight      - Grid height [m]
80.00               GridWidth       - Grid width [m] (should be >=
2*(RotorRadius+ShaftLength))
0                   VFlowAng        - Vertical mean flow (uptilt) angle
[degrees]
0                   HFlowAng        - Horizontal mean flow (skew) angle
[degrees]
```

```
--------Meteorological Boundary Conditions-------------------
"SMOOTH"             TurbModel       - Turbulence model ("IECKAI"=Kaimal,
"IECVKM"=von Karman, "GP_LLJ", "NWTCUP", "SMOOTH", "WF_UPW", "WF_07D",
"WF_14D", or "NONE")
"1-ED3"              IECstandard     - Number of IEC 61400-x standard
(x=1,2, or 3 with optional 61400-1 edition number (i.e. "1-Ed2") )
"A"                  IECturbc        - IEC turbulence characteristic
("A", "B", "C" or the turbulence intensity in percent) ("KHTEST" option
with NWTCUP model, not used for other models)
"NTM"                IEC_WindType    - IEC turbulence type ("NTM"=normal,
"xETM"=extreme turbulence, "xEWM1"=extreme 1-year wind,
"xEWM50"=extreme 50-year wind, where x=wind turbine class 1, 2, or 3)
default              ETMc            - IEC Extreme Turbulence Model "c"
parameter [m/s]
default              WindProfileType - Wind profile type
("JET","LOG"=logarithmic,"PL"=power law,"IEC"=PL on rotor disk,LOG
elsewhere, or "default")
84.2876              RefHt           - Height of the reference wind
speed [m]
18.2                 URef            - Mean (total) wind speed at the
reference height [m/s] (or "default" for JET wind profile)
default              ZJetMax         - Jet height [m] (used only for JET
wind profile, valid 70-490 m)
default              PLExp           - Power law exponent [-] (or
"default")
default              Z0              - Surface roughness length [m] (or
"default")

--------Non-IEC Meteorological Boundary Conditions------------
default              Latitude        - Site latitude [degrees] (or
"default")
0.05                 RICH_NO         - Gradient Richardson number
default              UStar           - Friction or shear velocity [m/s]
(or "default")
default              ZI              - Mixing layer depth [m] (or
"default")
default              PC_UW           - Hub mean u'w' Reynolds stress (or
"default")
default              PC_UV           - Hub mean u'v' Reynolds stress (or
"default")
default              PC_VW           - Hub mean v'w' Reynolds stress (or
"default")
default              IncDec1         - u-component coherence parameters
(e.g. "10.0  0.3e-3" in quotes) (or "default")
default              IncDec2         - v-component coherence parameters
(e.g. "10.0  0.3e-3" in quotes) (or "default")
default              IncDec3         - w-component coherence parameters
(e.g. "10.0  0.3e-3" in quotes) (or "default")
default              CohExp          - Coherence exponent (or "default")

--------Coherent Turbulence Scaling Parameters-------------------
"M:\coh_events\eventdata"  CTEventPath     - Name of the path where
event data files are located
"Random"             CTEventFile     - Type of event files ("LES", "DNS",
or "RANDOM")
```

```
true                Randomize       - Randomize the disturbance scale
and locations? (true/false)
 1.0                DistScl         - Disturbance scale (ratio of wave
height to rotor disk). (Ignored when Randomize = true.)
 0.5                CTLy            - Fractional location of tower
centerline from right (looking downwind) to left side of the dataset.
(Ignored when Randomize = true.)
 0.5                CTLz            - Fractional location of hub height
from the bottom of the dataset. (Ignored when Randomize = true.)
30.0                CTStartTime     - Minimum start time for coherent
structures in RootName.cts [seconds]

================================================
NOTE: Do not add or remove any lines in this file!
================================================
```

## Appendix D: MCrunch Input File

```
-----  MCrunch v1.00.00 Input File  ----------------------------------
--------
Test #01 (-Names, -Chans, +CC, -TSp, +Stats, -SwT, -SwX, +SF, -EE, -
Bins, -Bp, -PDF, -PDFp, -PSD, -PSDp, -PSDtxt, -PSDxls, +F, -FBR, -FBM,
+DEL, -CF, +FwDELt, -FwDELx, +FwRFt, -FwRFx, -FpBC, -FpPE, -FpCC, -FpRM,
+TbDEL, -Multi).
-----  Job Options  ---------------------------------------------------
---------
true        EchoInp           Echo input to <rootname>.echo as this
file is being read.
false             StrNames          Use channel names following a "$"
instead of numbers when specifying channels in this input file.
false             OutData           Output modified data array after
scaling and calculated channels. (currently unavailable)
"%11.3e"          RealFmt           Format for outputting floating-
point values.
"Cart_Agg"      AggRoot           Root name for aggregate output files.
-----  Input-Data Layout  ---------------------------------------------
---------
0                 TitleLine         The row with the file title on it
(zero if no title is available).
7                 NamesLine         The row with the channel names on
it (zero if no names are available or are specified below).
0                 UnitsLine         The row with the channel units on
it (zero if no units are available or are specified below).
9                 FirstDataLine     The first row of data.
0                 TotLines          The total number of data lines in
all files.  Set to a non-zero value to improve speed and reduce memory
usage.  Set to zero to let MatLab determine it.
0                 NumChans:         The number of channels in each
input file.
ChanTitleChanUnits    Scale  Offset     NumCols rows of data follow.
Title and units strings must be 10 characters or less.
-----  Filtering  -----------------------------------------------------
---------
-----  Calculated Channels  -------------------------------------------
---------
0                 NumCChan          The number calculated channels to
generate.
1234567890        Seed              The integer seed for the random
number generator (-2,147,483,648 to 2,147,483,647).
Col_Title   Units    Equation       Put each field in quotes.  Titles
and units are limited to 10 characters.  NumCChan rows of data follow.
-----  Generic Plot Information  --------------------------------------
---------
1.5               LineWidth         The width of curves on the plots.
210               FigLeftPos        The number of pixels from the left
side of the screen to the left side of the figures.
100               FigBottomPos      The number of pixels from the
bottom of the screen to the bottom of the figures.
776               FigWidth          The horizontal width of the figures
in pixels.
600               FigHeight         The vertical height of the figures
in pixels.
```

```
true              FigTitles         Add titles to each figure?
true               SaveFigs          Save the generated figures in files?
-----  Time-Series Plots  ------------------------------------------
---------
0                 NumTimeFigs       Number of time-series figures.
Each figure will have one or more subplots.
FigureName            #Rows      #Cols     Channel list (must number
#Rows*#Cols)    (NumTimeFigs rows of data follow)
-----  Moving Averages  -------------------------------------------
---------
-----  Time and Wind Speed  ---------------------------------------
---------
1                 TimeChan          The channel containing time.
2                 WSChan            The primary wind-speed channel
(used for mean wind speed and turbulence intensity, 0 for none).
-----  Load Roses  ------------------------------------------------
---------
-----  Azimuth Averages  ------------------------------------------
---------
-----  Crosstalk Removal ------------------------------------------
---------
-----  Peak Finding  ----------------------------------------------
---------
-----  Statistics and Extreme Events  -----------------------------
---------
true              DoStats           Generate statistics of all the
channels.
false             WrStatsTxt        Write the stats to a text file?
false             WrStatsXLS        Write the stats to an Excel file?
2                 NumSFChans        Number of channels that will have
summary statistics generated for them.
44 45             SFChans           List of channels that will have
summary statistics generated for them.  Must number NumSFChans.
0                 NumEETables       Number of tables of extreme events.
TableName           #ChansChanList
#InfoChansInfoChanList    (NumEETables rows of data follow)
-----  Binning  ---------------------------------------------------
---------
false             DoBins            Bin selected channels?
2                  NumDepChans       Number of dependent channels to bin.
false             UseBinAv          When reporting the location of 1-D
bins, use the average values instead of the bin centers.
true              PltBins           Plot the binned data?
true              PltRawData        Plot the raw data on top of the
binned data if there is only one independent channel?
false             WrBinsTxt         Write binning results to a plain-
text file?
false             WrBinsXLS         Write binning results to an Excel
workbook?
DepChanNumDims  IndChan1  BinWid1  IndChan2  BinWid2
  12        1         2       0.5
  80        2         2       0.5       19       0.5
-----  Peak and Valley Listing  -----------------------------------
---------
-----  Probablity Density  ----------------------------------------
---------
false             DoPDFs            Generate PDFs of all channels.
```

```
0                 NumPDFChans       Number of PDF channels.
80                PDFChans     List of PDF channels.
100               NumPDFBins        Number of bins for the PDFs.
false             WrPDFsTxt         Write PDFs to a plain-text file?
false             WrPDFsXLS         Write PDFs to an Excel workbook?
0                 NumPDFFigs        Number of figures for the PDFs.
Each figure will have one or more subplots.
FigureName            #rows    #columns    Channel list (must number
#rows*#columns)    (NumPDFFigs rows of data follow)
-----  Power Spectral Density  ----------------------------------------
---------
false             DoPSDs            Generate power spectral densities?
1                 NumPSDChans       Number of PSD channels.
80                PSDChans          List of PSD channels.
false             RmvMean           Remove the mean of the signal(s)?
true              Detrend           Remove linear trend of the
signal(s)?
true              CosTaper          Add a cosine taper to the ends of
the time series?
"hamming"         WindowType        Type of data window.
false             IntPSDs           Integrate the PSDs before plotting
or writing them to a file?
false             BinPSDs           Bin the PSDs before plotting or
writing them to a file?
0.1               BinWidth          Width of the PSD bins.
false             WrXLS             Write the PSDs to an Excel file?
true              WrTxt             Write the PSDs to a text file?
0                 NumPSDFigs        Number of figures for the PSDs.
Each figure will have one or more subplots.
FigureName       #rows    #columns    Channel list (must number
#rows*#columns)    (NumPSDFigs rows of data follow)
-----  Fatigue  -------------------------------------------------------
---------
true              DoFatigue         Do fatigue analysis.
2                 NumFatChans       The number of rainflow channels.
Next six lines ignored if zero.
0.0               FiltRatio         The fraction of the maximum range
of each channel used as a cutoff range for the racetrack filter.  Use
zero for no filter.
1                 RF_Per            Number of seconds in the rainflow
counting period.
false             BinCycles         Bin the rainflow cycles?
false             BinMeans          Bin by cycle means in addition to
ranges?
0.5               UCMult            Multiplier for binning unclosed
cycles.  (0 discards, 1 counts as a full cycle)
true              DoSimpDELs        Compute damage-equivalent loads?
false             DoLife            Do lifetime-related calculations?
10                RayAverWS         Rayleigh-average wind speed.
3                 WSmin             Starting value for the wind-speed
bins for the Rayleigh distribution.
2                 WSdel             Delta value for the wind-speed bins
for the Rayleigh distribution.
false             CumFatigue        Generate cycle data as cumulative
cycles?
true              WrRFTxt           Write rainflow data to plain-text
files?
```

```
false             WrRFXLS           Write rainflow data to an Excel
workbook?
true              WrDELsTxt         Write DELs to plain-text files?
false             WrDELsXLS         Write DELs to an Excel workbook?
true              WrLifeTxt         Write lifetime results to plain-
text files?
true              WrLifeXLS         Write lifetime results to an Excel
workbook?
false             PltBinCyc         Plot binned rainflow cycles?
false             PltProbExc        Plot probability of exceedance?
false             PltCumCyc         Plot cumulative rainflow cycles?
false             PltRngMean        Plot 3-D range and mean binned
rainflow cycles?
true              TblDELs           Generate an HTML table of damage-
equivalent loads?
Channel#  NSlopesSNslopeLstBinWidthTypeLMFLUltBinWidth not used when
BinCycles is false. NumChans rows of data follow.  LUlt>> LMF
44       1        10         100.0     5000      50000
46       1        10         100.0     5000      50000
0                 NumFatFigs        Number of figures for the rainflow
analysis.  Each figure will have one or more subplots.
FigureName              #rows    #columns    Channel list (must number
#rows*#columns)    (NumRFFigs rows of data follow)
-----  Statistical Extrapolation  ------------------------------------
---------
-----  Input Files  ---------------------------------------------------
---------
1                 NumFiles          The number of input files to read.
"cart_SFunc.out"
==EOF==                             DO NOT REMOVE OR CHANGE.  MUST COME
JUST AFTER LAST LINE OF VALID INPUT.
"DLC2.1_1.out"
"DLC2.3_2.out"
"DLC2.3_3.out"
"Wiki_RF_Examp.dat"
```

# Appendix E: Self-Optimizing Robust Control for Wind Turbine

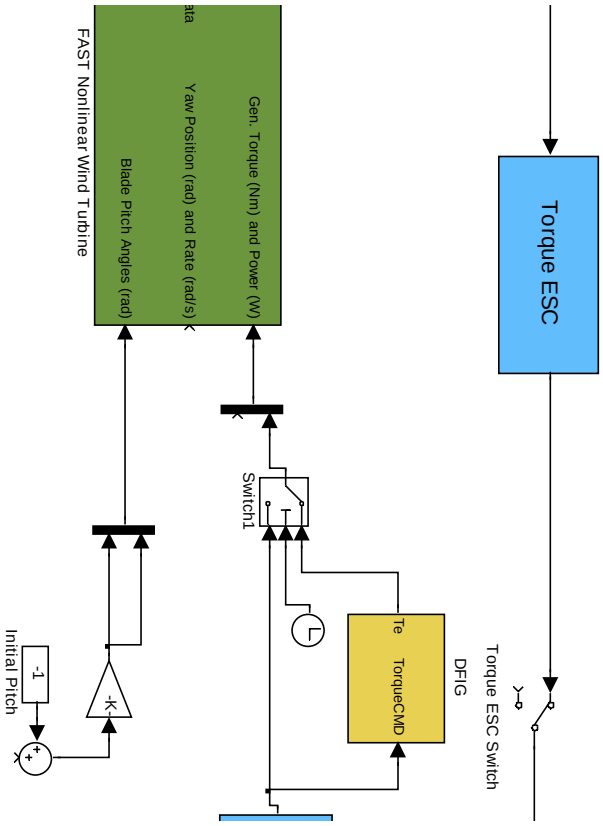

## Appendix E.1: Simulation Configuration Parameters

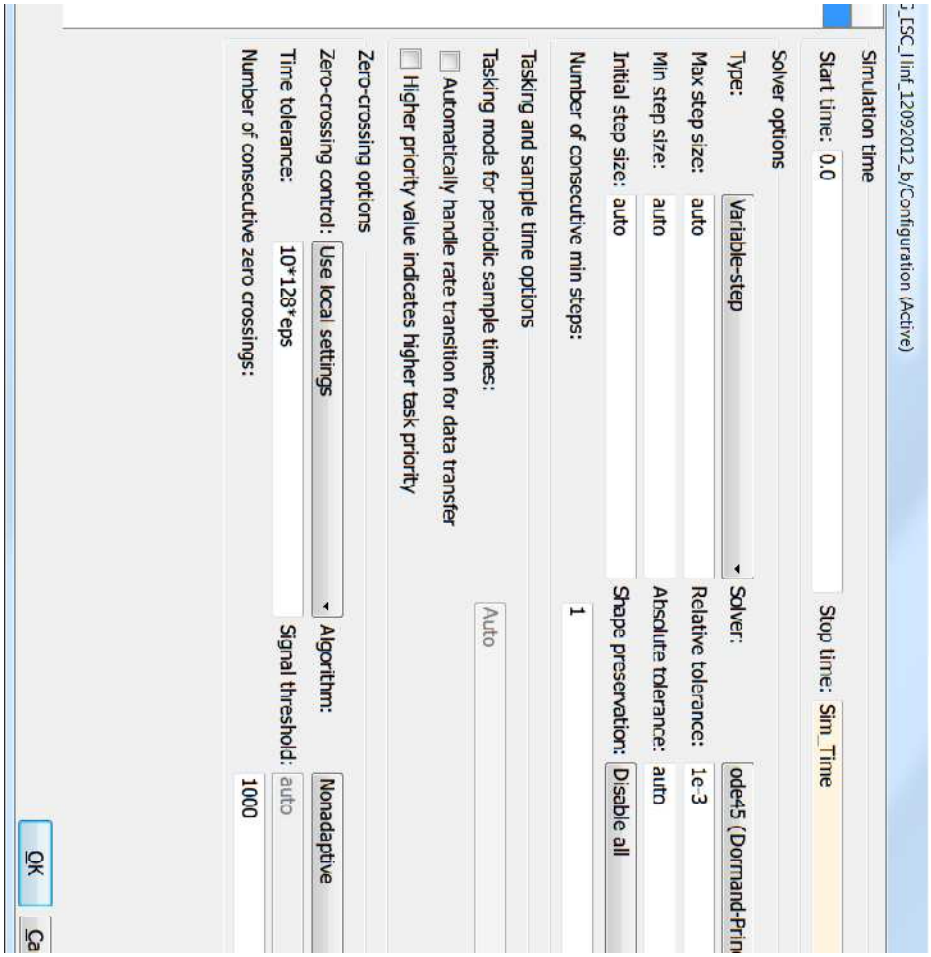

## Appendix E.2: Torque ESC Subsystem

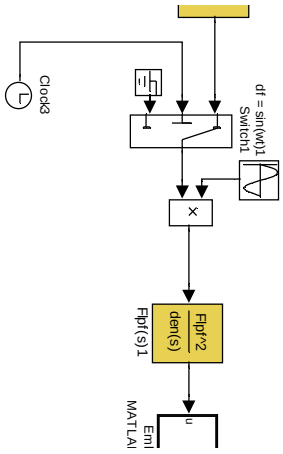

**Appendix E.3: Torque Calculation Subsystem**

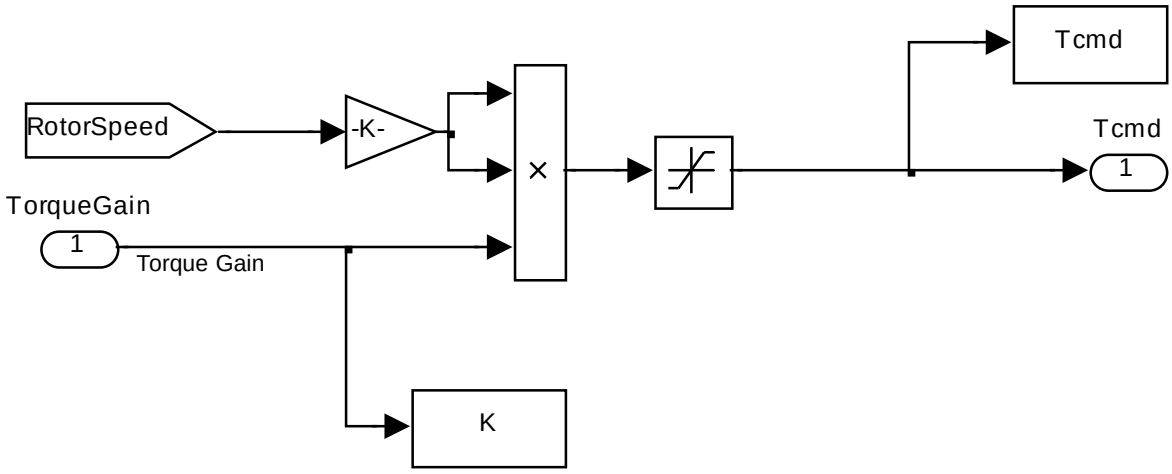

## Appendix E.4: DFIG Model Subsystem

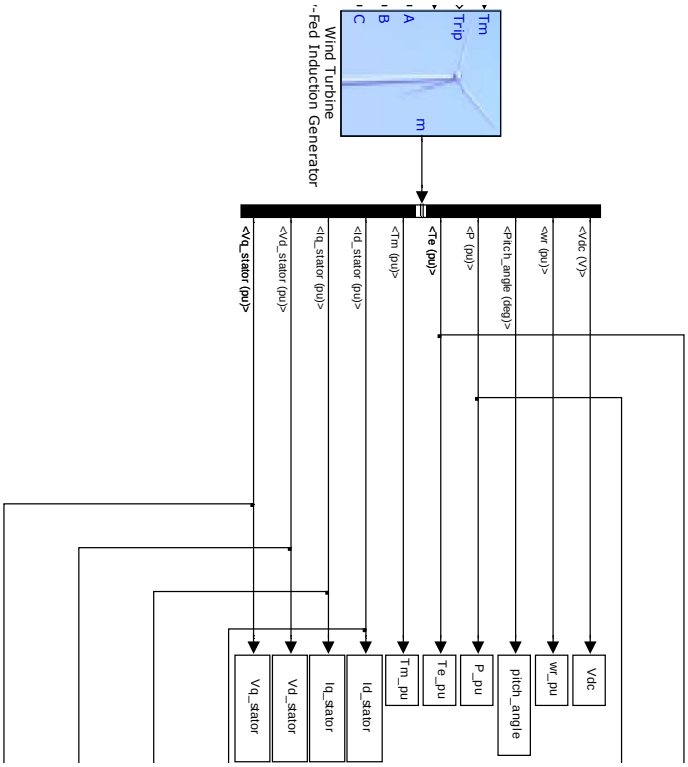

# Appendix F: Switching Control with CBT

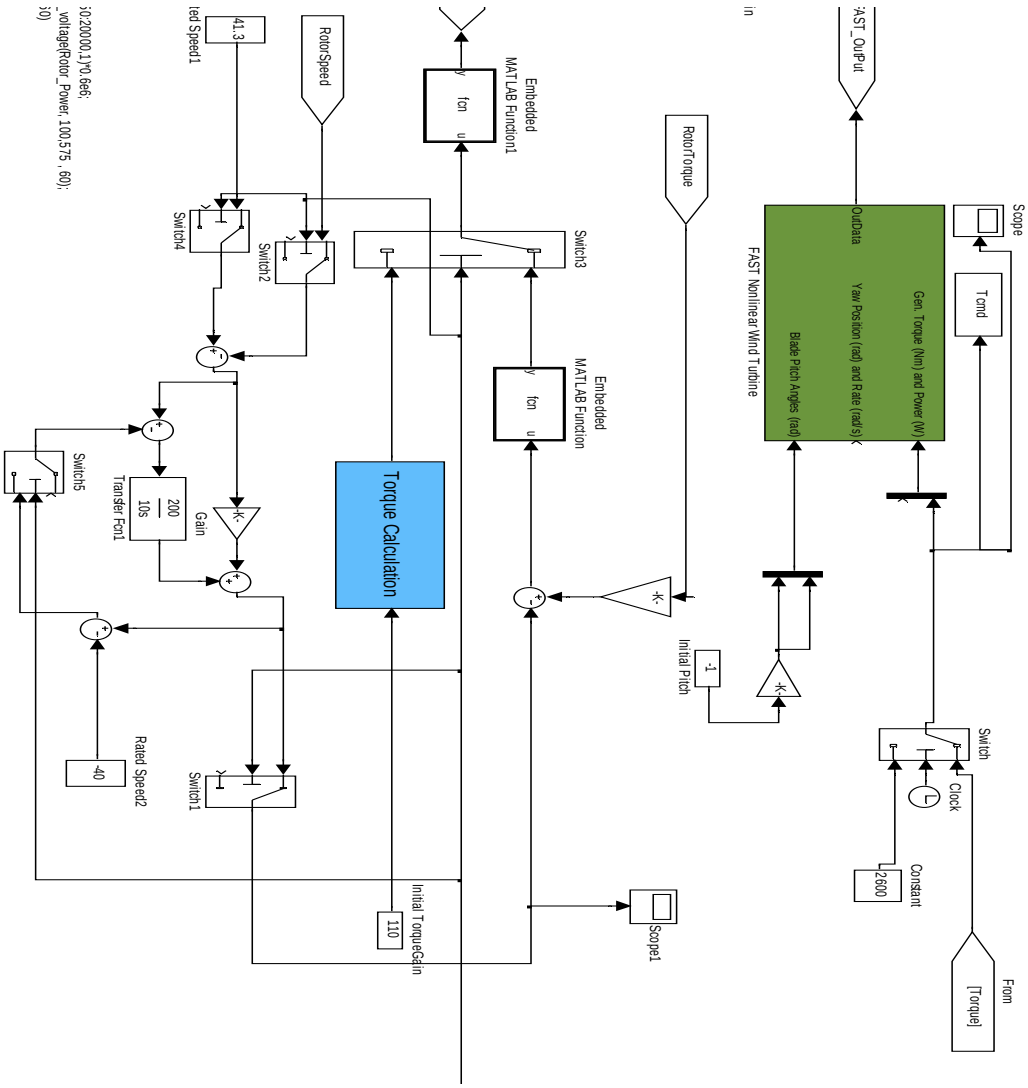

# Appendix G: Switching Control with LQBT